TÉCNICO LISBOA

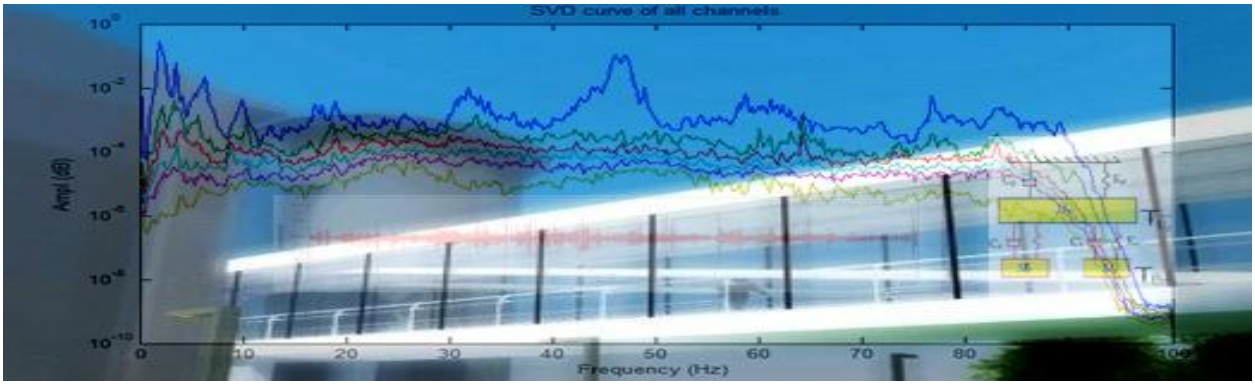

DYNAMICS OF FOOTBRIDGES THROUGH OPERATIONAL MODAL ANALYSIS AND VIBRATION CONTROL USING TUNED MASS DAMPERS

Gidewon Goitom Tekeste

Thesis to obtain the Master of Science Degree in

Civil Engineering

Supervisors: Prof. Jorge Miguel Silveira Filipe Mascarenhas Proença

Prof. Luís Manuel Calado de Oliveira Martins

Jury

Chairperson: Prof. José Joaquim Costa Branco de Oliveira Pedro

Supervisor: Prof. Jorge Miguel Silveira Filipe Mascarenhas Proença

Members of committee: Prof. Luís Manuel Coelho Guerreiro

JULY 2015

To Family and Friends

ABSTRACT

The development of output only analysis or Operational Modal Analysis (OMA) in the past two decades has brought a new attention to the experimental study of vibration induced effects in various civil engineering structures, including slender footbridges, without the need of artificial excitation source.

This dissertation focuses on the mathematical development of OMA estimation algorithms in the identification of dynamic behaviour and in the control of vibrations using Tuned Mass Dampers (TMDs). The application of TMDs to a case study steel footbridge in order to reduce pedestrian induced vibrations, including synchronization of pedestrians, making it less prone to resonance.

With regard to TMD tuning conditions, optimization of TMDs for better suppression of vibration amplitudes is studied assessing the ways for efficient tuning of TMDs. A MATLAB based Min-max optimization algorithm is developed and compared with the classic Den Hartog optimization Criteria. Its compliance range is determined and recommendation of its applicability range is done.

Peak-Picking, Enhanced Frequency Domain Decomposition (EFDD) and preliminary Stochastic Sub-Space Identification (SSI) methods are explored in depth and their implementation in the case study is presented. Comparison of EFDD MATLAB programmed algorithm and ARTeMIS standard software is performed for the footbridge and the ambient modal estimates are used in updating the FEM model for vibration serviceability check. TMD tuning is also checked and the footbridge responses at various TMD mass ratios are computed aiming at calibration of the effectiveness of TMDs in vibration control, and up to 50% reduction of responses is obtained.

Keywords: Operational Modal Analysis, Footbridge, Tuned Mass Dampers, Vibration Control, Enhanced Frequency Domain Decomposition, Stochastic Sub-Space Identification

RESUMO

O desenvolvimento da *Análise Modal Operacional* (OMA) nas últimas duas décadas trouxe atenção para o estudo dos efeitos da vibração induzida em várias estruturas de engenharia civil, incluindo passadiços pedonais, sem necessidade de fonte de excitação artificial.

Esta dissertação foca o desenvolvimento matemático de algoritmos de estimação OMA na identificação do comportamento dinâmico e controle de vibrações utilizando *Amortecedores de Massa Sintonizada* (TMDs). Estes algoritmos foram aplicados com o objectivo de reduzir as vibrações pedestres induzidas no passadiço, incluindo a sincronização dos peões, através da introdução de TMDs na estrutura tornando-a menos propensa à ressonância.

Considerando as condições de sintonização dos TMD, a optimização do seu dimensionamento para supressão das amplitudes de vibração é estudada, apresentando e desenvolvendo algoritmos de optimização Min-max baseados em MATLAB, sendo os mesmos comparados com o critério de optimização clássico de Den Hartog, procedendo-se à análise das condições de aplicação dos mesmos algoritmos.

São explorados em detalhe os métodos Peak-Picking, Enhanced Frequency Domain Decomposition (EFDD) e preliminary Stochastic Sub-Space Identification e a sua aplicação ao caso de estudo. É realizada a comparação do MATLAB programado EFDD com o ARTeMIS Standard para o passadiço e as estimativas modais ambientais são usados na atualização do modelo FEM para verificação das condicões de conforto em serviço. A sintonização dos TMDs também é verificada e as resposta do passadiço aos vários rácios de massa dos TMDs são calculadas com o objectivo de quantificar a eficiência dos TMDs no controle da vibração, obtendo-se uma redução de até 50% na resposta.

PALAVRAS-CHAVE: Análise Modal Operacional, Passadiços pedonais*, Amortecedores de Massa Sintonizada, Controle de Vibrações, Enhanced Frequency Domain Decomposition, Stochastic Sub-Space Identification*

ACKNOWLEDGEMENTS

The research presented in this dissertation is carried out at the Department of Civil Engineering, Architecture and Georresources (DECivil) of the Instituto Superior Técnico (IST), Lisbon. It is conducted under the supervision of Professor Jorge Miguel Proença. This dissertation is developed within the scope of the project signed between OZ. Lda. and the Instituto Superior Técnico, U Lisboa, regarding the operational modal analysis and structural health monitoring system of the pedestrian footbridges of the new corporative headquarters of EDP, Energias de Portugal. Lisbon. Through this document work, I would like to express my sincere appreciation and gratitude to:

− Professor Jorge Miguel Proença (Instituto Superior Tecnico, IST), for the scientific guidance and final text review. His permanent availability even to discuss the smallest details was more than helpful. His valuable advices, support and all the encouragement words, and relentless dedication for the work.

− Professor Carlos Oliveira (Instituto Superior Tecnico, IST), for stimulating me the need to investigate more and for providing me Artemis Dongle to run my records for modal estimation purposes as well as cross-checking and validating with MATLAB programmed results.

− Professor Mario Lopes (Instituto Superior Tecnico, IST) for provoking to take interest in dynamic behavior related scientific research issues in his classes.

− Professor Luis Guerreiro (Instituto Superior Tecnico, IST) for his presence when I needed support with Finite Element Modelling and sharing his ideas during my difficulties.

− Diagnóstico, Levantamento e Controlo de Qualidade em Estruturas e Fundações, Lda (OZ. Lda.) Company that made this study available for scientific purposes.

− AFACONSULT for supplying necessary documentation including FEM model of the project

− Ambiente e Sistemas de Informação Geográfica S.A.(AMBISIG) for assisting me during data collection, accessing their health monitoring apparatus and sending me necessary records.

− M.Sc. Student Timir Brayan Roy for all the helpful conversations about issues related with dynamic modelling, as well as for the sharing of knowledge and ideas for solving problems that arise from this study.

− My wife, Yohana A., and my parents for all their permanent support, especially during the moments when I was completely worn out and upset with problems that seemed never to end. To them I want to express my apologies for all the moments when I was prevented from giving them all the attention that they deserve.

TABLE OF CONTENTS

ABSTRACT ..... **iii**

RESUMO ..... **v**

ACKNOWLEDGEMENTS ..... **vii**

TABLE OF CONTENTS ..... **ix**

LIST OF TABLES ..... **xiv**

LIST OF FIGURES ..... **xiv**

LIST OF SYMBOLS AND ABBREVIATIONS ..... **xviii**

1 Introduction

1.1 Thesis Context **1**

1.1.1 Operational Modal Analysis 1

1.1.2 TMDs in Footbridges 2

1.1.3 Pedestrian Traffic on Footbridges 4

1.2 Thesis Objectives and Main Contributions **5**

1.2.1 Motivations and Objectives 5

1.2.2 Contributions of the Thesis 6

1.2.3 Organization and Structure of the thesis 6

2 Dynamic Models and Operational Modal Analysis

2.1 Introduction **9**

2.2 Multiple Degree of Freedom System **12**

2.2.1 Undamped Free Vibrations 12

2.2.2 Proportional or Rayleigh Damping 15

2.2.3 General Viscous Damping Systems 16

2.3 Finite Element Modelling 18

2.4 Frequency Domain Models 18

2.4.1 Laplace Transform and Transfer Function 18

2.4.2 Fourier Transform and Frequency Response Function (FRF) 20

2.4.3 Sampling, Discrete Fourier Transform, Z-transform and Fast Fourier Transform 21

2.4.4 Spectrum and Spectrum Estimation 22

2.4.5 Model Reduction 24

2.4.6 Frequency Domain Models 25

2.4.7 Summary 29

2.5 Frequency domain modal identification methods 29

2.5.1 Peak picking (PP) 29

2.5.2 Frequency Domain Decomposition (FDD) 32

2.6 Time Domain Models 36

2.6.1 Continuous Time State-Space Model 37

2.6.2 Discrete Time State- Space Model 38

2.6.3 Discrete Time Stochastic State-Space Model 41

2.6.4 Properties of Stochastic Systems 41

2.6.5 Summary 43

2.7 Time Domain Modal Identification Methods 43

2.7.1 Past' and 'Future' part of experimental signal 44

2.7.2 Data Driven SSI Method 45

2.8 Comparison of Identification Methods 50

2.9 Conclusion 50

3 Pedestrian traffic as a source of excitation

3.1 Introduction 51

3.1.1 Pedestrians as Source of Vibration 51

3.1.2 Forces Induced by Pedestrians 51

3.1.2.1 Patterns of Running and Walking 51

3.1.2.2 Vertical Component 52

3.1.2.3 Horizontal Component 53

3.2 Characteristics of Pedestrian Streams 53

3.3 Interaction between Pedestrians and Footbridges 54

3.3.1 Dynamic Properties of Footbridges under Human-Induced Loads 55

3.3.2 Synchronization between Pedestrians 55

3.3.3 Synchronization between Bridge and Pedestrians 56

3.4 Modelling of Pedestrian Loads 56

3.4.1 Vertical Load Model of Walking Pedestrian 56

3.4.2 Horizontal Load Model of Walking Pedestrian 60

3.5 Load Models for Group of Pedestrians 61

3.6 Load Model for Joggers 63

3.7 Sensitivity of Pedestrians to Vibrations of Footbridges 64

3.7.1 Sensitivity to Vertical Vibrations 64

3.7.2 Sensitivity to Horizontal Vibrations 64

3.8 Comfort Classes 65

4 Dynamic Control through Tuned Mass Dampers (TMDs)

4.1 Introduction 67

4.2 Frahm's Vibration Absorber 68

4.3 Equations of the Passive TMDs 74

4.4 Transfer Functions for Various External Excitations 77

4.5 Optimization Criteria for TMDs 77

4.5.1 H_∞ Optimization 78

4.5.2 H_2 Optimization 79

4.6 Single Degree-of-Freedom Systems with TMDs 80

4.6.1 TMD linked to an Undamped System and Optimized Tuning of TMDs 80

4.6.2 TMD Attached to a Damped System and Optimized Tuning of TMDs 85

4.7 Multi Degree-of-Freedom Systems with TMDs 89

4.8 Case study Footbridge with two TMDs tuned to the same Frequency 91

4.9 Design Considerations 93

5 Operational Modal Analysis of EDP's North footbridge

5.1 Description of the Footbridge 95

5.2 Ambient Records of North footbridge with and without TMDs Installed 96

5.2.1 Reduction of Errors from Records 99

5.2.1.1 Aliasing Error, Choice for Nyquist Frequency 99

5.2.1.2 Leakage, Windowing and De-Trending 99

5.2.2 Enhanced Frequency Domain Decomposition (EFFD) 100

5.2.2.1 EFDD Implementation using MATLAB Programmed Algorithm 100

5.2.2.2 EFDD Implementation using Artemis Modal Software 104

5.2.2.2.1 Creating Geometry, Importing, Managing Records and Analysis 104

5.2.2.2.2 Modal Estimation 106

5.2.2.3 Comparison of Modal Estimates 111

5.2.2.3.1 Comparison of FEM Estimates with OMA Estimates and FEM Updating 111

5.2.2.3.2 Comparison of Estimates Before and After TMD Installation 114

5.2.2.4 Assessment of Efficiency of TMD's in Attenuating Vibration 115

5.3 Summary and Conclusion 119

6 Conclusions and Future works

6.1 Conclusions 121

6.2 Future works 124

BIBLIOGRAPHY 125

Annex A 129

Annex B 131

Annex C 133

Annex D 139

Annex E 141

LIST OF TABLES

Table 2.1 Comparison of Modal parameters estimates from different algorithms

Table 3.1 Fourier coefficients proposed by several authors and codes

Table 3.2 Traffic classes

Table 3.3 Comfort classes according to 3rd international footbridge conference

Table 4.1 Simply supported beam FEM model with vibration absorber results

Table 4.2 Non-Dimensional Complex Transfer Functions (from Warburton, 1981)

Table 4.3 Optimized values comparison between Den Hartog criteria and MATLAB program

Table 4.4 Comparison between Den Hartog and Numerically optimized values for ξ_P=1%

Table 4.5 Comparison between Den Hartog and Numerically optimized values ξ_P=5%

Table 4.6 Properties of TMDs in North Footbridge

Table 5.1 Data collection sensor layout of the footbridge

Table 5.2 EFDD/CFDD modal estimates during construction and before TMDs installation using ARTeMIS standard.v.3.6

Table 5.3. MATLAB EFDD program modal estimates during construction and before TMDs installation

Table 5.4. ARTeMIS Modal estimates after completion of footbridge and after TMDs installed

Table 5.5. MATLAB EFDD program modal estimates after completion of footbridge and TMDs installed

LIST OF FIGURES

Figure 1.1 –Tuned Mass Damper and its components

Figure 1.2 - Organization of the thesis

Figure 2.1 - A system with output y; the input, comprising a determined input u and measured disturbance w, is assumed as white noise; v is an unmeasured disturbance

Figure 2.2 - Metallic Frame

Figure 2.3 - Natural Frequency and Modal shapes

Figure 2.5 - Trace of spectrum matrix

Figure 2.6 - Coherence of records

Figure 2.7- Singular values produced using EFDD method

Figure 2.8 - MAC value plot

Figure 2.10 - Natural frequency estimation from zero-crossing times and modal estimates (left) of EFDD program

Figure 2.11 - Singular values of projection matrix for model order computation

Figure 3.1 - Load Patterns of walking and running

Figure 3.2 - Loading curves of one pedestrian for different types of steps (Blanchard, 1977)

Figure 3.3 - Walking load patterns, lateral (left) longitudinal (right)

Figure 3.4 - Running load patterns, lateral (left) longitudinal (right)

Figure 3.5 - Traffic density versus Traffic velocity (Oeding, 1963)

Figure 3.6 - Pedestrian density

Figure 3.7 - Synchronizing effect of pedestrians

Figure 3.8 - Walking vertical/Longitudinal vs Lateral load function

Figure 3.9 - Application of Harmonic load according to mode shape

Figure 3.10 - Reduction Factor, ψ

Figure 3.11 -Reduction Factor, ψ, for running

Figure 4.1 - Frahm's vibration absorber

Figure 4.2 - Amplitude of transfer function with TMD (μ=0.05) and without TMD

Figure 4.3 - Amplitude of displacement transfer function for different mass ratios

Figure 4.4 - FEM model of a simply supported beam with TMDs (right) and without TMDs (left)

Figure 4.5 - FEM beam model maximum displacement versus mass ratio of vibration absorber

Figure 4.6 - Frahm's vibration absorber

Figure 4.7 - H_∞ optimization Criteria

Figure 4.8 - Displacement transfer function for q=0.9 and μ = 0.2 (ξ_p=0)

Figure 4.9 - Displacement Transfer Function for q=0.8 and μ = 0.2 (ξ_p=0).

Figure 4.10 -Transfer Function for undamped system (a) q=0.9 and (b) q=0.8 for values of ξ_S

Figure 4.11 -Transfer Function for *qOPT*, *0.95qOPT* and *1.05qOPT* (ξ_p=0)

Figure 4.12 -Transfer Function for $\xi_{S,OPT}$, $0.80\xi_{S,OPT}$ and $1.20\xi_{S,OPT}$(ξ_p=0)

Figure 4.13 - Amplitude of the Transfer Function variation with mass ratio μ (ξ_p=0).

Figure 4.14 - Modulus of the Transfer Function as function of ξ_P

Figure 4.15 - Amplitude of the Transfer Function (a) for ξ_P=1% and (b) for ξ_P=1% (μ = 0.2)

Figure 4.16 - Den Hartog versus Numerical solution comparison for optimized values a) freq. ratio, b) damping ratio

Figure 4.17 - TMDs location in the North Footbridge of EDP, plan view

Figure 4.18 - TMDs location in the North Footbridge of EDP, plan view

Figure 4.19 - North Footbridge sectional view at TMD location

Figure 5.1 - a) side view under construction and b) internal view after completion of the North Footbridge

Figure 5.2 - TMDs location in the span of the bridge and details of TMD

Figure 5.3 - MATLAB program singular value plot of records during construction and TMDs not installed

Figure 5.4- ARTeMIS singular value plot of footbridge records during construction and TMDs not installed

Figure 5.5 - Ambient vibration records after completion of the footbridge

Figure 5.6- Ambient vibration record at Mid-span in the vertical direction after completion of footbridge

Figure 5.7 – (a) Application of Hann window; (b) Application of de-trending

Figure 5.8 - Singular value plot for (a) MAC=0.9 and (b) MAC=0.8 [setup 4]

Figure 5.9 - MAC plot and SDOF bell curve for (a) MAC=0.9 and (b) MAC=0.8

Figure 5.10 - Free decay curve and damping estimation plot for (a) MAC=0.9 and (b) MAC=0.8

Figure 5.1 - Zero crossing times plot and corrected natural frequency estimation plot for (a) MAC=0.9 and (b) MAC=0.8

Figure 5.12 - Model order computed using SSI-DATA algorithm for ambient vibration records after completion of footbridge [setup 4]

Figure 5.13 - Geometry creation (left); Manage Measurements window (right) of ARTeMIS standard v.3.6

Figure 5.14 - Channel assignment (left); Analysis options window (right) ARTeMIS standard v.3.6

Figure 5.15 - Estimation window of ARTeMIS (left); Damping validation using Free decay (right)

Figure 5.16 - MAC validation between Modes in one method, EFDD, (left); between EFFD and CFDD of the same mode (right)

Figure 5.17 - MCF validation of first two modes from EFDD (right); MAC validation for first two modes in EFDD (left)

Figure 5.18 - Figure 5.17 MAC value matrix shown in bar-graphs for all modes after completion of footbridge

Figure 5.19 - Mode shapes calculated by OMA (after completion) and Finite Element method

Figure 5.20 - FEM updating trails, glass panel model (right) and cross bars model to simulate glass panels (left)

Figure 5.21 - Updated model with rotational springs at support, 1st vertical mode

Figure 5.22 - Averaged singular value plot for all setups before (left) and after (right) completion of the project for 1024 sampling points and no decimation

Figure 5.23 - SAP2000 model to simulate only the first mode of footbridge, f=1.09Hz

Figure 5.24 - Pedestrian load Traffic Class 5 (1st Harmonic) time history acceleration response at Mid-Span without TMD (left) and with TMD (right) tuned to the 1st mode with a mass ratio of 2% [units in m/s^2]

Figure 5.25 - Pedestrian load Traffic class 5 (1st Harmonic) time history displacement response at Mid-Span without TMD (left) and with TMD (right) tuned to the 1st mode with a mass ratio of 2% [units in m]

Figure 5.26 - Pedestrian load Traffic class 5(1st Harmonic) time history displacement (right) and acceleration (left) responses of TMD (joint 133) and footbridge mid-span node (joint 105) for the TMD tuned to the 1st mode with a mass ratio of 2% [units are in m and m/s^2]

Figure 5.27 - Percentage of reduction in footbridge response vs TMD mass ratio owing to TMDs, Mid-span displacement (left) and mid-span Acceleration (right)

Figure 5.28 - Relative displacement vs mass of TMD

Figure 5.29 - Total TMD stroke vs. TMD damping coefficient for 2% mass of TMD

Figure 5.30 - Footbridge vibration time history on final updated model, actual TMDs and TC5, with TMDs (left) and without TMDs (right) [m/s2]

LIST OF SYMBOLS AND ABBREVIATIONS

General Rules

-Matrix and Vector symbols are represented by bold type characters and capital letters.

-The transpose of a matrix is denoted by the superscript T

-Differentiation with respect to time is denoted by superposed dots (˙)

-Differentiation with respect to space is denoted by superscript primes (′)

-Complex conjugate (*) or (^{H})

-Inverse of a matrix ($^{-1}$)

-Eliminated mode (^{e})

-Retained mode(^{r})

Variables

a	Acceleration
a_{max}	Maximum acceleration
c	Damping coefficient
K_P	Stiffness of the primary system
K_S	Stiffness of the secondary system
m	Mass per unit length of a beam
m_P	Mass of the primary system
m_S	Mass of the secondary system
q	TMD frequency ratio
r_P	Ratio of the excitation to primary system natural frequencies
U_P	Displacement of the primary system
U_{Pst}	Static deflection of the primary system
U_S	Displacement of the secondary system
qOPT	Optimized frequency ratio
E	Young elasticity modulus
I	Moment of inertia of the beam cross-section

Greek Variables

α , β , γ	Parameters
δ(t)	Dirac delta function
ε( )t	Heaviside unit function
σ_f	Standard deviation
v_s	Velocity of pace [m/s]
G_k	Displacement transfer function
N_r	Number of pedestrians on bridge deck
μ	Secondary to Primary systems mass ratio
ω_0	First mode of vibration circular frequency of the undamped structure

ω_D	Circular frequency of the damped structure
ω_n	Circular frequencies of the *nth* vibration mode of the damped structure
ω_P	Natural frequency of the primary system
ω_S	Natural frequency of the secondary system
Φ	Dynamic amplification factor
ξ_n	Damping ratio of the *nth* vibration mode of the structure
ξ_P	Damping ratio of the primary system
ξs	Damping ratio of the secondary system
P	Persons
f_{sm}	Mean step frequency
A_{ri}	Denominator matrix polynomial
B_{ri}	Numerator matrix polynomial
C_d	Displacement response measurements
C_v	Velocity response measurements
C_a	Acceleration response measurements
ξ_i	Damping ratio of mode *i*
ϑ	Logarithmic decrement of damping
Ψ	Mode shape matrix
Φ	Mode shape vector
q_{mc}	Modal coordinate transformation
Λ_{com}	Eigen value matrix
Ω	Eigen frequency matrix
$\boldsymbol{I_{n_m}}$	Identity matrix
N/A	Not available
R_r	Residue
S_S	Spectrum Matrix
$H(s)$	Transfer Function
R_{xx}	Correlation Function
Δt	Time interval
$\mathbb{R}$	Real number
$\mathbb{Z}[\,]$	Z-Transform
$S^+{}_{yy}$	Half power spectra
$\boldsymbol{E}[\,]$	Expected value or mean value
L[ ]	Laplace transformation
γ	Modal participation factor
F[ ]	Fourier transformation

Vectors and Matrices

M	Mass matrix
C_2	Damping matrix
K	Stiffness matrix
F( )*t*	Vector of externally applied loads
U( )*t*	Displacement vector
$\dot{\boldsymbol{U}}$ ( )*t*	Velocity vector
$\ddot{\boldsymbol{U}}$( )*t*	Acceleration vector
$U(\omega_i)$	Unitary matrix
$S(\omega_i)$	Diagonal singular value matrix
φ	Mode shapes matrix

Abbreviations and Acronyms

ARMA	Auto-Regressive Moving Average
CL	Comfort Classes
CMIF	Complex Mode Indicator Function
COR	Correlation Functions
DFT	Discrete Fourier Transform
DLF	Dynamic Load Factor
DOF	Degree of Freedom
EDP	Energias de Portugal
EFDD	Enhanced Frequency Domain Decomposition
EMA	Experimental Modal Analysis
ERA	Eigen System Realization Algorithm
FDD	Frequency Domain Decomposition
FE	Finite Element
FEM	Finite Element Method
FRF	Frequency Response Functions
IOMAC	International Operational Modal Analysis Conference
IRF	Impulse Response Functions
LSCE	Least Squares Complex Exponential
MAC	Modal Assurance Criteria
MDOF	Multi Degree of Freedom
MTMD	Multiple Tuned Mass Damper
NDT	Nondestructive Testing
NExT	Natural Excitation Technique
OMA	Operational Modal Analysis
PFE	Partial Fraction Expansion
P-LSCF	Poly-reference Least Squares Complex Frequency

PP	Peak-Picking
PRCE	Poly-reference Complex Exponential
RMFD	Right Matrix Frequency Domain
SDOF	Single Degree of Freedom
SHM	Structural Health Monitoring
SLE	Synchronous Lateral Excitation
SP	Single Pedestrian
SSI	Stochastic Subspace Identification
SSI-COV	Co-variance driven Stochastic Subspace Identification
SSI-DATA	Data driven Stochastic Subspace Identification
SVD	Singular Value Decomposition
TMD	Tuned Mass Damper
TC	Traffic Class
TSA	Time Series Analysis
UMPA	Unified Matrix Polynomial Approach
ZOH	Zero-Order Hold

1

INTRODUCTION

1.1 Thesis context

1.1.1 Operational modal analysis

Operational Modal Analysis (OMA) deals with the identification of modal parameters of a structural system without measuring a controlled input excitation. Therefore, it is also known as Output-only Modal Analysis. The motivation to carry out OMA tests emerged initially from Civil Engineering because it is difficult and expensive to artificially excite structures such as buildings, bridges or dams. However, OMA has been also widely used in other fields, like mechanical engineering or aerospace engineering to measure the modal properties of different mechanical and aerospace objects like wing of an airplane. An extensive overview of applications of OMA with different scopes can be found in (Cunha et al, 2007; Hermans et al, 1999).

Ambient modal identification, also known as Operational Modal Analysis (OMA), aims at identifying the modal properties of a structure based on vibration data collected when the structure is under its operating conditions, i.e., no initial excitation or known artificial excitation. The modal properties of a structure include primarily the natural frequencies, damping ratios and mode shapes. In an ambient vibration test the subject structure can be under a variety of excitation sources which are not measured but are assumed to be 'broadband random'. The latter is a notion that one needs to apply when developing an ambient identification method. The specific assumptions vary from one method to another. Regardless of the method used, however, proper modal identification requires that the spectral characteristics of the measured response reflect the properties of the modes rather than those of the excitation.

Generally, OMA methods can be classified in two types: One of them comprehends the operational modal analysis methods used to process data from ambient vibration tests. Another one involves the long-term automated operational modal analysis methods, used to process continuous dynamic monitoring signals from data acquisition system. In ambient vibration tests, the structural ambient response is captured by one or more reference sensors at fixed positions, together with a set of roving sensors placed at different measurement points along the structure in different setups. The collected structural response is processed by two main groups of operational modal identification methods, namely non-parametric and parametric methods in both frequency and time domains. The purpose of the ambient vibration tests is the identification of structural dynamic properties in order to calibrate and update the finite element models, mitigate probable structural damage by preventing resonance problem, as well as to build a baseline for structural continuous dynamic monitoring.

Long-term automated operational modal analysis techniques mainly comprise a structural continuous dynamic monitoring system and fully automated output-only modal identification tools. The continuous dynamic monitoring system includes a series of permanently installed sensors such as strain gauges, displacement transducers, accelerometers, thermocouples, video cameras, inclinometers etc., collecting structural responses and environmental variations in operational conditions over a long period of time(can go up to several years). The continuous dynamic monitoring system not only provides vibration data for automated modal analysis, but also can be used to build a relatively simple alert system or to accurately characterize the structural performance, for instance evaluating experimentally fatigue damage. Automated modal identification procedures are responsible for processing the accumulated continuous monitoring vibration signals, excluding any user interaction, and tracking the variations of structural dynamic properties in order to reflect long term structural dynamic behavior. In recent years, automated operational modal analysis has gathered raising attentions with the formulation of algorithms relying on control theory and conventional signal processing techniques. Fruitful development of theory and applications is reviewed in (Rainieri and Fabbrocino, 2009).

1.1.2 TMDs in Footbridges

“Due to the trend of constructing ever lighter and filigree load-carrying structures, footbridges are becoming more susceptible to vibrations caused by pedestrians or wind. Usually, these vibrations impact only the serviceability of the bridges since the desired level of comfort is no longer attained. However, in some cases, the vibrations of the bridges are so extreme that damages can arise or, in extreme cases, the structural integrity of the bridge can be at risk. The primary reason for the occurrence of perturbing vibrations is resonance. In order to improve the dynamic behavior of a footbridge, the structural stiffness of the bridge has to be increased so that its natural frequencies are out of the range typically excited by pedestrians or wind, or structural damping of the bridge has to be increased. The most effective way to increase the structural damping and improve the dynamic behavior is the application of dampers (buffers, shock absorbers, Dampers) or TMDs (Tuned Mass Dampers) that significantly reduce resonance like excitation related vibrations”-Footbridge 2008, Third International Conference.

Moreover, as simulations of footbridge constructions become more prevalent, assuring that these simulations with reasonable accuracy represent the reality must be ensured. The comparison between simulated and measured dynamic properties is an important task in calibrating the finite element models, which will subsequently be used in the design phase as prediction tools. If the simulations indicate that the Eigen frequencies for the bridge will coincide with the walking frequencies of the pedestrians, action has to be taken. Either in redesigning the bridge or, if the design cannot be altered, by installing active or passive counter measures such as for instance tuned mass dampers (TMD) which is the subject in this thesis.

The advantage of using TMDs is that, unlike with the use of dampers, shock absorbers etc., no fixed-point are required. It is simply force-fitted to the structure. Compared to the additional structural mass that is

required to increase the structural damping conventionally, the necessary TMD mass is only a fraction, which allows also a subsequent application with no bigger improvements in the structural design. In this context the structural influence of TMDs on the dynamic properties of foot-bridge will be assessed under several conditions of relative masses and relative damping of the footbridge under study and TMDs installed.

“A tuned mass damper (TMD) is a device consisting of a mass, a spring, and a damper that is attached to a structure in order to reduce the dynamic response of the structure. The frequency of the damper is tuned to a particular structural frequency so that when that frequency is excited, the damper will resonate out of phase with the structural motion. Energy is dissipated by the damper inertia force acting on the structure. The TMD concept was first applied by Frahm in 1909 (Frahm, 1909) to reduce the rolling motion of ships as well as ship hull vibrations. A theory for the TMD was presented later in the paper by Ormondroyd and Den Hartog (1928), followed by a detailed discussion of optimal tuning and damping parameters in Den Hartog’s book on mechanical vibrations (1940). The initial theory was applicable for an undamped SDOF system subjected to a sinusoidal force excitation. Extension of the theory to damped SDOF systems has been investigated by numerous researchers. Significant contributions were made by Randall et al. (1981), Warburton (1981, 1982)”- Connor and Laflamme, Structural Motion Engineering.

The primary concept of TMDs is that each TMD installed at a given location (as with the case of multiple TMDs) will be preferably tuned to the natural frequency, related to the mode with higher amplitude at TMD position, so that the mode to which the TMD is tuned to will be suppressed yielding other two natural frequencies centered at the former natural frequency.

The primary concern is related to the frequency tuning of the TMDs as they are sensitive in this case, de-tuning may lead to non-usefulness of the TMDs in effectively suppressing structural vibration. In this image, tendency of changing stiffness of the structure over long period of time may lead to de-tuning of the TMDs. In this project the TMDs are designed with layers metal plates bundled together, as shown in Figure 1, in order to allow adjustment of the mass of the TMD by adding or removing metal plates, to increase and decrease the mass of the structure, so that the TMD will be tuned to the designed mode though stiffness change occurs in the foot-bridge. Detailed discussion can be found on chapter 4.

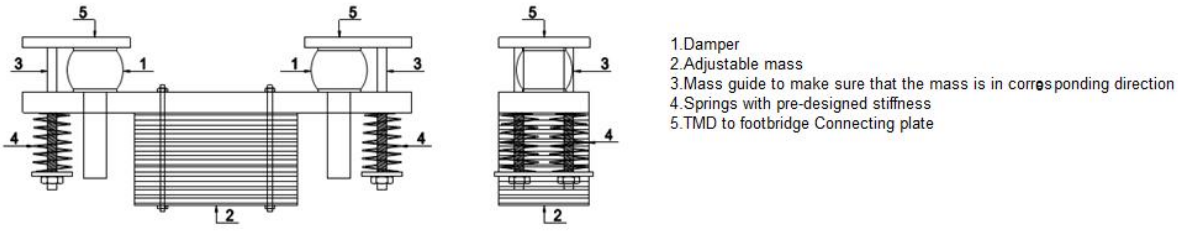

Figure 1.1-Tuned Mass Damper and its components

1.1.3 Pedestrian traffic on Footbridges

Footbridges are prone to pedestrian induced vibrations in vertical and lateral directions which has direct impact on the serviceability requirement of comfort level of pedestrians traversing it. Thus, in order to assess the dynamics of footbridges and actual vibration levels expected under various traffic levels, realistic modelling of pedestrian traffic load is crucial. When a pedestrian crosses a bridge a dynamic force is produced which has components in three different directions: vertical, lateral and longitudinal. Some forms of deliberate loading such as jumping or body swaying can also produce forces with different characteristics. The force produced in vertical direction by pedestrians is the one studied the most. The vertical component has the highest magnitude of the three components and has therefore been regarded as the most important (S.Živanovic, 2005). Vertical and longitudinal walking are characterized with 1.2-2.4Hz frequency range while lateral walking is characterized by half of the vertical frequency.

Dynamic forces are described as a function of time and space, periodically repeated with regular time intervals. Dynamic actions are the displacements, velocities, accelerations and energy produced by the vibration source. These actions can often not be predicted in a deterministic way which is why it can be suitable to consider them to be random. Several researches done to model pedestrian traffic resulted in diversified results which is attributed to its complexity involving human psychological situation.

Periodic load model of several harmonics was the most famous model. Nevertheless, several authors have diversified results, namely Blanchard, Bachmann etc., for the Fourier coefficients of the load model. However, recent researches done by HIVOSS and SYNPEX identified more sophisticated solution based on walking frequency parameter. In continuation, the need to model group of pedestrians makes this problem rather difficult due the synchronization effect of pedestrians. In this project, guidelines published by HIVOSS will be used for reference and load modelling.

The primary concept of modelling a group of pedestrians lies on the determination of equivalent number of synchronous pedestrians which is dependent on traffic density, structural damping of the structure and the walking frequency of pedestrians. As density increases, frequency of walking is reduced leading to higher synchronization of pedestrians but reduced dynamic input as speed of pedestrians is reduced. According to the statistics, the load can be increased with the square root of the number of pedestrian on the bridge. i.e. $\sqrt{N}$. Many researches done on synchronization use other approaches to define it.

Synchronous lateral excitation (SLE) is also an important aspect which was developed after the Millennium Bridge lateral resonant vibration phenomena. Several studies are done on that subject and brief discussion of this subject, and its influence for the project will be addressed.

1.2 Thesis Objectives and Main Contributions

1.2.1 Motivations and Objectives

The promising prospective of OMA inspired many researchers all over the world. Recent overviews, theory development and practical applications can be found in (Operational Modal Analysis of Civil Engineering Structures by Carlo Rainieri and Giovanni Fabbrocino).And more specifically, researches on a dynamic property improvement of structures equipped with TMDs using OMA as tool are rare. Modern footbridge structures tend to be lively structures due to the increasing strength of new materials, longer spans and greater slenderness for aesthetic requirements. These construction trends lead to vibration serviceability problems, footbridges becoming more susceptible to excessive sway motions resulted from moving pedestrian traffic or crowds. For example, the excessive lateral vibrations (lock-in) were clearly perceived by pedestrians in the opening day of the Millennium Bridge in London on 10th June 2000 (Dallard et al, 2001). This fact motivated the development of important investigations on footbridge vibrations, which was made evident on the International Footbridge Conference, launched in 2002 in Paris, and subsequent editions in Venice (2005) and Porto (2008). A review on footbridges research can be found in (Živanović et al, 2005) and a recent a book on Footbridge Vibration Design was edited by (Caetano et al, 2009). Considerable footbridge research attentions are paid to different aspects, namely, vibration source, path and receivers. However, the need to absorb the pedestrian traffic induced vibrations by equipping footbridges with TMDs has not been extensively investigated and well understood yet. For example, the influence of walking people on footbridge vibration properties, such as natural frequencies and modal damping ratios. Besides, though excessive vibration induced by pedestrians is regarded as a serviceability problem, it also may lead to early structural changes in normal operational conditions and thus, to solve the aforementioned problems, the effective use of active and/or passive TMDs can be proposed. Hence, proper understanding of OMA modal identification algorithms become a necessary tool.

In this context, the objectives of this thesis are concerned with such issues:

(i) Understanding and comparison of main OMA methods;
(ii) Implementation of chosen algorithms using MATLAB program with adequate accuracy in statistical terms and implementation of ARTeMIS for the same data for the purpose comparing MATLAB results with standard ARTeMIS modal results;
(iii) Updating Finite element modeling parameters in terms of frequency and damping ratios used for analysis under pedestrian loads;
(iv) Calibrating the effectiveness of TMDs in attenuating the amplitude of vibrations on the North footbridge (EDP building, Cais do Sodre, Lisbon) under study.

1.2.2 Contributions of the Thesis

To achieve the above mentioned objectives, the thesis is dedicated to solve these problems and its contributions are the following:

(i) Sample operational modal analysis techniques are reviewed synthetically. Generally, they are classified as frequency and time domain approaches, depending on the primary data type: frequency spectra of data using Fourier Transforms, or data in time domain.

(ii) A user- friendly MATLAB programs for operational modal analysis focusing on Enhanced Frequency Domain Decomposition (EFDD) and Data Driven Sub-Space Identification (SSI-DATA) are developed for modal identification methods.

(iii) The aforementioned operational modal analysis approaches are applied to ambient vibration test data from the North Footbridge of EDP building. In these applications, comparisons of the estimated modal parameters and FEM modal analysis results.

(iv) End use of ambient vibration modal estimation for FEM updating, applied to the North footbridge of EDP building.

(v) Recommendations for efficient tuning of TMDs based on the observations of the case study. It includes the ranges of mass ratio, frequency ratio and damping ratio of TMDs.

1.3 Organization and Structure of the Thesis

A chapter-by-chapter overview is presented in the following and inherent logic relations of them are manifested.

Chapter 1 introduces the investigation background and motivations, highlights the main work, as well as the organization of the thesis.

Chapter 2 begins with the classical dynamic vibration equations and transforms the structural vibration to modal model defined in system identification. Different parametric and non-parametric system identification approaches in both frequency and time domains are presented.

Chapter 3 presents pedestrian traffic as a source of excitation and explores the reliable modelling of pedestrian traffic for various levels of traffic using a periodic function. It considers loading models for walking and jumping in space dimensions.

Chapter 4 describes the philosophy behind TMDs, developing the dynamic equation of motion for an ideal two degree freedom system (structure modelled as single degree of freedom) by considering damped and undamped structure cases. Moreover, optimization criteria are set using H_∞ and H_2 approaches, and comparison of MATLAB programmed Min-max optimization and Den Hartog optimization criteria are compared to have confidence on the programmed outcomes.

Apart from that, TMDs design guidelines and definition of serviceability criteria for maximum of acceleration levels under pedestrian traffic are mentioned.

Chapter 5 is focused on the practical application of OMA modal identification algorithms implementation on the footbridge under study (North Footbridge of EDP's building, Lisbon). Data acquisition practice and methodology along with signal pre-processing tasks are also presented.

In this chapter, modal properties evaluation without TMDs installed is described in the first subsection and the same subject with TMDs installed is discussed in the second subsection. It explores the details of EFDD developed in MATLAB along with ARTeMIS outcomes. It also discusses the end of use of OMA in FEM updating applied to the footbridge and effective tuning of TMDs in setting TMD parameters in the case study is also discussed.

Chapter 6 ends the thesis with some conclusions and future works for further investigations relevant in the field of time domain OMA, vibration-based Structural Health Monitoring (SHM) and active control using TMDs, which would be the next task to be investigated if it were not for time-limit and scope.

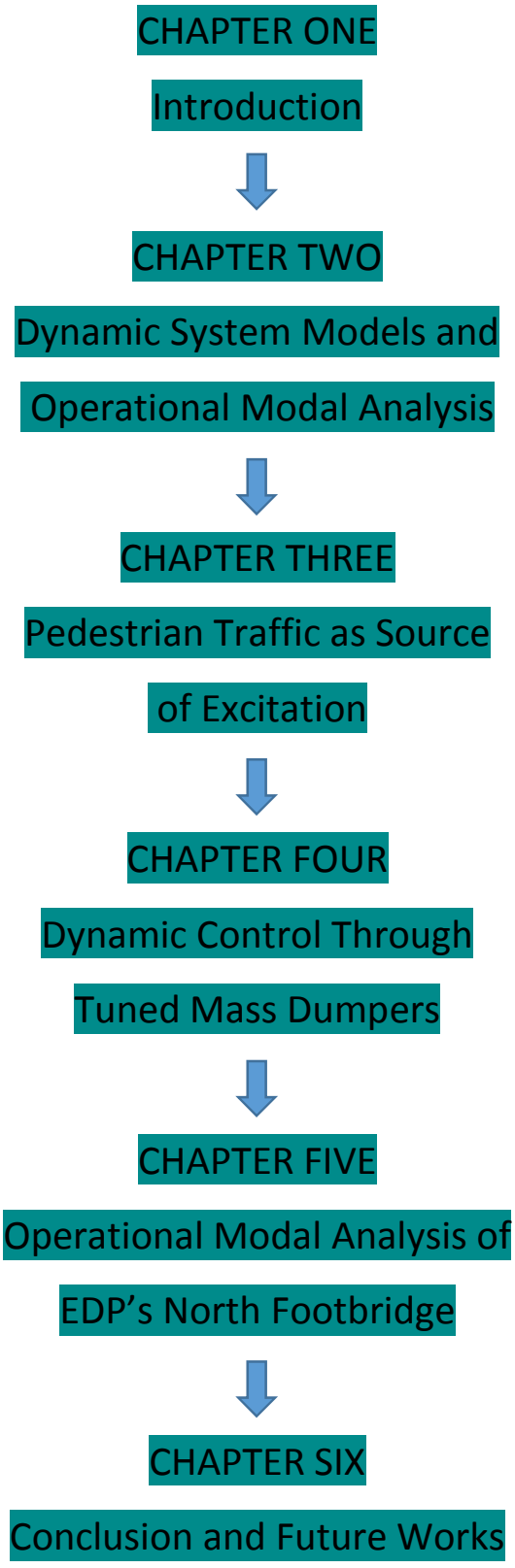

Figure 1.2-Organization of the thesis

2

MODELS OF DYNAMIC SYSTEMS AND OPERATIONAL MODAL ANALYSIS

2.1 Introduction

Operational modal analysis (OMA), rooting from classical experimental modal analysis (EMA) in mechanical engineering and time series analysis (TSA) in systems control engineering, has drawn great attention in the civil engineering community during the past two decades with applications in bridges, buildings, towers, etc. (Cunha et al, 2006,2007).

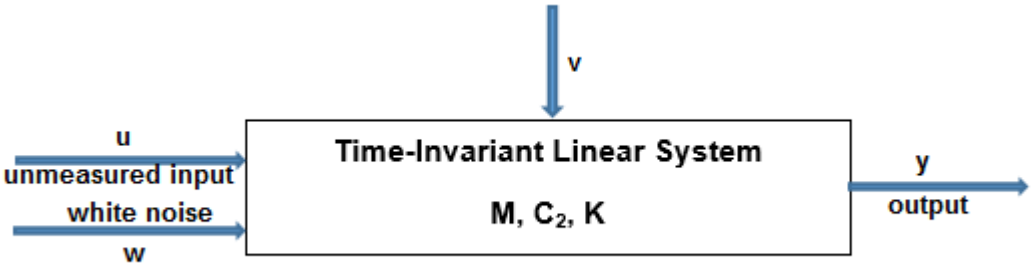

Figure2.1-A system with output y; the input, comprising a determined input u and measured disturbance w, is assumed as white noise; v is an unmeasured disturbance

OMA is also called as output-only '*system identification*'. A *system* is an object in which different kinds of variables interact and produce observable signals, illustrated by Figure. 2.1. The observable signals (*y*) that are of interest to use are usually called *outputs*. The *system* is also affected by external stimuli. External signals that can be manipulated by the observer are defined as determined inputs (*u*). Others are called *disturbances* and can be divided into those that are directly measured (*w*) and those that are only observed through their influence on the output (*v*). The distinctions between inputs (*u*) and measured or unmeasured disturbances (*w*, *v*) is often less important for the modelling process. The notion of a *system* is a broad concept. In this dissertation, a system is specified as a civil engineering structure. In OMA of civil engineering, the structures are naturally excited by ambient excitation forces e.g. wind, traffic, seismic activity, etc., which are difficult or even impossible to be measured. Elimination of this ambient excitation is often impossible and applying an artificial measurable force which exceeds the natural excitation is expensive and sometimes impractical. In these cases, only structural responses (*y*) are measured. The basic assumptions of OMA are:

- The output response is a realization of a stochastic process and the unmeasured input is a white noise. In this case, problems may arise as the structure tested go astray from this assumption; for example, cases where the excitation force is a combination of white noise and harmonic forces. Harmonic excitations can occur due to components like unbalanced rotors or fluctuating forces in electric actuators. The usual way to compute modal parameters in the presence of harmonic excitations is to treat harmonically excited frequencies to be virtual Eigen frequencies of the structure. However, if the frequency of the harmonic input is close to an Eigen frequency of the system, operational modal analysis procedures fail to identify the modal parameters properly. This is not a common problem in civil engineering structures as we deal with structures exposed to stochastic random processes as white noise due to wind, traffic, earth quake etc.
- System should be Linear Time-invariant, which requires the system to remain unchanged over the testing period of time. Again, this could be less problematic as in case of civil engineering elements, but it may pose problems as in case of mechanical parts, namely wind turbine modal analysis.

OMA directly evolved from traditional EMA, which can be regarded as a classical input-output approach, where the extraction of modal parameters is based on frequency response functions (FRFs), derived in frequency domain, or on the equivalent impulse response functions (IRFs), in time domain, using input-output measurements. Moving from one domain to the other is a matter of applying Fourier Transform. There are many technical publications on input-output modal identification (EMA) developed in last three decades. These methods are generally classified as frequency domain or time domain approaches. The frequency domain methods, based on the measurement of FRFs, comprise the simple 'peak-picking' (PP) or 'peak-amplitude' technique, the complex mode indicator function (CMIF) method (Shih et al, 1988) and the polyreference least squares complex frequency (P-LSCF) procedure (Guillaume et al, 2003). In parallel, the IRFs in time domain are normally calculated from the FRFs by an inverse Fourier transform, which leads to time domain methods comprehending the least-squares complex exponential (LSCE) method (Brown, 1979), the polyreference complex exponential (PRCE) method (Vold et al, 1982), the multiple reference Ibrahim time domain (MRITD) technique (Fukuzono, 1986) and the eigensystem realization algorithm (ERA) procedure (Juang and Pappa, 1985; Longman and Jung, 1989). In 1998, the unified matrix polynomial approach (UMPA) was proposed (Allemang et al, 1998). It demonstrates that most of the abovementioned techniques, both in the frequency and time domains, are particular cases of a more general polynomial formulation, and this helps to clarify the similarities among the various methods. More Comprehensive and detailed discussion of these methods can be found in (Heylen et al, 1995; Maia et al, 1997; Ewins, 2000). [According to Wei-Hua Hu, PhD dissertation presented at the University of Porto]

In early 1990s, the Natural Excitation Technique (NExT) was proposed (James, 1992). It is a significant breakthrough for modal identification, because only output measurements in the case of natural excitation are used for modal parameters estimation. The underlying principle of the NExT technique is that correlation functions (COR) between the responses can be expressed as a sum of decaying sinusoids. Each decaying

sinusoid has a damped natural frequency and damping ratio that is identical to the one of the corresponding structural mode. Therefore, CORs can be employed as IRFs to estimate modal parameters, which means that a modal identification procedure from traditional EMA can be further adopted for OMA. For example, in time domain, by replacing IRFs with CORs, ERA methods can be developed to NExT-ERA technique (Akaike, 1974; Benveniste and Funche, 1985; Aoki, 1987). This method is also named as Covariance driven Stochastic Subspace Identification (SSI-COV) method (Peeters, 2000). Similarly, in frequency domain, output spectra can be modeled in a similar way as FRFs under the assumption that the input is white noise. By replacing the FRFs matrix with the output spectral matrix, the traditional CMIF method and p-LSCF procedure evolved to frequency domain decomposition (FDD) method (Brincker et al, 2000,2001) and Polyreference Least Squares Complex Frequency techniques (PolyMAX®, Peeters, 2004,2005), respectively. Apart from EMA in mechanical engineering, OMA in civil engineering also root in TSA in control engineering because TSA methods model dynamic systems directly from output measurements, such as the auto-regressive moving average (ARMA) time series model and stochastic state-space (SS) model. It is demonstrated that the ARMA model is equivalent to the stochastic state-space model (Akaike, 1974; Basseville, 1985), however, the identification technique of stochastic SS model is better than of ARMA model because no non-linear search is required and computational complexity is dramatically reduced. The most important techniques for identifying ARMA model is the prediction-error method (PEM) (Ljung, 1999). By minimizing the prediction errors, the modal parameters identification is a nonlinear optimization problem, which makes ARMA model identification rather difficult to apply, especially for large dimension structures. Despite this drawback, efforts have been still made to apply PEM to identify modal parameters in civil engineering (Andersen, 1997). In the 1990´s, stochastic subspace identification (SSI) technique was developed in control engineering (Van Overschee, 1996). It starts by projecting the row space of the 'future' outputs into the row space of 'past' outputs, factorization of the projecting matrix leading to Kalman filter state sequence, which can be utilized to estimate system matrix by least square (LS) techniques. The identification procedure avoids non-linear iteration and is numerically reliable and effective. SSI has been adopted successfully for OMA in civil engineering (Peeters, 2000). Because of using the stochastic response data to identify modal parameters directly, it is also named Data driven Stochastic Subspace Identification (SSI-DATA).

In order to carry out OMA, one requires the consideration of three basic entities:

(1) A set of measured output responses (Acceleration, typical, velocity or displacement),

(2) Candidate models both in time and frequency domain and

(3) Algorithms for the identification of the candidate models using the output measured data.

In OMA testing, the only available information about the dynamic behavior of a structure is the output measurements. Different identification methods based on mathematical models in OMA are capable to provide accurate estimates of the modal parameters of the structure from output response. However, it is

necessary to obtain some kind of comprehension of how all kinds of models, both in frequency domain and time domain, relate to the modal parameters, that is, how they relate to the lumped mass-spring parameter model in structural analysis and how modal parameters can be identified by these models. The main purpose of this chapter is to provide such understanding. Therefore, this chapter starts with the description of the simple multi-degree-of freedom vibration model, subsequently, the analytical models are converted to frequency domain models and time domain state-space models followed by estimation algorithms.

2.2 Multi-degree-of-freedom systems

The dynamics of a mechanical system can be often idealized by discretizing in n_m masses connected by springs and dampers (DOFs), the corresponding motion being described by the following matrix differential equation of motion containing inertial, damping and restitution forces,

$$M\ddot{q}(\mathrm{t}) + C_2\dot{q}(t) + Kq(t) = \mathrm{f}(\mathrm{t}) = B_l u(t) \tag{2.1}$$

Where $M,\ C_{2,,}\ K \in \mathbb{R}^{n_m \times n_m}$ are the mass, damping and stiffness matrices; $q(\ddot{t}),\ \dot{q}(t), q(t) \in \mathbb{R}^{n_m}$ are displacement, velocity and acceleration vectors at continuous time, t, respectively; $\mathrm{f}(\mathrm{t}) \in \mathbb{R}^{n_m}$ is the excitation force vector, which can be factorized into a matrix $B_l \in \mathbb{R}^{n_m}$ specifying the locations of inputs and an input vector $u(t) \in \mathbb{R}^{n_m}$. In a practical modal experiment, output measurements are only a set of responses measured from well selected points, and not all n_m DOFs are described in FE model.

It is assumed that measurements are acquired at l points. In general case, the response can be measured using accelerometers, which is used for the case study in this dissertation, velocity or displacement transducers. In that case the observation equation y(t) is expressed as

$$\mathrm{y}(\mathrm{t}) = C_a\ddot{\mathrm{q}}(\mathrm{t}) + C_{\mathrm{v}}\dot{q}(t) + C_d q(t) \tag{2.2}$$

Where $\mathrm{y}(\mathrm{t}) \in \mathbb{R}^l$ are the outputs and $C_a, C_{\mathrm{v}}, C_d \in \mathbb{R}^{l \times n_m}$ are the selection matrices for the accelerations, velocities and displacements. These matrices contain only zeros and a few ones, indicating which output is measured as an acceleration, velocity or displacement. For example, if only accelerometers are used, $C_a = I, C_{\mathrm{v}} = 0\ and\ C_d = 0$.

In structural analysis, e.g. finite element (FE) analysis, the structure is discretized in a set of elements. The global mass matrix M and stiffness matrix K are obtained directly from the geometry and material properties. However, it is impossible to assemble the damping matrix C_2 in the same way as M and K due to lack of reliable material constants representing the global damping behavior of structure. Damping matrix C_2 can be modelled as symmetry and ordinary form: proportional damping and general viscous damping.

2.2.1 Undamped free vibration systems

Assuming the free vibration of an undamped system, equation 2.1 is transformed by ignoring the damping matrix C_2 and the external excitation $f(t)$ being null,

$$M\ddot{q}(t) + Kq(t) = 0 \tag{2.3}$$

Substituting the general solution to equation of motion $q(t) = \phi_i e^{\lambda_i t}$ in equation (2.3) leads to

$$K\phi_i = M\phi_i(-\lambda_i{}^2) \tag{2.4}$$

Where $\phi_i \in \mathbb{R}^{n_m}(\, i = 1,2,3 \ldots n_m\,)$ is an eigenvector and $\lambda_i{}^2$ is an eigenvalue. In an undamped vibration system, an eigenvalue is usually denoted as the square of an undamped natural frequency ω, that is:

$$\lambda_i = i\omega \tag{2.5}$$

Equation (2.4) can be rewritten using equation (2.5) in the following complete solution as

$$\boldsymbol{K\Phi} = \boldsymbol{M\Phi\Omega^2} \tag{2.6}$$

Where $\boldsymbol{\Phi} = [\, \boldsymbol{\Phi_1, \Phi_2, \Phi_3}, \ldots\ldots \boldsymbol{\Phi_{n_m}}] \in \mathbb{R}^{n_m \times n_m}$ is an eigen vector matrix of n_m degrees of freedom and n_m modes, and $\boldsymbol{\Omega} = [\ddots\ \boldsymbol{\omega_{i}}\ddots] \in \mathbb{R}^{n_m \times n_m}$ is a diagonal Eigen-frequency matrix. According to orthogonality conditions;

$$\boldsymbol{\Phi^T M\,\Phi} = [\ddots\ \boldsymbol{m_{i}}\ddots]\,\boldsymbol{,\ \Phi^T K\Phi} = [\ddots\ \boldsymbol{k_{i}}\ddots] \tag{2.7}$$

From which

$$\boldsymbol{\omega^2{}_i = k_i/m_i}$$

Where m_i and $k_i$are the modal mass and modal stiffness, respectively. The index '*T*' denotes transpose of a matrix.

It is important to realize that the eigenvalue matrix Ω is unique, because eigen frequencies are fixed quantities, while the eigenvector matrix Φ is subject to indeterminate scaling factors, which affect the amplitude of the eigenvectors ϕ_i.There are many scaling and normalization processes of Φ, the most common being mass-normalization. The mass-normalized eigenvector matrix is written as $[\Phi]_{nor}$ and has the particular property

$$\boldsymbol{\Phi^T{}_{nor} M \Phi_{nor} = I_{n_m},\ \Phi^T{}_{nor} K \Phi_{nor} = \Omega^2} \tag{2.8}$$

Where $\boldsymbol{I_{n_m}}$ is an identity matrix of dimension of $n_m \times n_m$

Matrices Φ and Ω describe the dynamic characteristics of the dynamic system. Hence, they constitute the modal model. Eigenvector ϕ_i is the *i*-th *mode shape* corresponding to the *i*-th undamped natural frequency ω_i. It is to be noted that in the undamped case the eigenvectors are real modal vectors.

Example

A metallic frame, shown in Figure 2.2, made of aluminum and Iron bars is idealized as a 3 degree of freedom undamped vibration model. In the current analysis, the density and modulus of elasticity of both aluminum and iron are evaluated as $\rho_A = 2.7 \times \frac{10^{3kg}}{m^3}$, $E_A = 65Gpa$ and $\rho_I = 7.7\frac{10^{3kg}}{m^3}$, $E_I = 210Gpa$, respectively. The total mass of each level, including the iron mass, the mass of each half part of support columns and the mass of connection elements, is calculated as $m_1 = m_2 = 67.15kg$ and $m_3 = 28.13kg$ .The stiffness provided by aluminum columns are 167.2kN/m, 167.2kN/m and 83.6kN/m. The mass and stiffness matrices have the following expression:

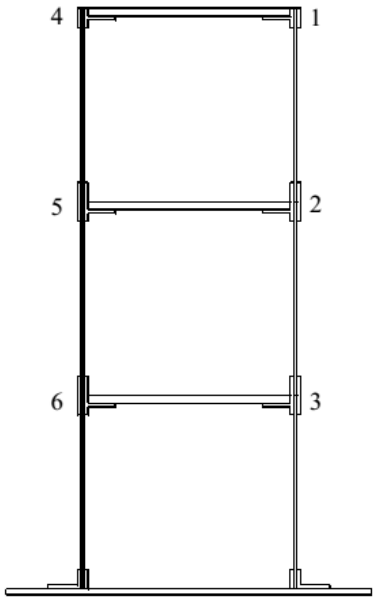

$$\boldsymbol{M} = \begin{bmatrix} \mathbf{15.67} & \mathbf{0} & \mathbf{0} \\ \mathbf{0} & \mathbf{15.67} & \mathbf{0} \\ \mathbf{0} & \mathbf{0} & \mathbf{13.28} \end{bmatrix} \boldsymbol{Kg}$$

$$\boldsymbol{K} = \begin{bmatrix} \mathbf{167.2} & \mathbf{-83.6} & \mathbf{0} \\ \mathbf{-83.6} & \mathbf{167.2} & \mathbf{-83.6} \\ \mathbf{0} & \mathbf{0-83.6} & \mathbf{83.6} \end{bmatrix} \boldsymbol{KN/m}$$

Figure 2.2- Metallic Frame [Lab model in FEUP, Porto]

According to equation (2.6), the Eigen frequency matrix Ω and the eigenvector matrix Φ are evaluated. The modal results are shown in Figure 2.3.

.

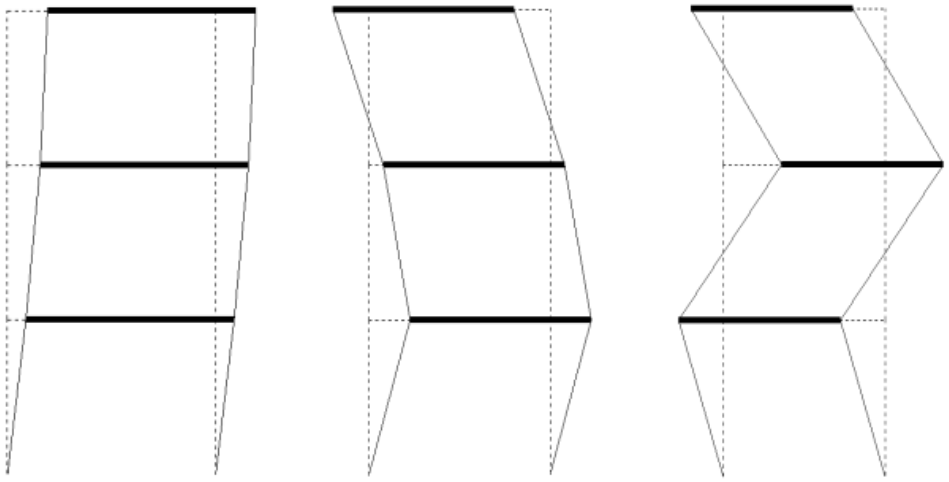

Figure 2.3-Natural Frequency and Modal shapes

2.2.2 Rayleigh or proportional damping systems

In a more general case of free vibration of a damped system, it is necessary to introduce some assumptions concerning the damping characters. Usually the damping is assumed as proportional, which means that the damping matrix C_2 is assumed as a linear combination of the mass and stiffness matrices, which is also called Rayleigh damping(α and β can estimated by considering a damping coefficient for the structure).

$$C_2 = \alpha M + \beta K \tag{2.9}$$

Where α, β are two scalar constants, then the equation of motion can be written in the form by pre-multiplying by ϕ^T and post multiplying M by $\phi\phi^{-1} = I$,

$$\phi^T M \phi \phi^{-1} \ddot{q}(\mathrm{t}) + \phi^T C_2 \phi \phi^{-1} \dot{q}(t) + \phi^T K \phi \phi^{-1} q(t) = \mathrm{f(t)} = 0 \tag{2.10}$$

And it can be re-arranged as

$$\phi^T M \phi \ddot{q}_p(\mathrm{t}) + \phi^T C_2 \phi \dot{q}_p(t) + \phi^T K q_p(t) = 0 \tag{2.11}$$

Where $\phi^{-1} q(t) = q_p(t)$ is a coordinate transformation. Assuming damping is small, it is acceptable to neglect the off diagonal elements in C_2 and it can be diagonal zed as

$$\boldsymbol{\Phi^T C_2 \Phi} = [\ddots \boldsymbol{c_i} \ddots] = [\ddots \boldsymbol{2\xi_i \omega_i m_i} \ddots] \tag{2.12}$$

Where $\boldsymbol{\xi_i = c_i / 2\omega_i m_i}$ is the modal damping ratio.

The solution of equation (2.11) with proportional damping has a form similar to the one of an undamped model solution $q(t) = \phi_{pi} e^{\lambda_i t}$ substituting this solution and equation (2.12) into equation (2.11) leads to a series of independent equations (decoupling of the equation of motion).

$$\lambda^2{}_i + 2\xi_i\omega_i\lambda_i + \omega^2{}_i = 0 \tag{2.13}$$

Up on solving equation (2.13),

$$\lambda_i, \lambda^*{}_i = -\xi_i\omega_i \pm j\sqrt{1-\xi^2{}_i}\ \omega_i \tag{2.14}$$

Where super index '*' denotes complex conjugate.

The particular advantage of using a proportional damping model in structural analysis is that the mode shapes are identical and the natural frequencies are similar to those of the simple undamped system. In fact, it is possible to derive the modal property of a proportional damping system by analyzing the undamped version and making a correction for the presence of the damping. However, it should be noted that it is only valid under the assumption that damping is distributed over the structure in the same way as the mass and the stiffness, which does not happen in real structures with local dampers, e.g. footbridges with tuned mass damper (TMDs) which is the case in this project. In order to model the damping mechanisms more accurately, general viscous damping assumption is discussed in the next sub-section.

2.2.3 General viscous damping systems

In case of a vibration model with general viscous damping, the damping matrix C_2 cannot be diagonalized. In order to solve the eigenvalue problem, it is necessary to recast equation (2.1) into so-called *state-space form*, the second order equation being reformulated as a first order equation.

Define a *state vector* $x(t)$ of order n=2n_m, containing both the displacement vector $q(t)$ and the velocity vector $\dot{q}(t)$,

$$x(t) = \begin{bmatrix} q(t) \\ \dot{q}(t) \end{bmatrix} \tag{2.15}$$

Assuming the solution $\mathrm{q(t)} = \phi_{\mathrm{gi}}\mathrm{e}^{\lambda_i \mathrm{t}}$,

$$x(t) = \begin{bmatrix} q(t) \\ \dot{q}(t) \end{bmatrix} = \begin{bmatrix} \phi_{\mathrm{gi}} \\ \lambda_i\phi_{\mathrm{gi}} \end{bmatrix}\mathrm{e}^{\lambda_i \mathrm{t}} = \varphi_i\mathrm{e}^{\lambda_i \mathrm{t}},\ \dot{x}(t) = \begin{bmatrix} \dot{q}(t) \\ \ddot{q}(t) \end{bmatrix} = \begin{bmatrix} \lambda_i\phi_{\mathrm{gi}} \\ \lambda^2{}_i\phi_{\mathrm{gi}} \end{bmatrix}\mathrm{e}^{\lambda_i \mathrm{t}} = \lambda_i\varphi_i\mathrm{e}^{\lambda_i \mathrm{t}} \tag{2.16}$$

Equation (2.1) can be then rewritten in state-space form as

$$P\dot{x}(t) + Qx(t) = F \tag{2.17}$$

Where:

$$P = \begin{bmatrix} C_2 & M \\ M & 0 \end{bmatrix},\ Q = \begin{bmatrix} K & 0 \\ 0 & -M \end{bmatrix},\ x(t)\begin{bmatrix} \phi_{\mathrm{gi}} \\ \lambda_i\phi_{\mathrm{gi}} \end{bmatrix}\mathrm{e}^{\lambda_i \mathrm{t}},\ F = \begin{pmatrix} B_l \\ 0 \end{pmatrix} u(t)$$

Substituting equation (2.16) in equation (2.17), this leads to a generalized eigen problem when *f*(*t*)=0,

$$P\Lambda_{com}\Psi + Q\Lambda_{com} = 0 \tag{2.18}$$

Whose solution comprises a set of n=2n_m eigenvalues, appearing in complex conjugate pairs.

Denoting the eigenvalues as $\Lambda \in \mathbb{C}^{n_m \times n_m}$ and the conjugate pairs as $\Lambda^* \in \mathbb{C}^{n_m \times n_m}$ the corresponding complex eigenvectors are,

$$\varphi = \begin{bmatrix} \Phi \\ \Phi\Lambda \end{bmatrix},\ \varphi^* = \begin{bmatrix} \Phi^* \\ \Phi^*\Lambda^* \end{bmatrix} \tag{2.19}$$

Λ_{com} and Ψ have the following structure

$$\Lambda_{\mathrm{com}} = \begin{bmatrix} \Lambda & 0 \\ 0 & \Lambda^* \end{bmatrix} = \begin{bmatrix} \ddots\ \lambda_i\ \ddots & 0 \\ 0 & \ddots\ {\lambda_i}^*\ \ddots \end{bmatrix},\ \Psi = [\varphi \quad \varphi^*] = \begin{bmatrix} \Phi & \Phi^* \\ \Phi\Lambda & \Phi^*\Lambda^* \end{bmatrix} \tag{2.20}$$

Where Λ and $\Phi \in \mathbb{C}^{n_m \times n_m}$ are the eigenvalues and eigenvectors of the original second order system. Substituting Λ_{com} and Ψ into equation (2.18) and it becomes

$$M\Lambda^2\Phi + \mathrm{C}_2\Lambda\Phi + \mathrm{K}\Phi = 0 \tag{2.21}$$

It is noted that eigen vectors matrix Φ can not diagonalize the matrices $M,\ C_2\ and\ K$ as happen when proportional damping is assumed. However, complex eigenvalues of equation (2.20), λ_i, are written as those analogous to proportional damping system

$$\lambda_i, {\lambda^*}_i = -\xi_i\omega_i \pm j\sqrt{1 - {\xi^2}_i}\ \omega_i \tag{2.22}$$

Pre-multiplying equation (2.17) by the eigenvector matrix Ψ^T, it is found that

$$\Psi^T P\Psi\dot{q}_{mc}(t) + \Psi^T Q\Psi q_{mc}(t) = 0$$

Where $q_{mc}(t) = \Psi^{-1}x(t)$ is the modal coordinate transformation. According to orthogonality conditions, matrices *P* and *Q* are diagonalized,

$$\Psi^T P\Psi = [\ddots\ a_i\ \ddots], \Psi^T Q\Psi = [\ddots\ b_i\ \ddots] \tag{2.23}$$

Where $[\ddots\ a_i\ \ddots]$and $[\ddots\ b_i\ \ddots]$are modal *a* matrix and modal *b* matrix, respectively.
Substituting (2.23) in (2.17),

$$\Lambda_{\mathrm{com}} = [\ddots\ \lambda_i\ \ddots] = -\left[\ddots\ {b_i}/{a_i}\ \ddots\right] \tag{2.24}$$

2.3 Finite Element Modelling (FEM)

The dynamic behavior of complex structures is generally analyzed by means of the Finite Element Method (FEM), which leads to an eigenvalue problem that is solved in terms of modal parameters (natural frequencies, modal damping ratios and mode shapes).The limitation of the FEM lies in the increase of model size required to properly describe complex structures with sufficient detail, which leads to high model construction and calculation times. More important restriction is inherent inaccuracy in modelling including model structure, parameter and order errors. To address these limitations, an experimental approach to modal analysis was developed to yield results which can be either as a model, or to validate and improve the FEM (Frisell and Mottershead, 1995). The resulting EMA and OMA approach have become a standard element of the mechanical product design and engineering process. In this project FE model is updated using ambient vibration estimates which will be presented in the subsequent chapters. Through this validation and updating of FEM results, actual tuning conditions of TMDs in the footbridge and vibration level checks under pedestrian traffic is performed. Detailed discussion is presented in chapter 5.

2.4 Frequency Domain Models

A standard OMA procedure consists of three basic stages: (1) performing ambient vibration tests under operational conditions and collection of output responses; (2) Consideration of a set of candidate models; (3) Application of algorithms in model fitting using the output data. The candidate models in OMA can be classified based on the domain in which the data is treated resulting in 'frequency domain models' and 'time domain models'. In time domain, the output responses can be used directly to build the model, while in frequency domain models it is necessary to perform a spectrum analysis by Fourier transform. In this section, the frequency models and corresponding algorithms will be introduced.

2.4.1 Laplace transform and transfer function

Laplace transform converts differential equations to algebraic ones, which are easier to manipulate. The one-sided Laplace transform of a function $x(t)$, denoted as $X(s)$, is defined as:

$$X(s) = L[x(t)] = \int_0^\infty x(t)e^{-st}dt \tag{2.25}$$

Where s is a complex quantity known as the Laplace variable. According to important property of the Laplace transform,

$$L[\dot{x}(t)] = sX(s) - x(0) \tag{2.26}$$

Applying the Laplace transform to equation (2.1) leads to:

$$L[M\ddot{q}(\mathrm{t}) + C_2\dot{q}(t) + Kq(t)] = \mathrm{M}[\mathrm{s}^2\mathrm{X}(\mathrm{s}) - \mathrm{s}x(0) - \dot{x}(0)] + C_2[sX(s) - x(0)] + K[X(s)]$$

$$=(\mathrm{Ms}^2 + C_2 s + K)\,\mathrm{X(s)} - Msx(0) - M\dot{x}(0) - C_2 x(0) \tag{2.27}$$

And

$$L[f(t)] = f(s) \tag{2.28}$$

If the initial displacement and velocity are equal to zero $(x(0) = and\ \dot{x}(0) = 0)$, equations 2.27 and 2.28 can be expressed as the ratio of the transformed response to the transformed excitation:

$$H(s) = \frac{Q(s)}{F(s)} = \frac{1}{\mathrm{Ms}^2 + C_2 s + Ks} = \frac{1}{Z(s)} = Z^{-1}(s) \tag{2.29}$$

Where $Z(s)$ is the dynamic stiffness as opposed to flexibility.

The denominator of equation (2.29), $\mathrm{Ms}^2 + C_2 s + Ks$, is identical to equation (2.21) yielding roots s_i expressed as Λ. Substituting s_i and the modal coordinates $q_{mc}(t) = \Psi^{-1} x(t)$ in equation (2.17), and pre-multiplying by Ψ^{T},

$$(s_i \Psi^{T} P \Psi + \Psi^{T} Q \Psi) q_{mc}(t) = \Psi^{T} F \tag{2.30}$$

According to orthogonality conditions shown in equations (2.23) and (2.24), it leads to

$$q_{mc}(t) = (s_i[\because a \because] - [\because a \because]\Lambda_{com})^{-1} \Psi^{T} F \tag{2.31}$$

Introducing $\Lambda_{\mathrm{com}} = \begin{bmatrix} \Lambda & 0 \\ 0 & \Lambda^* \end{bmatrix} = \begin{bmatrix} \because \lambda_i \because & 0 \\ 0 & \because \lambda_i^* \because \end{bmatrix}$, $\mathrm{V}_d = [\Phi \quad \Phi^*]$, $\Psi = \begin{bmatrix} \mathrm{V}_d \\ \mathrm{V}_d \Lambda_{com} \end{bmatrix}$ and considering $q_{mc}(t)$ in (2.31) equation (2.15) becomes

$$x(t) = \begin{bmatrix} q(t) \\ \lambda_i q(t) \end{bmatrix} = \Psi q_{mc}(t) = \begin{bmatrix} \mathrm{V}_d \\ \mathrm{V}_d \Lambda_{com} \end{bmatrix} (s_i[\because a \because] - [\because a \because]\Lambda_{com})^{-1} \begin{bmatrix} \mathrm{V}_d \\ \mathrm{V}_d \Lambda_{com} \end{bmatrix}^{T} \begin{pmatrix} f(t) \\ 0 \end{pmatrix} \tag{2.32}$$

The upper part of equation (2.32) is:

$$q(t) = [\mathrm{V}_d](s_i[\because a \because] - [\because a \because]\Lambda_{com})^{-1} [\mathrm{V}_d]^{T} \mathrm{f(t)} \tag{2.33}$$

Applying the Laplace transform to equation (2.33) yield

$$Q(s) = [\mathrm{V}_d](s[\because a \because] - [\because a \because]\Lambda_{com})^{-1} [\mathrm{V}_d]^{T} \mathrm{F(s)} \tag{2.34}$$

Then, transform function $H(s)$ in Partial Fraction Expansion (PFE) is obtained:

$$H(s) = \frac{Q(s)}{F(s)} = [\mathrm{V}_d](s[\because a \because] - [\because a \because]\Lambda_{com})^{-1} = \sum_{i=1}^{n_m} \left(\frac{1}{a_i} \frac{\Phi_i \Phi^{T}{}_i}{s - \lambda_i} + \frac{1}{a^*{}_i} \frac{\Phi^*{}_i \Phi^{H}{}_i}{s - \lambda^*{}_i}\right)$$

$$= \sum_{i=1}^{n_m} \left(\frac{\Phi_i \gamma^{T}{}_i}{s - \lambda_i} + \frac{\Phi^*{}_i \gamma^{H}{}_i}{s - \lambda^*{}_i}\right)$$

$$= \sum_{i=1}^{n_m} \left(\frac{R_{ri}}{s-\lambda_i} + \frac{R^*_{ri}}{s-\lambda^*_i}\right) \quad (2.35)$$

The transform function $H(s)$ is described as a sum of modal contributions, which is called *modal decomposition*. In classical modal analysis, λ_i, λ^*_i are named as system poles and coincide with equation (2.22):

$$\lambda_i, \lambda^*_i = -\xi_i \omega_i \pm j\sqrt{1-\xi^2_i}\ \omega_i \quad (2.36)$$

φi , γi and Rri are defined as *mode shape vector*, *mode participation vector* and *residue*, respectively. A so-called *'modal model'* is characterized by natural frequencies,$\omega_i i$, modal damping ratios ξi , mode shapes Φi and *mode participation factors* γi .

The equation (2.29) can also be expressed as:

$$H(s) = Z^{-1}(s) = \frac{Z_{adj}(s)}{|Z(s)|} \quad (2.37)$$

Where the numerator $Z_{adj}(s)$ is the adjoint matrix of ($n_m \times n_m$) dimension containing polynomials in s of order $2(n_m - 1)$ and the denominator is a polynomial in s of order $2n_m$. Therefore, equation (2.37) can also be written as (Verboven, 2002)

$$H(s) = \frac{B_{ri}(s)}{A_{ri}(s)} = \frac{\begin{bmatrix} B_{r(1,1)}(s) & \cdots & B_{r(1\times n_m)}(s) \\ \vdots & \ddots & \vdots \\ B_{r(n_m\times 1)}(s) & \cdots & B_{r(n_m\times n_m)}(s) \end{bmatrix}}{A_{ri}(s)} \quad (2.38)$$

Which is called a *common denominator model* or also *scalar matrix fraction description.* This expression can also be considered as a special case of multivariable transfer function models described using a Right Matrix Fraction Description (RMFD) (Kailath, 1980; Guillaume et al, 1996).

$$H(s) = B_{ri}(s)(A_{ri}(s))^{-1} \quad (2.39)$$

Based on this relation, the modal participation factor can be estimated directly together with poles. Afterwards, the mode shape can be estimated by linear least-squares frequency domain (LSFD) method.

2.4.2 Fourier Transform and Frequency Response Function (FRF)

If the complex Laplace variable *s* is restricted to purely imaginary value $s = j\omega$, where ω is any frequency of interest, the Laplace transform is converted into the Fourier transform:

$$X(s) = \boldsymbol{F}[x(t)] = \int_0^\infty x(t)e^{-j\omega t}dt \quad (2.40)$$

The FRF can be denoted replacing s by $j\omega$ in the transform function. It can be written in PFD, also in *modal decomposition* form

$$H(j\omega) = \sum_{i=1}^{n_m}\left(\frac{\mathrm{R}_{ri}}{s-\lambda_i} + \frac{\mathrm{R}^*_{ri}}{s-\lambda^*_i}\right) \tag{2.41}$$

And in RMFD

$$H(j\omega) = B_{ri}(s)(A_{ri}(s))^{-1} \tag{2.42}$$

The Fourier transform is a mathematical tool that converts a time signal into the frequency domain, and its great popularity in practical application stems from the efficient algorithm known as Fast Fourier Transform (FFT) (Cooley and Tukey, 1965).

2.4.3 Sampling, *z*-transform, Discrete Time Fourier Transform and Discrete Fourier Transform

In previous sections all equations are expressed in terms of infinite length in continuous time or frequency, but in experimental world observations of inputs and outputs are finite length in discrete time because of data-acquisition mode. In order to fit models to real measurements, it is then necessary to convert the above models to discrete time form. It is assumed that measurements are observed at the *sampling instants* $tk = k\Delta t\ , k = 0{,}1{,}2\ \ldots N-1\ \in \mathbb{N}$ where internal Δt is called *sampling interval*. Most often, *a zero-order hold* (ZOH) assumption is adopted, which means that the response, for example the displacement $q(t)$, is piecewise constant between the sampling instants i.e. step function,

$$q(t) = q_k, for\ k\Delta t \le t \le (k+1)\Delta t \tag{2.43}$$

Under ZOH, the equation of motion is converted as

$$M\ddot{q}_k + C_2\dot{q}_k + Kq_k = f_k \tag{2.44}$$

Where $\ddot{q}_k, \dot{q}_k, q_k\ and\ f_k$ are the sampled displacement, velocity, acceleration and force vectors respectively. The *z*-transform can be considered as a discrete equivalent of the Laplace transform. One-sided *z*-transform is defined as (0 to ∞)

$$X(z) = \mathbb{Z}[x_k] = \sum_{k=0}^{+\infty} x_k z^{-k} \tag{2.45}$$

Where $z\ \in \mathbb{C}$ is a scalar complex variable. An important property of the *z*-transform is

$$\mathbb{Z}[x_{k+1}] = \sum_{k=0}^{+\infty} x_{k+1} z^{-(k+1)} = z(X(z) - x_0) \tag{2.46}$$

Assuming that initial condition $x_0 = 0$, a forward shift in time domain corresponds to a multiplication by *z* in the *z*-domain,

$$\mathbb{Z}[x_{k+1}] = zX(z) = z\mathbb{Z}[x_k] \tag{2.47}$$

The Discrete-Time Fourier transform (DTFT) is the discrete equivalent of the Fourier transform shown in equation (2.40),

$$X(e^{-j\omega\Delta t}) = \boldsymbol{F}[x_k] = \sum_{k=0}^{+\infty} x_k e^{-j\omega k\Delta t} \tag{2.48}$$

Comparing equations (2.48) and (2.45), it is observed that the DTFT is a special case of *z*-transform when z is replaced by $z = e^{j\omega\Delta t}$, which is can be interpreted as the z-transform around the unit circle in the complex plane. In practical evaluation of the inputs and outputs during an experiment, only finite length sequences with *N* points are available. Thus, equation (2.48) may be paraphrased as

$$X(e^{-j\omega\Delta t}) = \boldsymbol{F}[x_k] = \sum_{k=0}^{N-1} x_k e^{-j\omega k\Delta t} \tag{2.49}$$

If *N* is a power of 2, above equation can be efficiently computed at uniformly-spaced discrete frequencies,

$$\omega = \frac{l_n}{N}\frac{2\pi}{\Delta t}, (l_n = 0,1,2 \ldots\ldots N-1) \tag{2.50}$$

across one period (2π), by using FFT recognized as Discrete Fourier Transform (DFT). By using DFT, a finite length discrete signal in time domain is converted into discrete frequency spectrum.

2.4.4 Spectrum and spectrum estimation

As input is unknown in OMA testing, power spectra is frequently used to identify the system model and extract modal parameters. In this section, spectrum analysis and practical aspects of spectrum estimation technique are introduced.

The power spectrum is defined as the Fourier transform of the autocorrelation function $R_s(t)$, if the signal can be treated as a stationary stochastic process, given by

$$S_S(j\omega) = \int_{-\infty}^{+\infty} R_S(t) e^{-j\omega t} dt \tag{2.51}$$

As mentioned in the very first, OMA assumes that the excitation (input) is a zero mean $\boldsymbol{E}[x(t)] = 0$, white noise sequence. The autocorrelation function can be written as

$$R_{xx}(\tau) = \boldsymbol{E}[x(t)x(t+\tau)] = R_{xx}\delta(\tau) \tag{2.52}$$

Where τ is the time lag, $R_{xx}(\tau) \in \mathbb{R}^{m\times m}$ is a constant matrix and $\delta(\tau)$ is the Dirac delta function. It can be defined as

$$\int_{-\infty}^{+\infty} f(t)\delta(t-a)dt = f(a) \tag{2.53}$$

For any function $f(t)$ which is continuous at time a considering the property of Dirac delta function, the power spectrum of unknown input is a constant matrix also called *'flat' spectrum matrix*,

$$S_x(j\omega) = \int_{-\infty}^{+\infty} R_S(t)e^{-j\omega t}dt = S_{con} \tag{2.54}$$

Again, return to real experimental world and recall that the output measurements. The measured output vector in l selected points is discretized as y_k, and thus output correlation matrices $R_r \in \mathbb{R}^{l\times l}$ are defined as

$$R_r = \boldsymbol{E}[y_{k+r}{y_k}^T] \tag{2.55}$$

Where r is an arbitrary time lag similar to τ in continuous time. If the measured output vector with N points is assumed as an ergodic random process $y_k, k = 0,1,2,\ldots..N-1 \in \mathbb{N}$, the correlation matrices are estimated as

$$\hat{R}_r = \frac{1}{N}\sum_{k=0}^{N-1} y_{k+r}{y_k}^T \tag{2.56}$$

The Full spectrum of a stochastic process is defined as the double sided *z*-transform of

$$S_{yy}(z) = \sum_{r=-\infty}^{r=+\infty} R_r z^{-r} \tag{2.57}$$

Using discrete autocorrelation function R_r property,

$${R_{-r}} = {R_r}^T \tag{2.58}$$

The spectrum in equation (2.57) can be rewritten as

$$S_{yy}(z) = {S^+}_{yy}(z) + ({S^+}_{yy}(z^{-1}))^T \tag{2.59}$$

Where

$${S^+}_{yy}(z) = {R_0}/{2} + \sum_{r=1}^{r=+\infty} R_r z^{-r} \tag{2.60}$$

The so-called *half spectrum*, having a positive time lag r, can be calculated by DTFT in equation (2.47) as

$$S_{yy}(e^{j\omega\Delta t}) = {R_0}/{2} + \sum_{r=1}^{r=+\infty} R_r z^{-j\omega r\Delta t} \tag{2.61}$$

In practical structure testing only a finite number of record length is available and so the spectrum indicated in equation (2.61) cannot be directly computed up to infinity. Consequently, the spectrum used in practice is estimated by finite sample sequence using DFT. The most popular spectrum estimation method may be *weighted averaged periodogram* (*modified Welch's periodogram*) (Welch, 1967) and *weighted correlogram* (Tukey and Blackman, 1958). The term *weighted* in these two methods means that a window function is applied to the signal (Hamming, Hann) to reduce leakage. The *averaged periodogram* operates directly on the output signal sequences, while the *correlogram* approach first estimates the correlations in time-domain and then the power spectra are obtained by transferring the correlations to the frequency-domain. The

weighted averaged periodogram method starts with dividing output sequences into L segments of M_s samples according to the number of sample points defined (by default welch uses M_s=8),

$$L \leq N/\,Ms \tag{2.62}$$

Each segment $y_{Ms}^{l}(m_s)$ are formed as

$$y_{Ms}^{l}(m_s) = y(m_s + (l-1)Ms) \begin{cases} 0 \leq m_s \leq Ms-1 \\ 1 \leq l \leq L \end{cases} \tag{2.63}$$

The L modified or windowed periodogram can be defined as

$$S_{yy^l}(e^{j\omega\Delta t}) = \frac{1}{\sum_{ms=0}^{Ms-1}\|win(m_s)\|^2}(\sum_{ms=0}^{Ms-1} win(m_s)y_{Ms}^{l}(m_s)e^{-j\omega m_s\Delta t})(\sum_{ms=0}^{Ms-1} win(m_s)y_{Ms}^{l}(m_s)e^{-j\omega m_s\Delta t})^T \tag{2.64}$$

Where *win* means window function (Hann, Hamming) to reduce leakage. If Ms is a power of 2, the spectrum of this segment is efficiently calculated by DFT at the discrete frequency points (desired for efficiency).

$$\omega = \frac{l}{M_s}\frac{2\pi}{\Delta t}, (l = 0,1,2 \ldots\ldots M_s - 1) \tag{2.65}$$

The spectrum estimation S_{yy} is computed by averaging all spectra based on L segments of sequence yk. The value of M_s can be changed until the desired accuracy is obtained in frequency resolution.

$$\hat{S}_{yy} = \frac{1}{L}\sum_{l=1}^{L} S_{yy^l}(e^{j\omega\Delta t}) \tag{2.66}$$

$\hat{S}_{yy}$ is the asymptotically unbiased estimate of the spectrum. Because the window function reduce the contributions of the data at the beginning and at the end of the record, introducing an overlap between the adjacent segments is advisable (usually 50% is the default, e.g. welch spectrum).

Another correlogram approach starts by estimating the correlation functions as indicated in equation (2.56). Then, the correlation functions are transferred to the frequency domain by taking the DFT to obtain the power spectrum. Note: averaged period gram will be adopted for reasons that will be discussed later.

$$\hat{S}_{yy} = \frac{1}{L}\sum_{r=-L}^{L} w_k \hat{R}_k(e^{-j\omega r\Delta t}) \tag{2.67}$$

In this section, the spectrum analysis and spectrum estimation techniques are introduced. The spectrum of stationary stochastic output is primary data in frequency domain OMA.

2.4.5 Model reduction

In real operational modal analysis, the ambient vibration experiment is always *band-limited*, which means that the signal only contains information over a certain frequency band. Only modes whose frequencies are within the bandwidth will show up in data and certain modes out of bandwidth are eliminated. This is called model reduction in operational modal analysis altered by the choice of Nyquist frequency of data.

Recall equation (2.41), the FRF can be rearranged with components within the bandwidth and parts out of the bandwidth as

$$H(j\omega) = \sum_{i=1}^{n_{re}} \left(\frac{\mathrm{R}_i}{j\omega - \lambda_i} + \frac{\mathrm{R}_i^*}{j\omega - \lambda^*_i} \right) + \sum_{i=1}^{n_m} \left(\frac{\mathrm{R}_i}{j\omega - \lambda_i} + \frac{\mathrm{R}_i^*}{j\omega - \lambda^*_i} \right) \tag{2.68}$$

Where n_{re} is the number of retained modes. In identification from experimental data, only modal parameters located in the test frequency range are estimated, while the contributions of out-of-band modes corresponding to the second part of the right hand side of equation (2.68) are neglected as

$$H(j\omega) = \sum_{i=1}^{n_{re}} \left(\frac{\mathrm{R}_i}{j\omega - \lambda_i} + \frac{\mathrm{R}_i^*}{j\omega - \lambda^*_i} \right) \tag{2.69}$$

The modal reduction is then a step closer to real experimental world.

2.4.6 Frequency domain models

a) *Half positive power spectra matrix*

In OMA, the relation between the constant input spectrum S_{con} and the output spectrum S_{yy} can be expressed as (Bendat and Piersol, 1980)

$$S_{yy}^{+}(j\omega) = H(j\omega) S_{con} H(j\omega)^H \tag{2.70}$$

Where $S_{yy}^{+}(j\omega) \in \mathbb{C}^{l \times l}$ and $S_{con} \in \mathbb{C}^{m \times m}$ are the power spectra matrices of the output and input measurements, and l, m are the number of output and input responses respectively. $H(j\omega) \in \mathbb{C}^{l \times m}$ is the frequency response function matrix. The superscript $(\,)^H$ denotes complex conjugate and transpose.

The equation (2.70) leads to a simple *non-parametric* frequency domain spectrum model derived from the FRF in PFE form, and a more complex *parametric* model based on FRF in RMFD format. In this paragraph, two models widely used in current frequency domain OMA are introduced. The purpose of OMA in frequency domain is to identify these models and extract modal parameters based on the output spectra matrix S_{yy}^{+}.

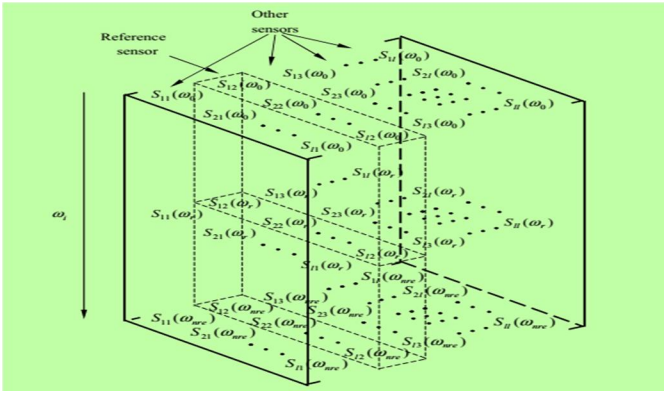

Figure 2.4-Schematic representation of spectra matrix [Wei-Hua Hu, FEUP, Porto]

Example

The half positive power spectra is a 3-dimension matrix consisting of auto and cross power spectra based on the experimental signals acquired in each setup. Considering the two vertical sensor's (tri-axial accelerometers) records used in each setup of the ambient vibration test of the North footbridge before final construction stage, the output spectrum S_{yy}^{+} can be written, according to Figure 2.4, as

$$S_{yy}^{+}(j\omega) = \sum_{i=0}^{n_{re}} \begin{bmatrix} S_{11}(\omega_i) & S_{12}(\omega_i) \\ S_{21}(\omega_i) & S_{22}(\omega_i) \end{bmatrix}$$

Where $\begin{bmatrix} S_{11}(\omega_i) & S_{12}(\omega_i) \\ S_{21}(\omega_i) & S_{22}(\omega_i) \end{bmatrix}$ refer a floor-matrix at discrete frequency points ω_i, $S_{11}(\omega_i)\ are\ S_{22}(\omega_i)$, are the auto power spectra calculated by experimental acceleration signals, while $S_{12}(\omega_i)\ and\ S_{21}(\omega_i)$ correspond to cross power spectra. Summation above indicates that the half positive power spectra $S_{yy}^{+}(j\omega)$ comprehends sub-matrix at all discrete frequency points $\omega_i\ (i = 0{,}1 \dots, n_{re})$.

b) Half positive power spectra model in PFD

Substituting the equation (2.69) into equation (2.70), the output spectra matrix evaluated at discrete frequency points as follows

$$S_{yy}(j\omega) = \sum_{i=0}^{n} \sum_{i=0}^{n} \left(\frac{\phi_i {\gamma_i}^T}{j\omega - \lambda_i} + \frac{{\phi_i}^* {\gamma_i}^H}{j\omega - {\lambda^*}_i} \right) S_{con} \left(\frac{\phi_s {\gamma_s}^T}{j\omega - \lambda_s} + \frac{{\phi_s}^* {\gamma_s}^H}{j\omega - {\lambda^*}_s} \right)^H \quad (2.71)$$

Multiplying the two partial fraction factors and making use of the *Heaviside partial fraction theorem*, the output spectra $S_{yy}\ (j\omega)$ can be converted to the partial fraction form (Hermans and Van der Auweraer, 1999; Peeters, 2000; Brincker, 2001)

$$S_{yy}(j\omega) = \sum_{i=1}^{n_r} \frac{\phi_i {g_i}^T}{j\omega - \lambda_i} + \frac{{\phi_i}^* {g_i}^H}{j\omega - {\lambda^*}_i} + \frac{g_i {\phi_i}^T}{-j\omega - \lambda_i} + \frac{{g_i}^* {\phi_i}^H}{-j\omega - {\lambda^*}_i} \quad (2.72)$$

Where $g_i \epsilon\ \mathbb{C}$ is the *operational reference vector* for mode *i*, which replaces the modal participation factors in cases where only output responses are available in OMA. The power spectra matrix derived above has a 4-quadrant symmetry because the OMA modal model contains, $\lambda_i, -\lambda_i,\ {\lambda^*}_i\ and - {\lambda^*}_i$ as poles, positive $(\lambda_i, {\lambda^*}_i)$ and negative $(-\lambda_i, -{\lambda^*}_i)$. The power spectra matrix S_{yy} modally decomposed into 4-quadrant symmetric terms, is called full power spectra matrix.

The counterpart of the full power spectra matrix S_{yy} in time domain is the correlation function matrix,

$$C_{yy}(\tau) = \sum_{i=1}^{n_r} (\phi_i {g_i}^T e^{\lambda_i \tau} + {\phi_i}^* {g_i}^H e^{{\lambda_i}^* \tau} - g_i {\phi_i}^T e^{-\lambda_i |\tau|} - {g_i}^* {\phi_i}^H e^{-{\lambda_i}^* |\tau|}) \quad (2.73)$$

In this equation, the first two terms, having positive poles, correspond to positive time lags, whereas the last two terms, with negative poles, correspond to the negative time lags. The full power spectra matrix is normally estimated by the spectrum estimation methods introduced in section 2.4.4. Because the power

spectra matrix is estimated from a limited amount of data in OMA, which are typically characterized by significant noise levels, a tradeoff must be made between stochastic uncertainties and bias errors introduced by leakage. The drawbacks caused by the spectrum estimation methods can be overcome by the unbiased estimation of correlation functions with only positive lags according to equation (2.54) (Hermans et al, 1998; Cauberghe, 2004). The first two terms in equation (2.73) are retained as

$$C_{yy}^{+}(\tau) = \sum_{i=1}^{n_r}(\phi_i {g_i}^T e^{\lambda_i \tau} + {\phi_i}^* {g_i}^H e^{{\lambda_i}^* \tau}) \tag{2.74}$$

Its counterpart in the frequency domain can be written as

$$S_{yy}^{+}(j\omega) = \sum_{i=1}^{n_r} \frac{\phi_i {g_i}^T}{j\omega - \lambda_i} + \frac{{\phi_i}^* {g_i}^H}{j\omega - {\lambda^*}_i} \tag{2.75}$$

The output spectra matrix with only positive poles is called *half positive power spectra* matrix. The first kind of frequency model begins from some mathematical manipulation of equation (2.72) under the assumption of light damping. The term $\phi_i {g_i}^T$ in equation (2.72) is a function of the modal parameters and the constant power spectrum matrix of the unknown random input excitation.

$$\phi_i {g_i}^T = (\phi_i {\gamma_i}^T) S_{con} (\sum_{i=1}^{n_r} \frac{\phi_i {\gamma_i}^T}{j\omega - \lambda_s} + \frac{{\phi_i}^* {\gamma_i}^H}{j\omega - {\lambda^*}_s})^H \tag{2.76}$$

When λ_s approaches $\lambda_i = -\xi_i \omega_i \pm j\sqrt{1-{\xi^2}_i}\ \omega_i$, the contribution of the *i-th* mode is given by

$$\phi_i {g_i}^T = \frac{(\phi_i {\gamma_i}^T) S_{con} (\phi_i {\gamma_i}^T)^H}{2\xi_i \omega_i} \tag{2.77}$$

If damping ratio is low, $\phi_i {g_i}^T$ becomes proportional to the mode shape as

$$\phi_i {g_i}^T \propto (\phi_i {\gamma_i}^T) S_{con} (\phi_i {\gamma_i}^T)^H = d_i \phi_i {\phi_i}^T \tag{2.78}$$

Where d_i is a scalar constant.

Around a certain frequency ω_i, only a limited number of modes contribute significantly and these modes are denoted as $Sub(\omega)$. Thus, the half positive power spectra matrix can be expressed in PFD form as

$$\underbrace{S_{yy}^{+}(j\omega)}_{\omega \to sub(\omega_i)} = \sum_{i \in sub(\omega)} \frac{d_i \phi_i {\phi_i}^T}{j\omega - \lambda_i} + \frac{d_i \phi_i {\phi_i}^H}{j\omega - {\lambda^*}_i} \tag{2.79}$$

According to this equation, a relation between the output spectrum, the system poles, $\lambda_i \; and \; {\lambda_i}^*$, and the mode shape ϕ_i is established, which leads to the identification algorithm of *peak-picking, frequency domain decomposition (FDD) and the enhanced frequency domain decomposition (EFDD).*

c) *Half positive power spectra model in RMFD* [According to Wei-Hua Hu, PhD dissertation, FEUP]

The frequency model described in equation (2.79) is only valid for a slightly damped structure. In order to estimate modal parameters of highly damped structures, another frequency model derived from RMFD shown in equation (2.42) is proposed (Peeters et al, 2004). It is observed that the half positive spectra matrix $S_{yy}^{+}(j\omega)$ is similar to the $H(j\omega)$ and they are parameterized in the same way. Therefore, the left side of equation (2.42), $H(j\omega)$ can be replaced by positive power spectra considering only the positive lags of the output spectra matrix $S_{yy}^{+}(j\omega)$.

$$S_{yy}^{+}(j\omega) = B_{ri}(j\omega)(A_{ri}(j\omega))^{-1} \tag{2.80}$$

Where $B_{ri}(s) \in \mathbb{C}^{l\times m}$ is the numerator matrix polynomial and $A_{ri}(s) \in \mathbb{C}^{m\times m}$ is the denominator matrix polynomial. They are defined as

$$B_{ri}(j\omega) = \sum_{r=0}^{p} \Omega_r(\omega)\beta_r \tag{2.81}$$

$$A_{ri}(j\omega) = \sum_{r=0}^{p} \Omega_r(\omega)\beta\alpha_r \tag{2.82}$$

With $\Omega_r(\omega)$ as the polynomial basis function and p is the user defined polynomial order. A pth order model based on m outputs contains mp poles. Theoretically, the indication of the model order can be counted as twice the number of peaks in the frequency-plot of a non-parametric spectrum. In practice it is better to over-specify the model order, a stabilization diagram being used to extract modal parameters from this model.

For a discrete-time domain model, the function $\Omega_r(\omega)$ is usually defined as;

$$\Omega_r(\omega) = e^{-j\omega\Delta tr} \tag{2.83}$$

Where Δt is the sampling time.

The polynomial coefficients $\beta_r \in \mathbb{R}^{l\times m}$ and $\alpha_r \in \mathbb{R}^{m\times m}$ are the parameters to be estimated and are assembled in following matrices:

$$\beta_o = \begin{pmatrix} \beta_{o_0} \\ \beta_{o_1} \\ \beta_{o_2} \\ \cdot \\ \cdot \\ \cdot \\ \beta_{o_p} \end{pmatrix} \in \mathbb{R}^{(p+1)\times m} \text{ ,(o=1, 2, 3,…,l) } \alpha = \begin{pmatrix} \alpha_0 \\ \alpha_1 \\ \alpha_2 \\ \cdot \\ \cdot \\ \cdot \\ \alpha_p \end{pmatrix} \in \mathbb{R}^{m(p+1)\times m}, \theta = \begin{pmatrix} \beta_1 \\ \beta_2 \\ \beta_3 \\ \cdot \\ \cdot \\ \beta_l \\ \alpha \end{pmatrix} \in \mathbb{R}^{(m+1)(p+1)\times m} \tag{2.84}$$

From this model, the output spectra $S_{yy}^{+}(j\omega)$ can be written as function of the coefficients $S_{yy}^{+}(\omega_k, \theta)$. By fitting the measured output spectra $S_{yy}^{+}(j\omega)$ with this model by coefficient θ at each frequency point ω_k, the system poles λ_i and operational reference vector g_i can be estimated. From this frequency model, a *poly-*

reference least squares frequency domain algorithm *(*p-LSCF*)* is used to identify modal parameters. Completing this section with two frequency domain models in equations (2.79) and (2.80), the path has now been paved for a discussion on the modal identification techniques.

2.4.7 Summary

This section presents half positive power spectra frequency domain models in both *PFD* and *RMFD* form. The evolution from analytical second order vibration equation to OMA frequency models is in following steps: converting analytical model to transfer function in continuous time domain and to classical FRF in discrete-time domain. The introductions of sampling, DFT technique, spectrum estimation and model reduction are further step to real experimental world. Finally, frequency models based on half positive power spectra in different forms leads to different identification methods that will be discussed comprehensively in next section.

2.5 Frequency Domain Modal Identification Methods

In the context of operational modal analysis (OMA) in civil engineering, structures such as bridges and buildings are excited by unmeasured input forces and only output measurements are available. Under the assumption that the input is a stochastic process (e.g. white noise), the structural behavior can be idealized by mathematical models in the frequency domain proposed, as described in previous section, in order to establish the relation between the output spectra matrix and the structural modal parameters. In this chapter, an overview of the main frequency domain modal identification methods is presented. They comprise *peak-picking* (PP) and *frequency domain decomposition* (FDD) algorithms and *poly-reference least squares complex frequency* (p-LSCF) technique. The PP and FDD methods are called *non-parametric* methods, because modal parameters are estimated by just looking at signal-based features without fitting or estimating a parametric model. Despite their simplicity and quickness, *non-parametric* methods are rather subjective in estimating modal parameters. On the contrary, p-LSCF is called a *parametric* method. A right matrix fraction model is selected and it is parameterized as a function of a parameter vector θ. By fitting this model with spectra of the output measurements in a linear least square (LS) sense, θ is determined and further leads to the estimation of the modal parameters more accurately.

2.5.1 Peak-picking (PP)

The Peak-Picking (PP) is the simplest and most popular approach to estimate structural modal parameters in OMA. The key step of this method is the natural frequencies are simply taken from the observation of the peaks on the graphs of the magnitude of the spectrum plot under the basic assumption that the modes have well-separated frequencies. Assuming that the spectrum around any frequency ω_i is dominated by a single mode, equation (2.79) can be expressed as

$$S_{yy}(j\omega) = -\frac{d_i \phi_i {\phi_i}^H}{\xi_i \omega_i} \tag{2.85}$$

By defining the scalar constant α_i as

$$\alpha_i = -\frac{d_i}{\xi_i \omega_i} \tag{2.86}$$

The approximated spectrum at resonance can be expressed as

$$S_{yy}(j\omega) \approx \alpha_i \phi_i {\phi_i}^H \tag{2.87}$$

From the point of view of Peak-Picking method, the interpretation of equation (2.85) is that at the resonance frequency ω_i each column (or equivalently row) of the spectra matrix can be considered as an estimate of the observed mode shape up to some scaling factor, as shown in Figure 2.5. If the column (or row) corresponds to a DOF of the structure that is situated at a node of a certain mode, this mode cannot be identified. In order to ensure all of the natural frequencies of a structure are identified, a practical implementation of the Peak-Picking method was firstly developed by Felber (1993). It is suggested to consider the averaged normalized power spectrum density (ANPSD) of all measured locations, which means the diagonal elements of the spectrum matrix $S_{yy}^{+}(j\omega)$.

The determination of damping ratios is then usually based on the half-power bandwidth method. However, this is a rather inaccurate procedure. Using simple peak-picking method, the damping ratio is likely difficult to be determined. When peak-picking method is applied to identify modal shapes, instead of estimating the spectrum matrix $S_{yy}^{+}(j\omega)$ only the spectra between the reference sensor and all sensors are calculated. The reason is that only one column (or row) of the spectrum matrix suffices to obtain the mode shape estimates. Some refinements of the peak-picking method are also proposed in (Felber, 1993). Coherence function between two sensors can assist in selecting natural frequencies, because the coherence function tends to be 1 around the resonance damped frequencies because of high signal-to-noise ratio at those frequencies. For instance, consider a structure under investigation shows two bending modes in orthogonal direction -x and y directions-and a torsional mode in a certain frequency range. When torsional modes are considered, the coherence shows a value close to 1 if either the two channels are in the same direction or in two orthogonal directions On the contrary, bending modes show low values of coherence when it is computed for two orthogonal modes The phase angles of the cross spectra are also helpful for determining the damped natural frequencies since the phase angles should be either $0\ or\ 180^0$ .The combination of information from the coherence, spectra and phase angle will be used to identify the structural modes. The detailed procedure for identifying modal parameters can be found in (Felber, 1993).

Example

Before applying various modal identification methods, the experimental data collected during construction of the footbridge under study i.e. before roof covering and installing the dampers, sampled at 200Hz were

pre-processed: They were decimated with factor 2 to reduce the size of data from 36,200 to 18,100 samples. The data were filtered with an eight-order Chebyshev type I lowpass filter with a cutoff frequency of 0.8*200/2/2=40Hz. Afterwards, the data were resampled with a lower sampling rate *fs*=200/2=100Hz. Subsequently, the decimated data were de-trended to remove the linear component.

When the preprocessed signals were treated by peak-picking method, the spectrum matrix was estimated by the *weighted averaged periodogram* method. 16384 of total 18,100 sample points were used and divided into 16 segments of 1024 points, for smooth spectra, with 50% overlapping; after multiplication by a Hann window, FFT was applied to each segment. Finally, the 4 FFTs were averaged to yield the spectrum estimates with frequency resolution 100/1024=0.09784Hz.

The trace of the spectrum matrix is shown in Figure 2.5. It is the sum of auto power spectra produced by each signal acquired from individual sensors. The frequencies are identified by picking the peaks with certain degree of uncertainty as the modes are close to each other, the mode frequencies are indicated in Figure 2.5 with data box. Moreover, coherence of channels is computed to verify the spectra peaks are real structural modes. Left coherence plots in Figure 2.6 are computed by considering vertical channel as a

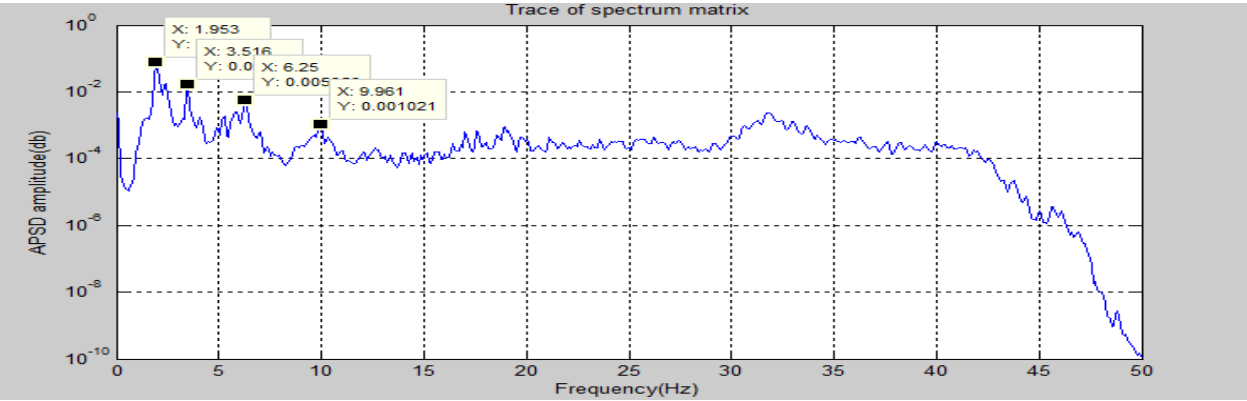

Figure 2.5-Trace of spectrum matrix

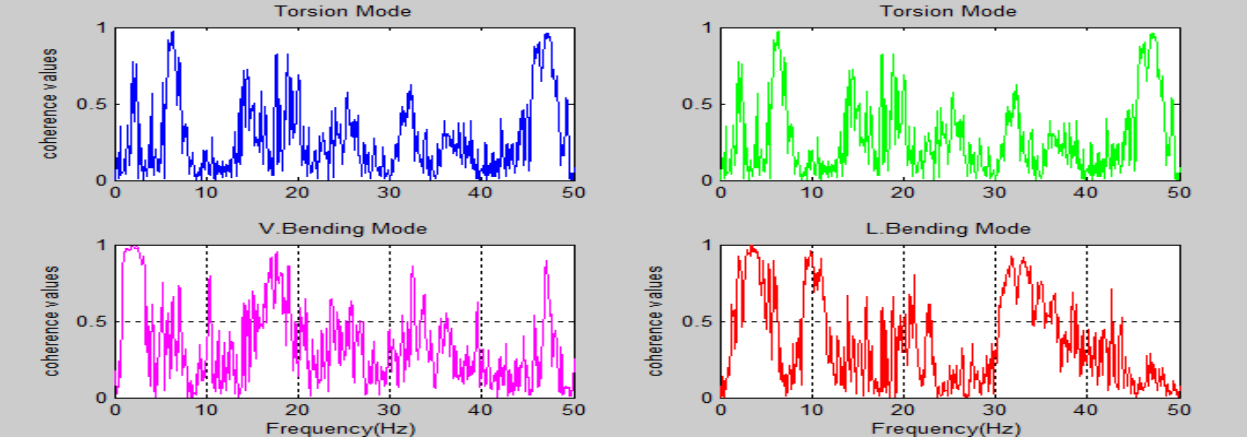

Figure 2.6-Coherence of records, left, bottom and top, coherence figures are with vertical channel as reference while right, bottom and top, coherence figures are with lateral channel as reference sensor

reference sensor, having being treated with other vertical channel it coherence close to unity is obtained at vertical bending mode frequency, while treating it with other lateral channel lead to coherence values of near unity around torsional mode of frequency. Similarly, coherence plots of the Right side of Figure 2.6 are done by considering other lateral channel as reference sensor, and thus treating it with other lateral channel leads to identification of lateral bending mode but torsion modes if computed against vertical channel. The corresponding modal identification results are listed and compared with those yielded from other methods in Table 2.1 at the end of this chapter.

2.5.2 Frequency Domain Decomposition (FDD)

The key step of FDD method is the Singular Value Decomposition (SVD) of the spectra matrix at each discrete frequency ω_i. SVD is a mathematic tool that is typically used for counting the rank of a matrix, because the number of non-zero singular values equals the rank of the matrix. It is also interpreted in modal analysis that the FRF or spectrum matrix evaluated at a certain frequency is only determined by a few modes, and the number of these modes coincides with the rank of the spectrum matrix. SVD of the spectrum matrix is used as a tool to count the number of modes of a vibrating system subjected to natural excitation (Prevosto, 1982). Subsequently, this method was applied to FRFs to count the number of modes in modal testing and it was named as Complex Mode Indication Function (CMIF). It was also extended to identify the modal parameters from FRFs (Shih, 1988). Similarly, SVD of output spectra matrix was further developed to estimate modal parameters in OMA (Brincker et al 2000, 2001).

When applying the FDD method in frequency domain for modal parameters identification, the first step is also the estimation of the half positive spectra matrix $S_{yy}^{+}(j\omega)$ based on output measurements. A simple way to understand this technique is response signals is from their decomposition into participations from the different modes $[\Phi]$ expressed via the modal coordinates $q(t)$ as

$$y(t) = [\Phi]\, q(t) \tag{2.88}$$

Using equation (2.88) in the expression of the correlation matrix of the response y we get

$$[C_{yy}(\tau)] = E\{y(t+\tau)y^T(t)\} = E\{[\Phi]\, q(t+\tau)[\Phi]^H q^H(t)\} = [\Phi]C_{qq}(\tau)[\Phi]^H \tag{2.89}$$

Applying the Fourier transform in equation (2.89), power spectra is obtained.

$$S_{yy}(j\omega) = [\Phi]G_{qq}(j\omega)[\Phi]^H \tag{2.90}$$

Then, by taking the SVD of $S_{yy}^{+}(j\omega)$ at each discrete frequency ω_i (floor) it can be decomposed as follows

$$S_{yy}^{+}(j\omega_i) = U(\omega_i)S(\omega_i)U^H(\omega_i) \tag{2.91}$$

Where $S(\omega_i)$ is a diagonal matrix holding the singular values sorted in descending order $S(\omega_{ij}), j = 1,2,\ldots..l$, $U(\omega_i) = [u_1(j\omega_i), u_2(j\omega_i), \ldots\ldots u_l(j\omega_i)]$ is a unitary matrix holding the singular vectors(columns

of U) $u_j(j\omega_i)$ are orthogonal to each other as modal coordinates are uncorrelated to each other due the assumption that $G_{qq}(j\omega)$ is diagonal. When the frequency approaches a certain resonance frequency ω_r, the power spectra matrix can be approximately decomposed as a rank one matrix,

$$\underset{\omega \to \omega_r}{S_{yy}^{+}(j\omega_r)} = \begin{bmatrix} S_{11}(\omega_r) & S_{12}(\omega_r) \dots \dots & S_{1l}(\omega_r) \\ S_{21}(\omega_r) & S_{22}(\omega_r) \dots \dots & S_{2l}(\omega_r) \\ \vdots & \vdots & \vdots \\ S_{l1}(\omega_r) & S_{l2}(\omega_r) \dots \dots & S_{ll}(\omega_r) \end{bmatrix} \overset{SVD}{\to} S_{11}(\omega_r) u_1(\omega_r) {u_1}^H(\omega_r) \tag{2.92}$$

If only one mode is dominating at the resonance frequency ω_r, the corresponding singular vector $u_1(\omega_r)$ is an estimate of the corresponding mode shape with unitary normalization,

$$\hat{\phi}_r = u_1(\omega_r) \tag{2.93}$$

And the corresponding singular value is the auto power spectra function of the corresponding single degree of freedom (SDOF) bell curve system associated with equation (2.79). In the case of repeated modal frequencies, the rank of the power spectra matrix is equal to the multiplicity number of the modes. Therefore, the singular value which is a function of frequencies sorted in descending order can be adopted as the modal indication function. Modal frequencies can be located by the peaks of the singular value plots. Mode shapes can be obtained from the corresponding singular vectors assuming the mode shapes are orthogonal. Because SVD has the ability to separate the signal space from noise space, the modes can be indicated from singular value plots with noisy measurements, and closely spaced modes or even modes with repeated modal frequencies can be easily detected.

Initially, FDD could only estimate modal frequencies and mode shapes. To identify modal damping ratio, the enhanced FDD (EFDD) technique was proposed (Brincker et al, 2001). After estimating mode shapes according to equation (2.93), the corresponding singular value is the auto power spectral density function of the corresponding single degree of freedom system. This power spectral density function is identified around the peak by comparing the mode shape estimation $\hat{\phi}_r$ with the singular vectors for the frequency lines around the peak. MAC (Modal Assurance Criterion) value is computed between the SDOF singular value and the singular values of frequency lines centered at this resonance frequency as

$$MAC_i = \frac{\left(\hat{\phi}_r {\phi_i}^T\right)^2}{(\hat{\phi}_r {\phi_i}^T)(\hat{\phi}_r{}^T \phi_i)} \tag{2.94a}$$

If a singular vector ϕ_i is found to have high Modal Assurance Criterion (MAC) value (user defined value, commonly 0.8 as a starting value), with $\hat{\phi}_r$, the corresponding singular value is included in the definition of the SDOF auto spectra function. In addition, mode complexity factor can be used for validation of modes given by

$$MCF_i = 1 - \frac{(S_{yy} - S_{xx})^2 + 4S_{xy}^2}{(S_{yy} + S_{xx})^2} \tag{2.94b}$$

Where $S_{xx} = Re\{\phi_i\}^T Re\{\phi_i\}$, $S_{yy} = Im\{\phi_i\}^T Im\{\phi_i\}$, and $S_{xy} = Re\{\phi_i\}^T Im\{\phi_i\}$

The Later distinguishes real (0 value) and imaginary mode (1 value) and is given in %. It can interpreted as, a given mode with significant complexity has mode shape in which the maximas does not occur at the same time. Complexity plots can be prepared also for single or group of modes where the distribution of mode shape vector is displayed around a unit circle.

From the fully or partially identified SDOF auto spectra function, an approximation of the correlation function of the SDOF system is obtained by taking the spectral density function back to time domain by inverse FFT. From this free decay function in time domain (the correlation function of the SDOF system), the natural frequency and the damping is found by estimating crossing times and logarithmic decrement. Firstly, all peaks r_{pk} on the correlation function are found. The logarithmic decrement δ_k at kth frequency is calculated as [Note: '2' in equation (2.95) is due to use of negative peaks of correlation function are also used]

$$\delta_k = \frac{2}{p}\ln\left(\frac{r_{0k}}{|r_{pk}|}\right) \tag{2.95}$$

Where r_{0k} the initial peak value of the correlation is function and r_{pk} is the *p*th peak at the kth mode. In order to avoid noise interference, the correlation function is normalized and peak values between 0.95-0.3 are taken for computation of δ_k. And the damping ratio is estimated by

$$\xi_k = \frac{\delta_k}{\sqrt{\delta_k + 4\pi^2}} \tag{2.96}$$

The damped natural frequency ω_{dk} is found by making a linear regression between the crossing times and the times corresponding to the peaks. The natural frequency ω is found by

$$\omega_k = \frac{\omega_{dk}}{\sqrt{1-\xi^2{}_k}} \tag{2.97}$$

Example

The SVD was applied to the estimated spectrum matrix constructed with the preprocessed experimental signals of the incomplete footbridge. Figure *2.7* shows the singular values as a function of frequency. Because only two channels were used to in each setup giving to a 2×2 output spectrum matrix as the example discussed in section 2.4.6 which yields 2 singular value vectors according to equation (2.87). A MATLAB program is written for computing the spectra matrix as shown below yielding s_{yy} .

```
Syy =

    [2049x1 double]    [2049x1 double]
    [2049x1 double]    [2049x1 double]
```

Each cell contains nfft/2+1 values of PSD samples

Most importantly, the EFDD algorithm is implemented as MATLAB program to compute singular value plots for peak picking, mode shapes, damping values and corrected natural frequencies(detailed explanation of the MAT LAB EFDD program is presented in Annex C & D).The results are presented below:

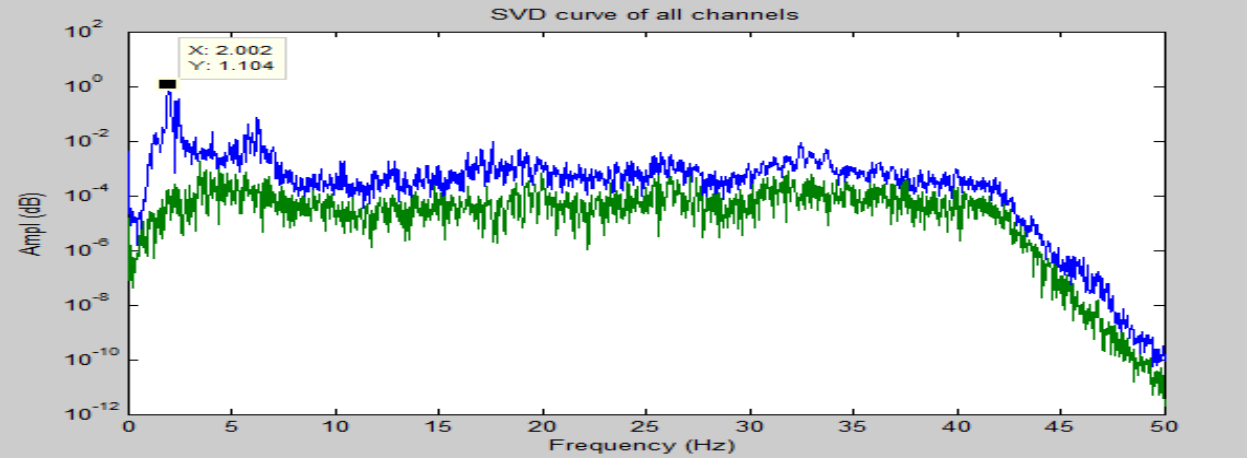

Figure 2.7-Singular values produced using EFDD method

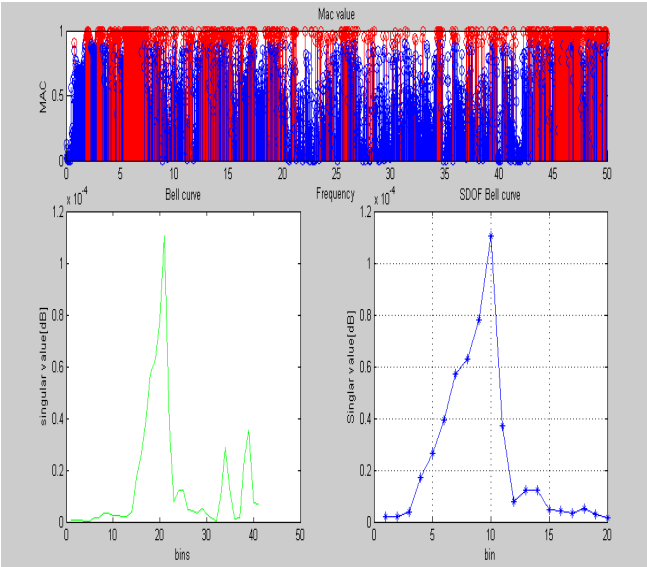

Figure 2.8-Top plot -MAC value against frequency at the first mode, bottom-left plot, singular values at 1Hz frequency range centered at first mode and bottom-right plot, SDOF curve for 1st mode with MAC of 0.9

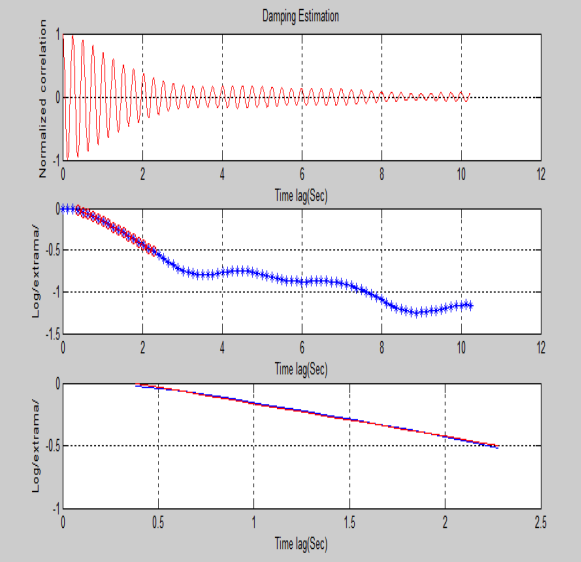

Figure 2.9-Damping estimation, correlation function of SDOF Bell curve,$|p_k|$ plot against time lag and curve fitting for $\delta_k$computation, respectively from top to bottom

The peak around 2.002Hz (1st mode) is picked from the singular value plot for computation and the corresponding SDOF is shown in Figure 2.8. The mode shape $\hat{\phi}_{2.002Hz}$ is estimated. The singular vectors of the neighboring frequency lines around the peak were compared against the mode shape $\hat{\phi}_{2.002Hz}$ by

calculating the MAC value. The frequency lines with MAC value higher than 0.9 were selected and regarded as the auto correlation function of a SDOF system, as shown Figure 2.8 (bottom right).By applying inverse FFT to the selected frequency lines, the free decay function in time domain is obtained (Figure 2.9(top most)). The natural

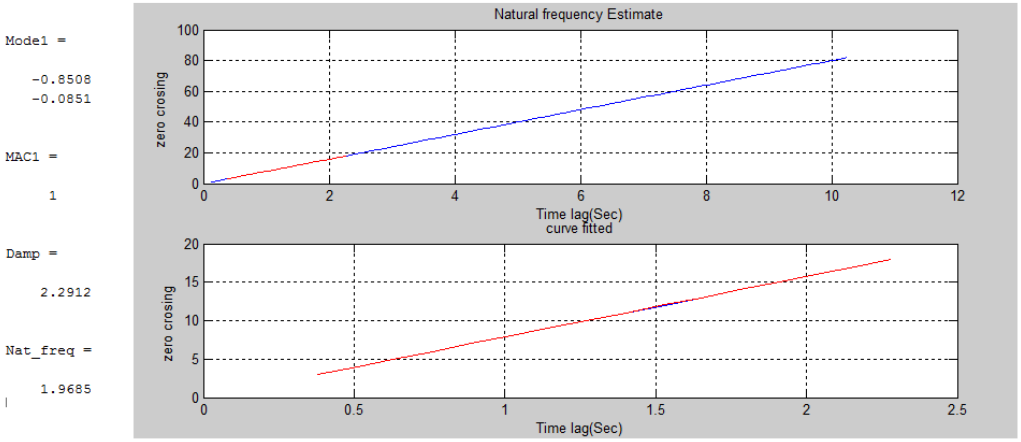

Figure 2.10-Natural frequency estimation from zero-crossing times and modal estimates (left) of EFDD program

frequency and the damping were evaluated by estimating crossing times and logarithmic decrement of the fitted envelope according to equations (2.96-2.97).The estimation results are presented at the end of this chapter. The modal parameters estimated by the program are shown in Figure 2.10 along with the natural frequency estimate from zero-crossing times.

The basic assumption of FDD is that the structure is lightly damped. Moreover, only truncated data near the peak of the singular value plot are utilized for the inverse FTT to calculate approximate correlation functions of the corresponding SDOF system, which may cause bias error in damping estimation. To estimate damping ratio more accurately, the parametric *poly-reference least squares complex frequency* (p-LSCF) algorithm for identification of modal parameters based on half positive output spectra matrix was proposed from the frequency model in RMFD (Peteers et al, 2005) which will not be discussed in this paper as its analogy in time domain (SSI-Data driven) is presented in the next section.

2.6 Time Domain Models

Time domain state-space (SS) model originate from control engineering. This model reveal the inherent relation between modal model of vibration systems and output measurements. Without converting from the signals to frequency domain, the modal parameters can be fitted directly from time series analysis (TSA) based on *parametric* models. It is utmost useful to inspect these time domain representations of vibration signals. The modal identification results estimated by these models in time domain can be compared with the results produced by frequency domain models. It is worth to identify the main disparity between the two approaches (time domain and frequency domain) in order to reach a conclusion on the effectiveness of each methodology and find conditions suitable to apply a given method.

2.6.1 Continuous-time state-space model

a) The state equation

The equation of motion in state-space form can be written as

$$P\dot{x}(t) + Qx(t) = F \tag{2.98}$$

Where

$$P = \begin{bmatrix} C_d & M \\ M & 0 \end{bmatrix} \quad Q = \begin{bmatrix} K & 0 \\ 0 & M \end{bmatrix} \quad , x(t) = \begin{bmatrix} q(t) \\ \lambda q(t) \end{bmatrix}, \quad F = \begin{pmatrix} B_l \\ 0 \end{pmatrix} u(t)$$

Pre-multiplying equation (2.98) by P^{-1}

$$\dot{x}(t) = A_c x(t) + B_c u(t) \tag{2.99}$$

Where the sub index '*c*' denotes continuous time,$A_c \in \mathbb{R}^{n \times n}$ is the state matrix and $B_c \in \mathbb{R}^{n \times n}$ is the input matrix. They are given by

$$A_c = P^{-1}Q = \begin{bmatrix} C_d & M \\ M & 0 \end{bmatrix}^{-1} \begin{bmatrix} K & 0 \\ 0 & M \end{bmatrix} = \begin{bmatrix} 0 & I \\ -M^{-1}K & -M^{-1}C \end{bmatrix} , \quad B_c = P^{-1} \begin{pmatrix} B_l \\ 0 \end{pmatrix} = \begin{bmatrix} 0 \\ M^{-1}S \end{bmatrix} \tag{2.100}$$

b) The observation equation

In a practical vibration experiment, accelerations $\ddot{q}(t)$, velocities $\dot{q}(t)$ and displacements $q(t)$ may be measured simultaneously in well selected l positions as described in equation (2.2),

$$\mathrm{y(t)} = C_a \ddot{\mathrm{q}}(\mathrm{t}) + C_{\mathrm{v}} \dot{q}(t) + C_d q(t) \tag{2.101}$$

Using the second order equation of motion (2.101) and the definition of the state vector $x(t)$ in equation (2.98), the observation equation (2.101) can be expressed as

$$y(t) = C_c x(t) + D_c u(t) \tag{2.103}$$

Where the sub index '*c*' denotes continuous time,$C_c \in \mathbb{R}^{l \times n}$ is the output matrix and $D_c \in \mathbb{R}^{l \times n}$ is the direct transmission matrix. They are given by

$$C_c = (C_d - C_a M^{-1} K \quad C_v - C_a M^{-1} C_2) \, , D_c = C_a M^{-1} B_l \tag{2.104}$$

Combining equations (2.99) and (2.103), the classical continuous-time state-space (SS) model is given by

$$y(t) = C_c x(t) + D_c u(t) \ , \quad \dot{x}(t) = A_c x(t) + B_c u(t) \tag{2.105}$$

The equation of motion is written in state-space form and it can also be used to compute the response $y(t)$ of the structure with a given input $u(t)$.

2.6.2 Discrete-time state-space model [According to Wei-Hua Hu, PhD dissertation, Porto]

Similarly, it is necessary to convert the state-space model expressed in the continuous time domain to discrete time domain, in order to fit the models to discrete measurements. In section 2.4.3, the concepts of sampling and assumption of zero-order hold (ZOH) have been introduced. The continuous-time state-space model described in equation (2.116) can be then converted to the discrete-time state-space model:

$$y_k = Cx_k + Du_k \tag{2.106}$$

$$x_{k+1} = Ax_k + Bu_k \tag{2.107}$$

Where $x_k = x(k\Delta t) = \begin{pmatrix} q_k \\ \dot{q}_k \end{pmatrix}$ is the discrete-time state vector consisting of the sampled displacements and velocities; u_k, y_k are the sampled input and output vectors respectively; *A*, *B*, *C* and *D* are the discrete state matrix, discrete input matrix, discrete output matrix and direct transmission matrix respectively. It can be expressed by its continuous-time counterparts as

$$A = e^{A_c \Delta t}\ , B = \int_0^{\Delta t} e^{A_c \tau} B_c\, \delta\tau = (A - I)A_c^{-1}B_c\ \ , C = C_c,\ D = D_c \tag{2.108}$$

The classical derivation of the above relations can be found in (Juang, 1994)

a) Modal parameters

The purpose of this section is to reveal the relations between matrices A and C, and the modal parameters, including natural frequencies ω_i, modal damping ratios ξ_i and mode shapes ϕ_i .

It is observed that the state matrix A_c in continuous-time state-space model in equation (2.100) comprises all information about the structural system. According to orthogonality conditions of P and Q in equation (2.23), as well property in equation (2.24), A_c is rewritten as a standard eigenvalue problem,

$$A_c = P^{-1}Q = -\Psi[\ddots\ 1/a_i\ \ddots]\ \Psi^T\Psi^{-T}[\ddots\ 1/b_i\ \ddots]\Psi^{-1} = \Psi\Lambda_{com}\Psi^{-1} \tag{2.109}$$

Where Λ_{com} and Ψ are complex eigenvalue and eigenvector matrices defined in equation (2.20) as

$$\Lambda_{\text{com}} = \begin{bmatrix} \Lambda & 0 \\ 0 & \Lambda^* \end{bmatrix} = \begin{bmatrix} \ddots\ \lambda_i\ \ddots & 0 \\ 0 & \ddots\ \lambda_i{}^*\ \ddots \end{bmatrix},\ \Psi = [\varphi \quad \varphi^*] = \begin{bmatrix} \Phi & \Phi^* \\ \Phi\Lambda & \Phi^*\Lambda^* \end{bmatrix}$$

Which is called modal decomposition of matrix A_c.

The matrix A in discrete-time stochastic state-space model is found by inserting the modal decomposition of the continuous state matrix A_c into equation (2.108),

$$A = e^{A_c \Delta t}\ = e^{\Psi\Lambda_{com}\Psi^{-1}\Delta t} = \Psi e^{\Lambda_{com}\Delta t}\Psi^{-1} = \Psi\Lambda_d\Psi^{-1} = \Psi[\ddots\ \mu_{i\ddots}]\Psi^{-1} \tag{2.110}$$

Where

$$\mu_i = e^{\lambda_i \Delta t}$$

Thus, the system poles are determined as

$$\lambda_i = \frac{\ln(\mu_i)}{\Delta t} \tag{2.111}$$

The connection between $\lambda_i, \omega_i \; and \; \xi_i$ is specified in equation (2.22).

Similarly, *transformation* of the *state vector* $x(t)$ to the (complex) *modal state vector* $x^m(t) \in \mathbb{C}^n$ is defined as

$$x(t) = \Psi x^m(t) \tag{2.112}$$

And the corresponding discrete time format,

$$x_k = \Psi x_k^m \tag{2.113}$$

The *modal state-space model* in discrete time format is obtained by inserting the modal decomposition of A in equation (2.106) and (2.107),

$$x^m{}_{k+1} = \Lambda_d x_k^m + L^T u_k \tag{2.114}$$

$$y_k = V x_k^m + D u_k \tag{2.115}$$

Where L^T and V are the discrete modal participation matrix and the observed mode shape matrix respectively, given by

$$L^T = \Psi^{-1} B, V = C\Psi$$

The relation between the observed mode shape matrix V and the mode shape matrix Φ of the second order equation of motion (2.1) can be clarified by inspecting $V = C\Psi$ based on the definition of C (equation (2.108)), C_c (equation (2.104)) and Ψ (equation (2.20)).

$$V = C\Psi = C_c\Psi = (C_d - C_a M^{-1} K \qquad C_v - C_a M^{-1} C_2) \begin{bmatrix} \Phi & \Phi^* \\ \Lambda\Phi & \Lambda^*\Phi^* \end{bmatrix} \tag{2.116}$$

Case-1: If only displacements are measured, $C_a = C_v = 0$, the mode shape matrix V becomes

$$V = C_d(\Phi \;\; \Phi^*) \tag{2.117}$$

Case-2: If only velocities are measured, $C_d = C_a = 0, \; V$ yields

$$V = C_v(\Lambda\Phi \;\; \Phi^*\Lambda^*) \tag{2.118}$$

Case-3: If output measurements are only specified as accelerations ($C_d = C_v = 0$), which is the most widely used in vibration experiment, V can be derived by also considering equation (2.116) and (2.20) as

$$V = C_a(\Phi\Lambda^2 \;\; \Phi^*\Lambda^{*2}) \tag{2.119}$$

From equations (2.117-2.119), $C_d, C_v \; and \; C_a$ are selecting the components of the mode shape corresponding to the output positions, Λ, Λ^* and, Λ^2, Λ^{*2} are diagonal matrices that are only scales of mode shape Φ. It is concluded that observed mode shape matrix V denotes the part of mode shapes from output measurements.

This section reveals the relation between matrices A and C and the modal parameters. Once matrices A and C are identified from the state-space model, modal parameters including natural frequencies ω_i, modal damping ratios ξ_i and modal shapes Φ_i will be obtained.

b) Model reduction

As experiments are performed using a certain sampling frequencies, only the contribution of a limited number of modes is acquired. The model reduction can be derived by eliminating higher modes from the modal state-space model. The discrete time modal state-space model in equations (2.106/7) is divided with the n_r to-be-retained modes and $(n - n_r)$eliminated modes as

$$\begin{matrix} n_r \\ n-n_r \end{matrix} \updownarrow \begin{pmatrix} {x^r}_{k+1} \\ {x^e}_{k+1} \end{pmatrix} = \begin{bmatrix} \Lambda_d & 0 \\ 0 & \Lambda_d \end{bmatrix} \begin{pmatrix} {x^r}_k \\ {x^e}_k \end{pmatrix} + \begin{pmatrix} L^r \\ L^e \end{pmatrix}^T u_k \tag{2.120}$$

$$y_k = (V^r \quad V^e) \begin{pmatrix} {x^r}_k \\ {x^e}_k \end{pmatrix} + Du_k \tag{2.121}$$

Where ${x^r}_k$ is the discrete-time state vector of the reduced system and ${x^e}_k$ is the state vector to be eliminated. The *modal decomposition* of direct transmission term *D* can be expressed as a sum of *n* rank-one matrices as (Peeters, 2000).

$$\begin{aligned} D = D_c &= V_c\Lambda_c^{-1}L_c^T = V(\Lambda_d - I)^{-1}L^T \\ &= D^r + D^e \\ &= V^r(\Lambda_d^r - I)^{-1}L^{rT} + V^e(\Lambda_d^e - I)^{-1}L^{eT} \end{aligned} \tag{2.122}$$

Model reduction can be obtained by putting next states that have to be eliminated equal to the current state, i.e. ${x^e}_{k+1} = {x^e}_k$.By introducing the resulting ${x^e}_k$ into the observation equation, the reduced modal state-space model is obtained as

$${x^r}_{k+1} = \Lambda_d^r {x^r}_k + L^{rT}u_k \tag{2.123}$$

$$y_k = V^r{x^r}_k + D^r u_k \tag{2.124}$$

The reduced model reflects the real experimental world, where only the modes within a certain frequency bandwidth are contained in the experimental data

2.6.3 Discrete-time stochastic state-space model

The discrete-time state-space model in equations (2.123/4) shows that the system is only driven by the input u_k. However, the noise in real measurements has to be considered to model the vibration system accurately. Therefore, stochastic components can be modeled and the *discrete-time combined deterministic-stochastic state-space model* (Van Overschee and De Moor, 1996) is obtained as

$$y_k = Cx_k + Du_k + v_k \tag{2.125}$$

$$x_{k+1} = Ax_k + Bu_k + w_k \tag{2.126}$$

Where $w_k \in \mathbb{R}^n$ represents the noise caused by disturbances and modelling inaccuracies and $v_k \in \mathbb{R}^l$ means the measurement noise due to sensor inaccuracy.

In real experiments, it is impossible and unimportant to distinguish the terms u_k and the noise terms w_k and v_k. By substituting $Bu_k + w_k$ by w_k and $Du_k + v_k$ by v_k as stochastic input, above two equations become a *discrete-time stochastic state-space model* as

$$y_k = Cx_k + v_k \tag{2.125}$$

$$x_{k+1} = Ax_k + w_k \tag{2.126}$$

It is assumed that unmeasured signal vectors w_k and v_k are white zero mean, and their covariance matrices having the following property:

$$E\left[\begin{pmatrix} w_p \\ v_p \end{pmatrix}\begin{pmatrix} w_q^T & v_q^T \end{pmatrix}\right] = \begin{pmatrix} Q & S \\ S^T & R \end{pmatrix}\delta_{pq} \tag{2.127}$$

Where E is the expected value operator; δ_{pq} is the Kronecker delta, which means that $\delta_{pq} = 1$, if $p = q$, otherwise $\delta_{pq} = 0$ if $p \neq q$ i.e. any two arbitrary time instants. $Q \in \mathbb{R}^{n\times n}$, $S \in \mathbb{R}^{n\times l}$ and $R \in \mathbb{R}^{l\times l}$, where n is the order of the system.

The discrete-time stochastic state-space model in equation (2.125/6) assumes implicitly that the input is modelled by a white noise. If this assumption of white noise is not valid, for example, if the input contains some dominating frequency components, these frequency components cannot be separated from the Eigen frequencies of the system, appearing as spurious poles of the state matrix A (Peeters, 2000).

2.6.4 Properties of stochastic systems

The main properties of linear time-invariant stochastic system are briefly discussed in this section. These properties lead to different identification algorithms one of which will be described in section *2.7.* More detailed and complete derivation can be found in (Van Overschee and De Moor, 1996).

It is assumed that the stochastic process x_k is stationary

$$E(x_k) = 0,\ E(x_k x_k^T) = \sum \tag{2.128}$$

Where the state covariance matrix Σ is independent of the time k. This implies that matrix A is stable (all poles are in inside a unit circle) In this section, the *forward model* and *forward innovation model* are introduced, which leads to *covariance driven subspace stochastic identification* and data *driven subspace stochastic identification*.

a) Forward model

Since noise terms w_k and v_k in equation (2.125/6) are zero mean white noise vector sequences and independent of x_k, then

$$E(x_k w_k^T) = E(x_k v_k^T) = 0 \tag{2.129}$$

Recall the definition of output correlation matrices in equation (2.54),

$$R_i = E[y_{k+i} y_k^T]$$

Where i is an arbitrary time lag. The 'next state-output' covariance matrix $G \in \mathbb{R}^{n \times l}$ is defined as

$$G = E[x_{k+1} x_k^T] \tag{2.130}$$

Hence it is be deduced that,

$$\begin{aligned} \sum = \ & E(x_{k+1} x_{k+1}^T) = A \sum A^T + Q \\ \mathrm{R}_0 = & E[y_k y_k^T] = C \sum C^T + R \\ G = & E[x_{k+1} y_k^T] = A \sum C^T + R \end{aligned} \tag{2.131}$$

Where i=1,2,3,….

$$\begin{aligned} R_i &= C A^{-1} G \\ R_{-i} &= G^T (A^{-1})^T C^T \end{aligned} \tag{2.132}$$

This equation reveals an important relation between the output covariance sequence and system matrices *A* and *C*, which means that *A* and *C* can be identified by decomposing the estimated output covariance matrix. This property leads to the *covariance driven subspace stochastic identification* algorithm which is not discussed in this dissertation.

b) Forward innovation model

The *discrete-time stochastic state-space model* can be converted into a *so-called forward innovation model* by applying a Kalman filter to the stochastic SS model in equation (2.127). The Kalman filter is described in many books. An elaborate explanation can be found in (Juan, 1994). The purpose of the Kalman filter is

to estimate the optimal prediction of the state vector x_{k+1}, denoted as Kalman filter state vector $\hat{x}_{k+1}$. It is given as

$$x_{k+1} = Ax_k + Ke_k \tag{2.133}$$

$$y_k = Cx_k + e_k \tag{2.134}$$

Where e_k are called innovations sequence, the corresponding covariance matrix being,

$$E(e_k e_k^T) = R_0 - CPC^T$$

K is a (forward) kalman gain, (2.135)

$$K = (G - APC^T)(R_0 - CPC^T)^{-1}$$

and P is the forward state covariance matrix. It can be solved by *discrete Riccati equation* from a generalized Eigen value problem,

$$P = APA^T + (G - APC^T)(R_0 - CPC^T)^{-1}(G - APC^T)^T \tag{2.136}$$

Based on this forward innovation model, the *data driven subspace stochastic identification* method is proposed to identify the state matrices A and C.

2.6.5 Summary

In this section it is described how a structural system subjected to white noise excitation can be parameterized by a stochastic state space model in time domain. The relation between a state space model and a modal model is revealed and thus modal parameters can be identified from the state space model. The concept of model reduction is also explained in state-space model, which makes a closer step to the real experiment field. Introduction of important properties of the state space model pave a solid path for the different time domain identification techniques.

2.7 Time Domain Modal Identification Methods

In this section modal identification methods involving time domain mathematical models of vibrating systems are explained. The main concern is related with the stochastic subspace identification (SSI) methods. A first group of algorithms is called covariance-driven SSI methods, because the output covariance matrix is used as primary data, which is based on the factorization property in equation (2.132). Another group is named data-driven SSI methods, because it identify models directly from the time signals, which stems from the Kalman filter state sequence shown in equation (2.133/4).

2.7.1 'Past' and 'Future' part of experimental signal

Before explaining the identification algorithm, the data reduction and smoothing procedure for dividing experimental signal into 'past' and 'future' part is introduced. The Toeplitz and Hankel matrices consist of these two parts of signals. To determine experimental mode shapes, modal test always involve a batch of measurement setups. In each setup, l sensors (mostly accelerometers) are placed at certain nodes of the structure. The discrete samples y_k can be described as sample matrix,

$$y_k = [y_m^n] = \begin{bmatrix} y_1^n \\ y_2^n \\ \vdots \\ y_l^n \end{bmatrix} = \begin{bmatrix} y_1^0 & y_1^1 & \dots & y_1^N \\ y_2^0 & y_2^1 & \dots & y_2^N \\ \vdots & \vdots & & \vdots \\ y_l^0 & y_l^1 & \dots & y_l^N \end{bmatrix} \tag{2.137}$$

Where y_m^n refers the *n-th* (*n*=0,1,…*N*) sample point from the *m-th* (*m*=1,2,…,*l*) sensor in a certain setup. The Hankel matrix $H \in \mathbb{R}^{2li \times j}$ can be divided into a *past* part y_p and a *future* part y_f in equation (2.138).

$$H_{0|2i-1} = \frac{1}{\sqrt{j}} \begin{pmatrix} y_0 \\ y_1 \\ \vdots \\ y_{i-1} \\ y_i \\ y_{i+1} \\ \vdots \\ y_{2i-1} \end{pmatrix} = \left[\begin{array}{cccc} y_{1\to l}^0 & y_{1\to l}^1 & \dots\dots & y_{1\to l}^{j-1} \\ y_{1\to l}^1 & y_{1\to l}^2 & \dots\dots & y_{1\to l}^{j} \\ \dots\dots & \dots\dots & \dots\dots & \dots\dots \\ y_{1\to l}^{i-1} & y_{1\to l}^{i} & \dots\dots & y_{1\to l}^{j+i-2} \\ \hline y_{1\to l}^{i} & y_{1\to l}^{i+1} & \dots\dots & y_{1\to l}^{i+j-1} \\ y_{1\to l}^{i+1} & y_{1\to l}^{i+2} & \dots\dots & y_{1\to l}^{i+j} \\ \dots\dots & \dots\dots & \dots\dots & \dots\dots \\ y_{1\to l}^{2i-1} & y_{1\to l}^{2i} & \dots\dots & y_{1\to l}^{j+2i-2} \end{array}\right] = \begin{pmatrix} Y_{0|i-1} \\ Y_{i|2i-1} \end{pmatrix} = \begin{pmatrix} Y_p \\ Y_f \end{pmatrix} = \frac{"past"}{"future"} \tag{2.138}$$

Where the number of block rows $i(\text{order})$ is a user defined index which is theoretically larger than the maximum order of the system. It is noted that the matrix *H* consists of $2li$ rows since each block row include l (number of output measurement) rows. The number j is typically equal to $N - 2i + 2$, which implies that all samples are used.

The subscripts of $Y_{i|2i-1}$ and $Y_{0|i-1}$ are subscripts of the first and last element in the first column of the block Hankel matrix of past and future matrices. The subscripts *p* and *f* stand for *past* and *future Henkel matrices*. The past matrix $Y_{0|i-1}$ and future matrix $Y_{i|2i-1}$ are defined by splitting the Hankel matrix $H_{0|2i-1}$ in two parts with i block rows. Another division is defined by omitting the first block row of future matrix and adding these block rows at the end of past matrix, which can be explained as

$$H_{0|2i-1} = \frac{1}{\sqrt{j}} \begin{pmatrix} y_0 \\ y_1 \\ \vdots \\ y_i \\ y_{i+1} \\ y_{i+1} \\ \vdots \\ y_{2i-1} \end{pmatrix} = \left[\begin{array}{cccc} y_{1\to l}^0 & y_{1\to l}^1 & \dots\dots & y_{1\to l}^{j-1} \\ y_{1\to l}^1 & y_{1\to l}^2 & \dots\dots & y_{1\to l}^{j} \\ \dots\dots & \dots\dots & \dots\dots & \dots\dots \\ y_{1\to l}^{i} & y_{1\to l}^{i+1} & \dots\dots & y_{1\to l}^{j+i-1} \\ \hline y_{1\to l}^{i+1} & y_{1\to l}^{i+2} & \dots\dots & y_{1\to l}^{i+j} \\ y_{1\to l}^{i+2} & y_{1\to l}^{i+3} & \dots\dots & y_{1\to l}^{i+j+1} \\ \dots\dots & \dots\dots & \dots\dots & \dots\dots \\ y_{1\to l}^{2i-1} & y_{1\to l}^{2i} & \dots\dots & y_{1\to l}^{j+2i-2} \end{array}\right] = \begin{pmatrix} Y_{0|i} \\ Y_{i+1|2i-1} \end{pmatrix} = \begin{pmatrix} Y_p^+ \\ Y_f^- \end{pmatrix} = \frac{"past"}{"future"} \tag{2.139}$$

2.7.2 Data-driven SSI method

In this dissertation Data-driven SSI method will only be discussed as the two (Covariance-Driven SSI and Data-Driven SSI) methods are similar in the concept used for modal identification. Modal parameters can be identified by data-driven SSI method (Overschee and De Moor). Detailed description of this method can be found in (Van Overschee and De Moor, 1996; Ljung, 1999). Instead of computing output covariance of output measurements as in case of covariance-driven SSI method, the data-driven SSI method starts with projecting the row space of future outputs into the row space of past outputs. Actually, the purpose of both covariance and projections in different methods is to cancel out the uncorrelated noise. The following steps in data-driven SSI method are SVD and Least Squares, similar to covariance-driven SSI method. The principles of data-driven SSI algorithm are the Kalman filter states and the factorization property of projection matrix.

a) Kalman Filter States

The Kalman filter states play a crucial role in data-driven SSI method. The purpose of Kalman filter is to estimate the Kalman filter state $\hat{x}_k$together with the observation of the outputs up to time $k-1$, system matrices and the noise covariance according to the forward innovation model indicated in section 2.6.4. If the initial state estimates $\hat{x}_0 = 0$, the initial covariance of the state estimates,

$$P_0 = E\left[\hat{x}_0 {\hat{x}_0}^T\right] = 0$$

And the output measurements $y_0, y_1, y_2 \ldots\ldots y_{k-1}$ are observed. The non-steady state Kalman filter state estimates $\hat{x}_k$, the Kalman filter gain matrix K_{k-1} and Kalman state covariance matrix $P_k$can be derived as

$$\hat{x}_k = A\hat{x}_{k-1} + K_{k-1}(y_{k-1} - C\hat{x}_{k-1})$$

$$K_{k-1} = (G - AP_{k-1}C^T)(R_0 - CP_{k-1}C^T)^{-1} \quad (2.140)$$

$$P_k = AP_{k-1}A^T + (G - AP_{k-1}C^T)(R_0 - CP_{k-1}C^T)^{-1}(G - AP_{k-1}C^T)^T$$

The Kalman filter state sequence is defined as $\widehat{X}_i \in \mathbb{R}^{n\times j}$ is defined as

$$\hat{X}_i = [\hat{x}_i \quad \hat{x}_{i+1} \quad \ldots \quad \hat{x}_{i+j-1} \quad] \quad (2.141)$$

$$\hat{X}_0 = [0 \quad 0 \ldots \quad 0], \quad P_0 = 0$$

Y_P

$$\begin{bmatrix} y_0 & y_q & y_{j-1} \\ \vdots & \vdots & \vdots \\ y_{i-1} & y_{i+q-1} & y_{i+j-2} \end{bmatrix}$$

$\widehat{X}_i$ $\quad [\ \hat{x}_i \quad \hat{x}_{i+q} \quad \ldots \hat{x}_{i+j-1}\ ]$ Kalman state

This sequence in equation (2.141) can be written as a linear combination of the past output measurements and is generated by a batch of non-steady state Kalman filters working in parallel on each columns of the block Hankel matrix of past outputs Yp, which is illustrated above. This observation implies that the Kalman filter state sequence $\hat{X}_i$ can be determined directly from output data (Van Overschee and De Moor, 1996).

b) Factorization Property of Projection Matrix

The projection matrix is defined as projecting the row space of future outputs onto row space of past outputs as

$$P = Y_f/Y_p = Y_f Y_p^T (Y_p Y_p^T)^\dagger Y_p \tag{2.142}$$

Where $Y_f \in \mathbb{R}^{li\times j}$, $Y_p \in \mathbb{R}^{li\times j}$ are the block hankel matrices containing future and past matrices respectively. The projection matrix is also equal to the product of the extended observability matrix O_i and the Kalman filter state sequence$\hat{X}_i$,

$$P = O_i \hat{X}_i \tag{2.143}$$

This relation is based on the main theorem of SSI (Van Overschee and De Moor, 1996). From equations (2.142/3), it is observed that the Kalman filter state sequence $\hat{X}_i$ can be determined by projecting the future outputs on past outputs.

In practice, projection is computed by *RQ* factorization based on the Hankel matrix defined in equations (2.139/40).Nevertheless, direct computation is possible.

$$Y_{0|2i-1} = P = Y_f/Y_p = Y_f^+/Y_p^- = RQ^T \tag{2.144}$$

Where $Q \in \mathbb{R}^{J\times j}$ is an orthonormal matrix and $Q \in \mathbb{R}^{2li\times j}$ is a lower triangular matrix.

Projecting the row space of future outputs Y_f onto row space of past outputs Y_p can be achieved by the RQ factorization of projection P_i:

$$P_i = Y_f/Y_p = \begin{matrix} li \\ l \\ l(i-1) \end{matrix} \updownarrow \begin{bmatrix} R_{11} & 0 & 0 \\ R_{21} & R_{22} & 0 \\ R_{31} & R_{32} & R_{33} \end{bmatrix} \begin{pmatrix} Q_1^T \\ Q_2^T \\ Q_3^T \end{pmatrix} \begin{matrix} \updownarrow li \\ \updownarrow l \\ \updownarrow l(i-1) \end{matrix} \tag{2.145}$$

Substituting equation (2.145) in equation (2.142), projection matrix P_i is expressed by the product of *R* and *Q* submatrices as:

$$P_i = \begin{pmatrix} R_{21} \\ R_{31} \end{pmatrix} Q_1^T \tag{2.146}$$

Similarly, projection P_{i-1} is computed by the alternative expression of future outputs Y_f^- and past outputs Y_p^+,

$$P_{i-1} = (R_{31} \quad R_{32}) \begin{pmatrix} Q_1^T \\ Q_2^T \end{pmatrix} \tag{2.147}$$

The factorization property applied to projecting matrices play a crucial role in data-driven SSI method. Once the projection of matrix P_i and P_{i-1} are available, the structure modal parameters can be estimated using these matrices.

c) Estimation of system matrix

Finally, SVD is applied to estimate the rank of projection matrix. Theoretically, the rank is equal to the system order *n* and the number of the non-zero singular values. After omitting the zero singular values and corresponding singular vectors, the projection matrix is given as

$$P_i = U_1 S_1 V_1^T \tag{2.148}$$

Where $\in \mathbb{R}^{li \times li}$, $S \in \mathbb{R}^{li \times li}$ and$V \in \mathbb{R}^{li \times li}$. This step explains why these algorithms are called *subspace algorithms*: Only the subspaces consisting of singular vectors corresponding to non-zero singular values of the projection matrix are used to identify the system matrices.

Combining equations (2.148) and (2.143), the extended observability O_i is given by (Van Overschee and De Moor, 1996)

$$O_i = U_1 S_1^{1/2} \quad and \quad X_i = S_1^{1/2} V_1^T \tag{2.149}$$

From equation (2.143), we have

$$\hat{X}_i = O_i^{\dagger} P_i \tag{2.150}$$

In order to identify system matrices A and C, another projection matrix is introduced by shifting one block row down in the Hankel matrix,

$$P_{i-1} = Y_f^- / Y_p^+ = O_{i-1} \hat{X}_{i+1} \tag{2.151}$$

The extended observability matrix O_{i-1} is simply obtained by deleting the last l rows of O_i,

$$O_{i-1} = O_i(1: l(i-1), :) \tag{2.152}$$

The state sequence $\hat{X}_{i+1}$ can be derived as

$$\hat{X}_{i+1} = O_{i-1}^{\dagger} P_{i-1} \tag{2.153}$$

Substituting state sequences $\hat{X}_{i+1}$ and $\hat{X}_i$ into stochastic state-space model (2.125/6), yields

$$\begin{pmatrix} \hat{X}_{i+1} \\ Y_{i|i} \end{pmatrix} = \begin{pmatrix} A \\ C \end{pmatrix} \hat{X}_i + \begin{pmatrix} W_i \\ V_i \end{pmatrix} \tag{2.154}$$

Where, W_i and V_i are residuals, and $Y_{i|i}$ is the ith block row of the Hankel matrix. It is easily written, according to *RQ* submatrices in equation (2.145),

$$Y_{i|i} = (R_{31} \quad R_{32} \quad R_{33}) \begin{pmatrix} Q_1^T \\ Q_2^T \\ Q_3^T \end{pmatrix} \tag{2.155}$$

Finally, state sequences $\hat{X}_{i+1}$, $\hat{X}_i$ and the block row $Y_{i|i}$ are determined from output measurements, and system matrices A and C can be computed by the least square method,

$$\begin{pmatrix} A \\ C \end{pmatrix} = \begin{pmatrix} \hat{X}_{i+1} \\ Y_{i|i} \end{pmatrix} \hat{X}_i^{\dagger} \tag{2.156}$$

Identification of matrices A and C is sufficient to estimate the modal parameters using the equations discussed in section 2.6.2. System poles and mode shapes are given as

$$A = \Psi[\ddots\ \mu_i \ddots]\Psi$$

$$V = C\Psi$$

$$\lambda_i = \frac{\ln(\mu_i)}{\Delta t}\ ,\ \omega_i = \frac{|\lambda_i|}{2\pi}\ ,\ \xi_i = -\frac{Re(\lambda_i)}{\omega_i}$$

It is to be noted that the matrices A and C identified from output measurements are only an estimation (denoted $\hat{A}$ as and $\hat{C}$) of the 'true' system matrices, because only finite data length is available.

Due to noise of the measurements in practice, the model order n cannot be determined easily by simply counting the number of non-zero singular values of matrix *S*1 (equation 2.148). The expected 'gap' between successive singular values is also not obvious in real experiments. To solve the order determination problem, a stabilization diagram is used as in case of P-LSCF and SSI-COV are methods. Models of different order are then obtained and used to construct a stabilization diagram by considering a different number of singular values and corresponding vectors in equation (2.148). Modal parameters are estimated by interpreting the stabilization diagram.

In order to construct the stabilization diagram, criteria for modal parameter comparison is set between modal parameters computed in each successive model order of the iteration. The user defined criterions may vary depending on the project type and precision required, but typically 1-2% for frequencies, 3-5% for both damping and mode shape correlations can be adopted. The construction of stabilization diagram is done in two stages as

i) Elimination of unexpected frequencies (out of range of $f_{max} to f_{min}$) and unexpected damping values (out of range of $\xi_{max} to \xi_{min}$);
ii) Elimination of modal parameters not pertaining to a user defined criterions using equations

$$\left|\frac{f_i - f_{i+1}}{f_i}\right| \leq \varepsilon_f, \quad \left|\frac{\xi_i - \xi_{i+1}}{\xi_i}\right| \leq \varepsilon_\xi \quad \text{and}$$

$$MAC_\phi\ (\phi_i, \phi_{i+1}) = \frac{|\phi_i^T \phi_{i+1}|^2}{(\phi_i^T \phi_i)(\phi_{i+1}^T \phi_{i+1})} \leq MAC_\phi \tag{2.157}$$

Where $\varepsilon_f \ and\ \varepsilon_\xi$ are user defined criterion e.g. $\varepsilon_f = 1\%$ and $\varepsilon_\xi = 5\%$, and MAC_ϕ MAC value of mode shape vector at same frequency lines of successive orders e.g. $MAC_\phi = 98\%$ or $(MAC_\phi - 1) = 2\%$. The quality of stabilization diagram can be improved further using covariance vector MAC criteria, detailed explanation can be found on Shock and Vibration Volume 2014 by E. Mrabet, M. Abdelghani and Ben Kahla.

Example

The preliminary SSI-DATA method was also applied to the preprocessed experimental data. The experience parameter i was set as 20. A MATLAB program is written for computing modal parameters using SSI-DATA for the same records used in the FDD example in section 2.5.2 The first step of SSI-DATA is to gather the output measurements in a block Hankel matrix with $2il \times N$ (2*20*2×2400=80*2400(reduced number of sampling points is taken so as for efficient performance of the MATLAB program)). Next, the Hankel matrix is divided in to future and past Hankel matrices followed by projection of row space of future matrix in to row space of past matrix for both P_i and P_{i-1} using equation (2.144). The observability matrix for both the projection matrices is computed by singular value decomposition and using equation 2.149.The non-zero singular values obtained are collected which indicates the order of the model provided that there exist no noise. But, it is clear that there exist noise commonly in stochastic process making it difficult to identify the system order from the number of non-zero singular values. It is observed from Figure 2.11 that 2 singular values are significant and that there is a "gap" between the 2nd and 3rd singular values, representing the first guess of the model order in the processed experimental data. Through this outcome we cannot conclude the model order. However, a stabilization diagram under various model orders should be constructed to find the stable system poles according to user defined stabilization ranges.

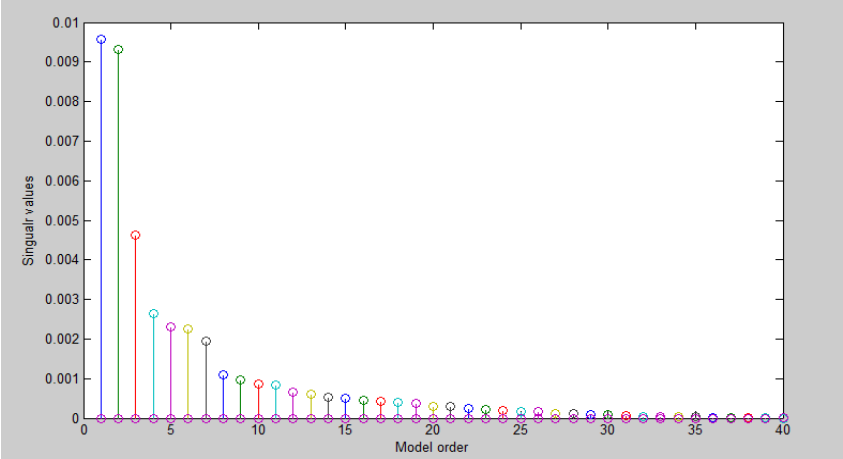

Figure 2.11-Singular values of projection matrix for model order computation

2.8 Comparison of identification methods

This section presents a comparison between the modal parameters computed or estimated by different models and modal identification methods for the example, footbridge two vertical channel records, presented to illustrate the identification methods. It is noted that the damping ratio cannot be computed directly by analytical models, being only estimated by experimental methods. The damping ratio results estimated by PP method are not listed because the half-power bandwidth damping ratio estimation method is not reliable and the EFDD method evolved from PP method can provide more objective and accurate estimation of modal damping ratios.

Theoretically, PP and EFDD modal identification techniques are usually classified as *non-parametric* estimation methods, because they do not employ a parametric model in the search for a best description, which induces that the identification procedure becomes a relatively subjective task in case of noisy civil engineering experimental data or weakly-excited modes. In contrary, time domain models, parametric models, maintain dependable results.

Computation speed can also be compared between the different algorithms. Generally, parametric models have less computation speed due to the need to estimate the parametric matrix (vector).

Table 2.1-Comparison of Modal parameters computed by parametric methods

		Method	**Frequency (Hz)**	**Damping (%)**	**Mode shape(Φ)**
Mode 1	Non-Parametric	PP	1.953	/	Vertical
		EFDD	1.974	1.829	
	Parametric	SSI-DATA	Model order of two		
Mode 2	Non-Parametric	PP	3.516	/	Lateral
		EFDD	3.495	0.742	
	Parametric	SSI-DATA	Model order of two		

2.9 Conclusion

This chapter presents a state of art of operational modal analysis (OMA) and describes in detail three of the most relevant methods used. Ambient vibration test of North footbridge, EDP, under construction was performed to enhance the understanding of abstract concepts of the theory described. Finally, the performance of different OMA methods is briefly compared; SSI-DATA is used only to determine model order.

Illustration of the aforementioned frequency domain modal estimation techniques and preliminary time domain modal estimation was implemented on the ambient vibration records taken at the construction stage of the footbridge by using two vertical channels only and the first two relevant modes are referred for a reason which will be discussed later.

3

PEDESTRIAN TRAFFIC AS A SOURCE OF EXCITATION

3.1 Introduction

3.1.1 Pedestrians as source of vibration

Pedestrians are more and more susceptible to create vibrations on footbridges as the design and building technologies constantly improve and slender and longer footbridges are being built. Human induced vibration become important as the footbridge becomes more slender, typically more than 30m with width less than 3m. Generally speaking pedestrian's loads are time-variant and may be classified in the "periodic load" category. In this paper pedestrian traffic load in terms of running and walking is categorized which enables to clarify the interaction between pedestrians and footbridges. To this end, the attention will go to the modeling of pedestrian loads.

3.1.2 Forces induced by pedestrians

The center of gravity of the human body is located at about 55% of its height and makes a sinusoidal motion during walking, both in vertical and horizontal directions. The force thus has three components: a vertical, a longitudinal and a lateral. The vertical sinusoidal component is the largest, up to 40% of the body weight. The lateral and longitudinal components are considerably smaller, the lateral force being the least, usually 4%-5%. Each component of body force is presented below.

3.1.2.1 Patterns of running a and walking

During normal walking the vertical forces are centered at a frequency in the range of 1.2Hz - 2.3 Hz (lower range represent the 5% slow and upper range represent 95% fast, SYNPEX), corresponding to the pace rate. For running the frequencies lie in the range 2Hz – 3.5 Hz. Normal walking follows a normal distribution with a mean value of 2.0 Hz and a standard deviation of 0.173 Hz, according to a research of Matsumoto (1978). In the other hand, the lateral forces fall in the frequency range 0.5Hz-1.2Hz, with the same implication of upper range of frequency as vertical frequency with 95% fast and, minimum range, 0.5Hz, attained from a recommendation of Millennium Bridge which caused Lock-in effect in 2000.

For the FEM modal analysis, performed on the footbridge by the OZ Lda. Company, Portugal, for vertical and longitudinal direction pedestrian frequency range of 1.2-2.3Hz is taken while the lateral direction was computed with frequency range of 0.5-1.2(approximately, half of the vertical direction frequency).The ranges are taken from SYNPEX.

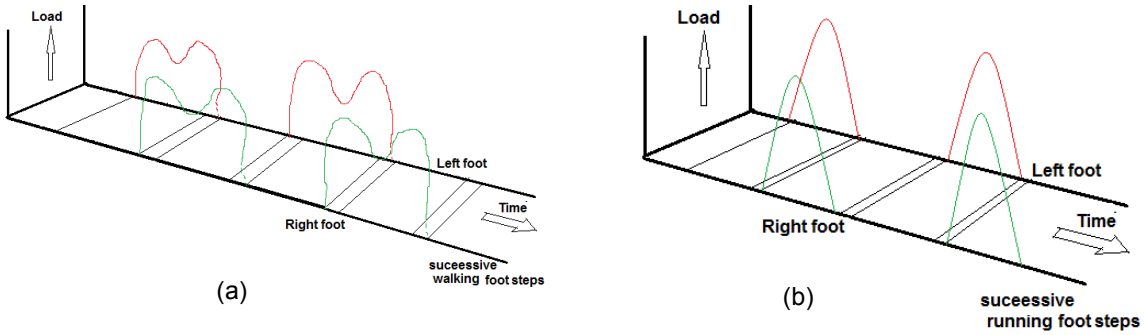

Figure 3.1-Load Patterns of (a) Walking and (b) Running (Sétra, 2006)

3.1.2.2 Vertical component

Early studies on pedestrian induced forces on footbridges were carried out by Blanchard et al. in 1977. Walking, running or jumping each produce a different loading curve over time as well as frequencies in which the oscillations can occur. Note that during walking always at least one foot is in contact with the ground (floor).

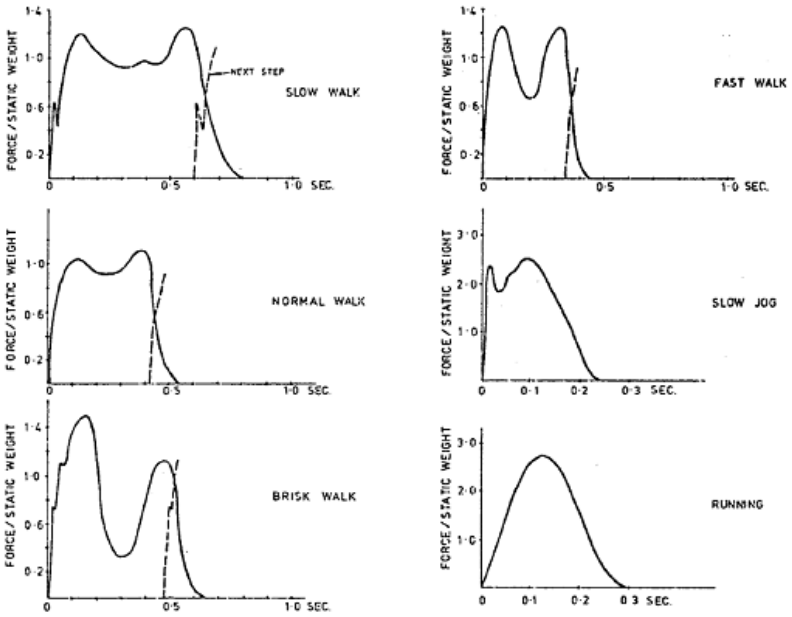

Figure 3.2-Loading curves of one pedestrian for different types of steps (Blanchard, 1977)

During walking, the vertical component shows a characteristic double hump, which is the result of the impact of the heel on the ground (first one) and the push off (second one). The maximum increase with increasing step frequency. Note that the next footfall begins just before the other one has finished. This phenomenon does not occur while running, as both foots can be off the ground at the same moment and the time that the foot is on the ground is relatively short. . [Iemke Roos, TUDelft, 2009]

3.1.2.3 Horizontal component

The horizontal force components are considerably lower than the vertical force. The pattern of these forces are shown in Figure 3.3 (walking) and Figure 3.4 (running).

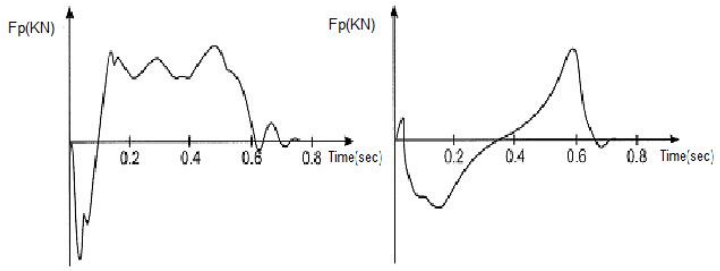

Figure 3.3-Walking load patterns, lateral (left) longitudinal (right) (Blanchard, 1977)

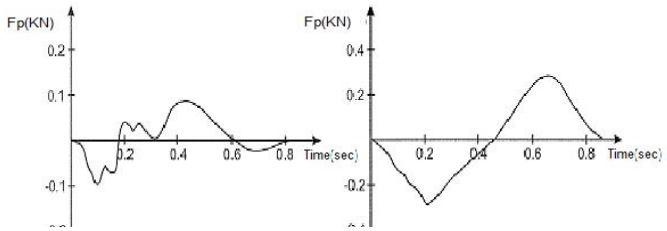

Figure 3.4-Running load patterns, lateral (left) longitudinal (right) (Blanchard, 1977)

Horizontal forces are periodic with half of the walking frequency, with a mean value of 1Hz, as the force changes its direction by each step and the longitudinal force is characterized by the retarding and the pushing walking period. The lateral force is caused by the lateral oscillation of the body. Runners seem to have a larger lateral stability, so that the lateral force is smaller than during walking. This can be manifested from the above diagram (Blanchard, 1977), in which the amplitude of running lateral load is smaller than walking lateral load. . [Iemke Roos, TUDelft, 2009]

3.2 Characteristics of pedestrian streams

The pedestrian density greatly influences the speed of the individual and is therefore important for the dynamic analysis. The relation between velocity and pedestrian density is given according to the Oeding measurements.

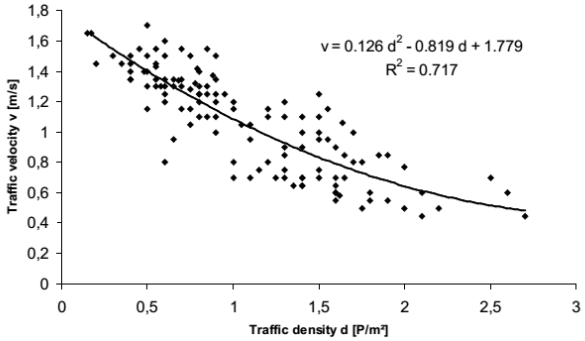

Figure 3.5-Traffic density versus Traffic velocity (Oeding, 1963)

The pedestrian density on the bridge structure can be calculated according to the following formula:

$$d = \frac{N_r}{L * b_{eff}} = \frac{\lambda}{v_s * b_{eff}} \ [\text{P/m}^2] \tag{3.1}$$

Where

d Pedestrian density [Persons/m²]

λ Rate of Pedestrian Arrival [Per/s]

v_s Velocity of Pace [m/s]

N_r Number of Pedestrians on Bridge Deck

b_{eff} Effective Width of Bridge

L Length of Bridge

A correlation between densities and step frequencies was evaluated by taking the mean value between walking speed and pedestrian traffic density from Oeding's measurements. The results for the mean step frequency $f_{s,m}$ and the corresponding standard deviation σ_f for a single pedestrian (not the deviation among all pedestrians) are given by [C. Butz, M. Feldmann, C. Heinemeyer, G. Sedlacek et al]

$$f_{s,m} = 0.7868V + 0.7886 \ [Hz] \tag{3.2}$$

$$\sigma_f = 0.0857V - 0.035 \ [Hz] \tag{3.3}$$

Where V is velocity of crossing.

3.3 Interaction between pedestrians and footbridges

It is well known that there is a certain degree of interaction between pedestrians and the structure, footbridges. Two different phenomena can be distinguished; one concerns the change of properties of the footbridge when humans are using the bridge. The other phenomenon is the synchronization of the walking pattern between pedestrians and synchronization of humans with the structure, under certain circumstances.

3.3.1 Dynamic properties of footbridges under human-induced loads

A change in dynamic properties is more likely to happen to light structures where human loading can have significant impact on the structure compared to a non-loaded structure; the mass and the damping can increase and thus this can have effect on the natural frequency of the footbridge.

3.3.2 Synchronization between pedestrians

Synchronization between pedestrians is mainly dependent on the pedestrian density on a footbridge. Figure 3.6 shows different density situations. At low densities, pedestrians are free to walk without obstacles (other pedestrians). When the path becomes denser, pedestrians are less free to choose their pace and adjust to the surrounding. The first restrictions occur at about 0.6 persons per square meter. At this stage passing becomes more difficult. At a density of 1.0 person per m² the freedom of movement is greatly inhibited. When the density reaches about 1.5 persons per m², walking become very difficult and pedestrians are greatly dependent on other users of the bridge. The velocity of the pedestrians decreases as the density increases. [Iemke Roos, TUDelft, 2009]

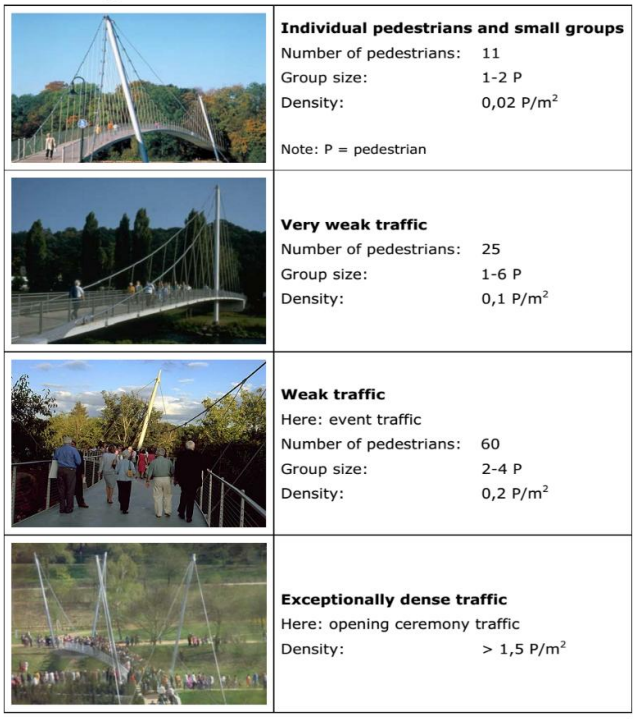

Figure 3.6-Pedestrian density (HIVOSS)

Hence it becomes clear that synchronization of pedestrians is more likely to occur at higher densities, when people are not able to walk freely and are dependent on other pedestrians. The density of pedestrians also influences their velocity and consequently their dynamic forces on the bridge. Synchronization between runners is less likely to occur, as the velocity is quite high and thus the density is lower. Beyond the upper limit value of 1,5 P/m² walking of pedestrians is impossible, so that dynamic effects significantly reduce. When a stream becomes dense, the correlation between pedestrians' increases, but the dynamic load tends to decrease.

3.3.3 Synchronization between bridge and pedestrians

The lock-in effect describes the phenomenon by which, when the structure exceeds a certain threshold value of displacement (depending on direction of vibration, type of activity, etc.), walking (or jumping, or running) person tends to adapt to and synchronize his/her motions in frequency and phase with the vibrating deck leading to further synchronization. . [Iemke Roos, TUDelft, 2009]

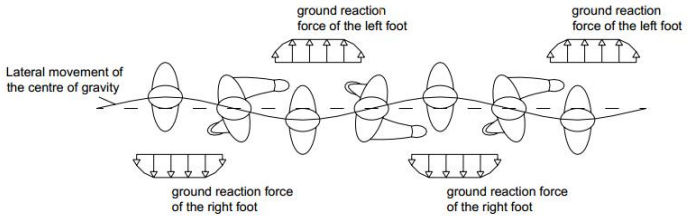

Figure 3.7-Synchronizing effect of pedestrians (HIVOSS)

Lock-in in transverse direction is most likely to occur during lateral synchronization and is also known as Synchronous Lateral Excitation (SLE). This is due to the fact that pedestrians are much more sensitive to lateral vibrations than to vertical vibrations (will be discussed below). A good example of a bridge on which such a phenomenon occurred is the Millennium Bridge in London, which vibrated several times laterally during opening in June 2000 when hundreds of people were walking over it. The maximum density has been estimated between 1.3 and 1.5 persons per m².

Dallard et al. investigated the Millennium Bridge and concluded that during SLE the produced dynamic force by the pedestrians is proportional to the lateral velocity of the deck: $F_L(t) = kV_L(t)$. By investigating more bridges, he found out that SLE could occur to any bridge with a lateral frequency of 1.3 Hz under the condition that sufficient number of people would cross the bridge at the same time. Later investigations reveal that, a slight lateral movement of the foot-bridge will cause pedestrians to adjust their movements involuntarily which in turn drive the bridge to vibrate more laterally.

3.4 Modelling of pedestrian loads

This paragraph illustrates the basics of modeling pedestrian loads. Several codes give different methods and values of coefficients for modelling. Load models for walking differ from the ones for running, as illustrated in previous sub-section. The walking load is much more complex than the running load. This paragraph focuses on walking pedestrian loads. Time domain models consist of modeling waveforms and determine the attenuation model that best fits the real load pattern. In case of the frequency domain model, one solves the spectrum of the load waveform that best fits the attenuation model.

3.4.1 Vertical load model of walking pedestrian

Vertical walking forces due to human footsteps can be divided into different periodic oscillations by a Fourier transformation,

$$F(t) = F_0 + \sum_i F_i \sin(2\pi i f_s t - \varphi_i) \quad (3.4)$$

Where:

F_0 Mean or static load (person's weight)

F_i Load component for frequency if_s

f_s Human step frequency

φ_i Phase angle of the load component F_i

i Natural number 1, 2, 3…..

Usually the first three harmonics are taken into account, as the fourth harmonic and higher do not have much influence on the pattern of the load model as their frequency are far away from the excitation frequencies. The ratio of actual force amplitude to the static load is defined as Dynamic Load Factor (DLF),

$$DLF = a = F/G \quad (3.5)$$

Where G=F_0, the static load (person's weight), equation (3.4) can be re-written as

$$F(t) = G(1 + a_1 \sin(2\pi f_s t - \varphi_1) + a_2 \sin(4\pi f_s t - \varphi_2) + a_3 \sin(6\pi f_s t - \varphi_3)) \quad (3.6)$$

Different results of investigations done by Bachmann among others show that the values of the DLF's scatter greatly. Table 3.1 presents the different Fourier coefficients proposed by several authors and codes; this is mainly due to uncertainties during the measurements, but also to the fact that there are differences between persons. This also applies for the phase angles. Note that these DLF's have been determined by walking on a rigid floor. Experimental results by Bachmann et al. manifest the great dependency of the coefficients, a (i.e.$F_i = aG$) and φ_i, with frequency of the steps taken by a person.

Moreover, the periodic force is not stationary. It moves with a constant speed along the bridge. Within the SYNPEX project, the relationship between step frequency and walking speed is found by measurements for a step frequency range of 1.3 to 1.8 Hz,

$$Vs = 1{,}271fs - 1 \quad (3.7)$$

Table 3.1-Fourier coefficients proposed by several authors and/or codes [HIVOSS]

Author(s)	Fourier coefficients/ phase angles	Comment	Type of activity and load direction
Blanchard et al.	$a_1 = 0.257$		Walking –vertical
Bachmann & Ammann	$a_1 = 0.4 - 0.5,\ a_2 = a_3 = 0.1$	For fp=2-2.4Hz	Walking –vertical
Schulze	$a_1 = 0.37, a_2 = 0.1, a_3 = 0.12$, $a_4 = 0.04, , a_5 = 0.015$	For fp=2Hz	Walking –vertical
Bachmann et al.	$a_1 = 0.4 - 0.5,\ a_2 = a_3 = 0.1$ $a_1 = a_2 = a_3 = 0.1$ $a_{1/2} = 0.1, a_2 = 0.2,\ a_1 = 0.1$ $a_1 = 1.6,\ a_2 = 0.7,\ a_3 = 0.3$ $\varphi_2 = \varphi_3 = \pi/2$	$\text{For fp} = 2 - 2.4\text{Hz}$ $\text{For fp} = 2$ $\text{For fp} = 2\text{Hz}$ $\text{For fp} = 2 - 3\text{Hz}$	Walking –vertical Walking –lateral Walking –longitudinal Running –vertical Walking –vertical/ lateral
Kerr	$a_1 = a_2 = 0.07,\ a_3 = 0.2$	$a_1$is frequency dependent	Walking –vertical
Young	$a_1 = 0.37(fp - 0.95) \leq 0.5$ $a_2 = 0.054 + 0.0088fp$ $a_3 = 0.026 + 0.015fp$ $a_4 = 0.01 + 0.0204fp$	Mean values for Fourier coefficients	Walking –vertical
Charles & Hoorpah	$a_1 = 0.4$ $a_2 = 0.05$ $a_3 = 0.2$		Walking –vertical Walking –lateral Walking –longitudinal
EC5,DIN1074	$a_1 = 0.4,\ a_2 = 0.2$		Walking –vertical

	$a_1 = a_2 = 0.1$ $a_1 = 1.2$		Walking –lateral jogging –vertical
SYNPEX Findings	$a_1 = 0.0115f_s^2 + 0.2803f_s - 0.2902$ $\varphi_1 = 0$ $a_2 = 0.0669f_s^2 + 0.1067f_s - 0.0417$ $\varphi_2 = -99.76f_s^2 + 478.92f_s - 387.8[°]$ $a_3 = 0.0247f_s^2 + 0.1149f_s - 0.1518$ $if\ f_s \leq 2.0Hz$ $\varphi_3 = 150.88f_s^3 + 819.65f_s^2 - 1431.35f_s + 811.93[°]$ $if\ f_s > 2.0Hz$ $\varphi_3 = 813.12f_s^3 - 5357.6f_s^2 + 11726f_s - 8505.9[°]$ $a_3 = -0.0039f_s^2 + 0.0285f_s - 0.0082$ $\varphi_4 = 34.19f_s - 65.14[°]$	Fourier coefficients and phase angles of step-by –step load model which represents real human reaction forces	Walking –vertical

Table 3.1-Fourier coefficients proposed by several authors and/or codes [HIVOSS]...continuation

In many Codes (e.g. EN 1995) the body weight P is given as 700 N or 800 N. The mean body mass given in the German 2004 census was 74.4 kg.

For example: As shown in table 3.1, Bachmann et al. proposed the following coefficients to be used for walking at a frequency of 2Hz.

$$a_1 = 0.4 \qquad a_2 = a_3 = 0.1 \qquad \varphi_1 = \varphi_2 \approx {}^{\pi}/_{2}$$

This leads to the following formula for the vertical load,

$$F(t) = G + 0.4\,G\cos(2\pi f_s\,t) + 0.1\,G\cos(4\pi f_s\,t) + 0.1G\cos(6\pi f_s\,t) \qquad 3.8)$$

3.4.2 Horizontal load model of walking pedestrian

Even if the horizontal forces caused by a pedestrian are much smaller than the forces in vertical direction, attention has to be paid to it. It can in some situations be one of the sources of serious problems, like the ones occurred on the Millennium Bridge. The longitudinal forces do not have much effect on the vibration of footbridges and will therefore not be further discussed here. The forces in lateral direction however will be.

Horizontal load can be represented by Fourier's transformation as in case of vertical load. The frequency of the lateral load is half of the vertical load, corresponding to the lateral oscillation of the center of gravity of the body. In order to be able to represent the load according to the vertical frequency, *fs*, the solution generally used is to modify the presentation in the following form,

$$F(t) = \sum_i F_i \sin(2\pi i f_s\,t - \varphi_i) \qquad (3.9)$$

Where *i has* the (non-whole) values of 1/2, 1, 3/2, 2, etc. The phase shifts are close to zero and therefore do not appear in the expression. As in case of vertical force, lateral force for walking occur at a frequency of 2Hz, the following force amplitudes are mainly used,

$$\alpha_1 = \alpha_3 = 0.05 \qquad \alpha_2 = \alpha_4 = 0.01$$

$$F(t) = 0.5\,G\sin(\pi f_s\,t) + 0.01G\,\sin(2\pi f_s\,t) + 0.5\,G\sin(3\pi f_s\,t) + 0.01G\,\sin(2\pi f_s\,t) \qquad (3.10)$$

Using SYNPEX coefficients for dynamic load factor and phase angle, the time domain periodic pedestrian loading is plotted as shown in Figure 3.8

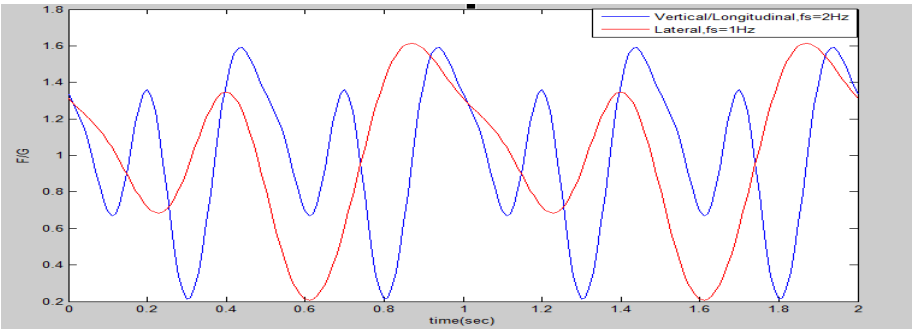

Figure 3.8-Walking vertical/Longitudinal vs Lateral periodic load function

3.5 Load models for group of pedestrians

A footbridge is rarely submitted to forces due to one pedestrian only. Groups of pedestrians are much more common. Each person has its own characteristics (weight, speed, frequency, initial phase shift, location on the bridge) which make the system much more complicated. Moreover, depending on the number of pedestrians on a bridge, people tend to walk more or less synchronous with each other, during which the natural pace of pedestrian changes. This behavior is nearly impossible to model correctly. The Euro code standardized traffic classes are presented below:

Table 3.2-Traffic classes (HIVOSS)

Traffic Class	Density d (P = pedestrian)	Description	Characteristics
TC 1*)	group of 15 P; d=15 P / (B L)	Very weak traffic	(B=width of deck; L=length of deck)
TC 2	d = 0,2 P/m²	Weak traffic 	Comfortable and free walking Overtaking is possible Single pedestrians can freely choose pace
TC 3	d = 0,5 P/m²	Dense traffic 	Still unrestricted walking Overtaking can intermittently be inhibited
TC 4	d = 1,0 P/m²	Very dense traffic 	Freedom of movement is restricted Obstructed walking Overtaking is no longer possible
TC 5	d = 1,5 P/m²	Exceptionally dense traffic	Unpleasant walking Crowding begins One can no longer freely choose pace

*) An equivalent pedestrian stream for traffic class TC1 is calculated by dividing the number of pedestrians by the length L and width B of the bridge deck.

According to the statistics, the load can be increased with the square root of the number of pedestrian on the bridge.i.e. $\sqrt{N}$. This means that a number of $\sqrt{N}$ are walking synchronously. However, this is only the case if initially none of the motions on the bridge are synchronous. In reality a (small) part of the crowd will be synchronized. Different codes and guidelines have set up load models for group of pedestrians. [Iemke Roos, TUDelft, 2009]. Generally, a uniformly distributed vertical harmonic load modelling for design which can simulate a stream of pedestrian can be calculated by:

$$p(t) = P \times cos(2\pi f_s t) \times n' \times \psi \tag{3.11}$$

Where,

P Force component for a pedestrian with frequecny of f_s

f_s Step frequency, assuming it to be equal to the bridge vibration mode

n' Equivalent number of persons (depends on the 95th percentile)

ψ Reduction coefficient that takes into account the probability that the frequency of walking approaches the critical frequency range into consideration, and this coefficient is different in different direction as shown in Figure 3.10.

The application of the oscillating distributed load, defined above, on the bridge is done in accordance to the mode shape as shown in Figure 3.9.

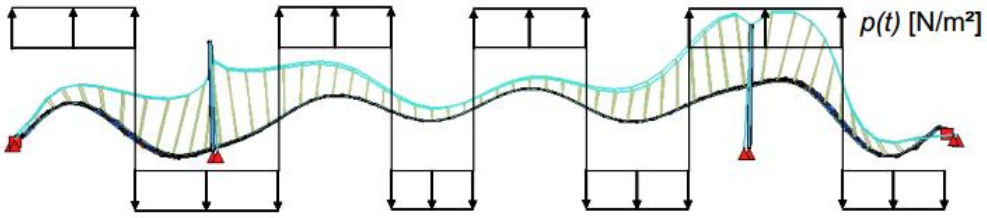

Figure 3.9-Application of Harmonic load according to mode shape (HIVOSS)

A uniformly distributed Harmonic load p(t) represents an equivalent loading of pedestrian stream. The load model for pedestrians of traffic class TC1 to TC3 considers free movement of pedestrians, while traffic classes TC4 and TC5 represent obstructed movement. The values of force components, P, which is a measure of the force introduced by each pedestrian in to the footbridge in respective direction, are given by

Table 3.2-Pedestrian load component (SYNPEX)

	Vertical	Longitudinal	Lateral
$P\ [N]$	280	140	35

For cases of traffic classes TC1 and TC3 (d<1P/m^2) [see section 3.5], the number of synchronized persons accessing the footbridge is given by

$$n' = \frac{10.8\sqrt{\xi \times n}}{S}\ [m^{-2}] \tag{3.12}$$

For cases of traffic classes TC4 and TC5 d≥1P/m^2)

$$n' = \frac{1.85\sqrt{n}}{S}\ [m^{-2}] \tag{3.13}$$

With

ξ structural damping ;

n Number os pedestains on the surface S(n=S*density);

S Loaded surface of the floor(according to some appraoches it dependes on mode shape of normal mode under consederation ,while other approaches consider the total loadable surface .

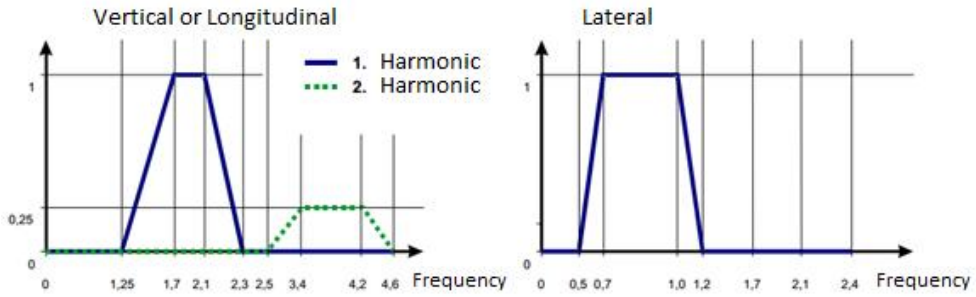

Figure 3.10-Reduction Factor, ψ(Setra, 2006)

3.6 Load model for joggers

The human ground reaction forces due to running are characterised by a lift-off phase, during which no foot is in contact with the ground. In comparison to walking the running induced forces depend more on the individual way of running and the type of shoes. That is the reason why this load model is very difficult to apply with currently used commercial structural analysis programs and may only be modelled by specialised software (e.g. ANSYS,DYNACS). The load model presented to the running movement consists of a single force that moves at a speed *v* whose value varies with time according to the following formula

$$P(v,t) = P * \cos(2\pi f t) \times n' \times \psi \tag{3.14}$$

$P * \cos(2\pi f t)$ is the harmonic action because of a single pedestrian running.

Where

P Force component in vertical, N/A for other directions, due to a single pedestrian with step frequency, f, P=1250N can be taken for design purposes according to human induced vibration of steel structure (HIVOSS)

f_s Natural frequency under consideration

n' Equivalent number of persons

ψ Reduction coefficient that takes into account the probability that the frequency of running approaches the critical frequency range into consideration

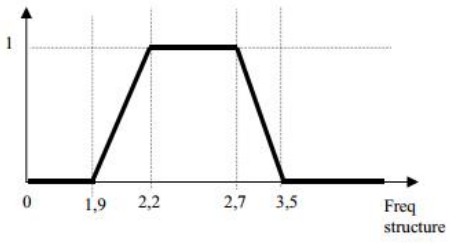

Figure 3.11-Reduction Factor, ψ, for running (Setra, 2006)

3.7 Sensitivity of pedestrians to vibrations of footbridges

Both vertical and horizontal vibrations can be considered as disturbing effects during traversing a footbridge and can therefore considerably influence the serviceability limit state condition. Perception of vibrations by humans is a rather complicated topic, as it has many influencing factors where human psychology plays an important role. Each person senses a vibration differently, but this is also dependent of the moment when the vibrations are perceived, the eventual sounds from the structure, e.g. music or even the height above the ground. Pedestrians can also get used to vibrations over the time and acceptance regarding to vibrations can rise.

It is important to distinguish the sensitivity in horizontal direction and vertical direction. Pedestrians are naturally much more sensitive to horizontal vibrations than to vertical ones. Therefore these two cases are being explained separately.

3.7.1 Sensitivity to vertical vibrations

Experiments have shown that pedestrians are more sensitive to vibration when standing still than when walking. Comfort criteria are being expressed by defining maximum limits of acceleration of the vibrations or corresponding speed and displacements can be used to define comfort. C.R.Smith investigated large amplitude vibrations which affected the normal walking considerably and found an upper bound of pedestrian tolerance. Vertical vibrations are especially sensible by pedestrians when the natural frequency of the bridge is higher than 4 Hz. [Iemke Roos, TUDelft, 2009]

3.7.2 Sensitivity to horizontal vibrations

Pedestrians are much more sensitive in horizontal direction (especially lateral) than in vertical direction. This is due to the fact that a person is more easily brought off balance with horizontal oscillations than with vertical ones. However, data on human perception of horizontal vibrations of bridges are scarce. Like for the vertical comfort criteria, the acceleration can be used to define a limit for the horizontal vibrations, but in this case with less threshold of acceleration.

Pedestrian tend to react differently in crowd situations than in normal situations. In crowd situations walking pedestrians have a lower standard for the lateral vibrations. Higher vibrations could then be permitted. Lateral vibrations are especially sensible by pedestrians when the lateral natural frequency of the bridge is below 2.5 Hz, more accurately below 1.2Hz. Accelerations of about 0.3 m/s² are clearly perceptible by pedestrians and can influence their walking behavior.

The lock-in trigger amplitude is expressed in terms of acceleration. Further frequency dependence could exist but has not been detected in measurements. Tests in France on a test rig and on the Passerelle Solferino indicate that a trigger amplitude of 0.1 to 0.15 m/s² exist when the lock-in phenomenon begin.

$$a_{lock-in} = 0.1 - 0.15\mathrm{m/s^2}$$ [Third International Footbridge Conference, Porto, Portugal]

On a different perspective, the research centered in the Millennium footbridge has led to an interpretation of lock-in as a phenomenon associated with the generation of a negative damping dependent on the number of pedestrians on the bridge. The triggering number of pedestrians for lock-in, that is the number of pedestrians N_L that could lead to a vanishing of the overall damping producing a sudden amplified response, has been defined as a function of the structural damping ratio ξ, of the modal mass m*, of the natural frequency f, and of a constant k as(HIVOSS),

$$N_L = \frac{8\pi\xi m^* f}{k} \tag{3.15}$$

On the basis of the Millennium footbridge tests, Dallard et al. derived the constant *k* to be approximately equal to 300 Ns/m over the range 0.5-1.0 Hz. Recent experiments on two footbridges in Coimbra and Guarda, Portugal have shown the adequacy of the Millennium formula to describe the triggering for lock-in. Amplitudes of acceleration of the order of 0.15-0.2 m/s^2 have been observed in correspondence, suggesting that the two approaches may be related. [Iemke Roos, TUDelft, 2009]

3.8 Comfort classes

The assessment of comfort classes is very delicate aspect which necessitate looking at vertical and lateral directions separately, and needs to consider the following minimally:

1. Number of people walking in the bridge
2. Frequency of walking
3. Height above ground
4. Position of human body (sitting, walking or running)
5. Harmonic or transient excitation characteristics
6. Transparency of the deck pavement and railing

Accelerations calculated should be checked for the assumed comfort level limit for acceleration.

Table 3.3-Comfort classes according to 3rd International Footbridge Conference, HIVOSS

Comfort class	Comfort Grade	a_{max}	
		Vertical	Horizontal
CL 1	Maximum	$< 0.5m/s^2$	$< 0.1m/s^2$
CL 2	Medium	$0.5 - 1m/s^2$	$0.1 - 0.3m/s^2$
CL 3	Minimum	$1 - 2.5m/s^2$	$0.3 - 0.8m/s^2$
CL4	Unacceptable	$> 2.5m/s^2$	$> 0.8m/s^2$

It should be noted that passing the footbridge with acceptable comfort classes 1-3 is possible. Table 3.3 shows that higher traffic density class can be acceptable for serviceability purposes under a lower comfort levels of acceleration as they are seldom in occurrence.

4

DYNAMIC CONTROL THROUGH TUNED MASS DUMPERS

4.1 Introduction

A passive tuned mass damper (TMD) is a structural dynamic response modification device composed essentially by a mass attached to the structure through spring and damper elements, tuned to a particular structural frequency of the footbridge. It is due to the damper that is possible to dissipate the energy of the system, which is accomplished whenever the mass of the TMD oscillates with no vanishing displacements or velocities relative to the primary system, enabling the transference of energy from the primary system to the TMD. Therefore, in order to obtain the maximum effectiveness of this control system, a careful tuning of TMD parameters has to be done. Since the mass of the TMD is usually much smaller than the structural mass, once excited, the TMD will resonate out of phase with the footbridge motion, i.e., the TMD mass oscillates in the opposite direction of the primary structure. This may generate large relative displacements between the two systems, so the possibility to accommodate the TMD system within the structure has also to be taken into account when designing it and the adverse effects of large relative displacements between the TMDs and primary structure should be assessed.

As mentioned earlier, the effectiveness of these types of devices is very much dependent on the frequency and device damping ratio assumed in its design, which depends, on the other hand, on the accuracy of the knowledge of the primary structure's dynamic characteristics in terms of mode shapes and frequencies which makes it sensitive in its implementation. This limitation can be overcome, or mitigated, by the use of multiple tuned mass dampers (MTMDs), which enables the control of more than one mode of a multi-degree-of-freedom structure by tuning each one of the TMDs to a specific mode shape, or by tuning the TMDs to frequencies in the vicinity of a mode of the primary system (S.S.Patil, S.B.Javheri, .G.Konapure,2012), effects of tuning in the vicinity versus mass addition in the modal modification criteria is assessed later in this paper. Additionally, OMA method can be adopted to find realistic modal estimates of the structure.

The TMD, even though being a simple physical system, can perform two important functions when attached to structures (Karoumi, 1998):

- It reduces the resonant response of the primary structure;
- Increases the overall damping of the structure through the attached dashpot, which provides an auxiliary source for energy dissipation

One of the main reasons for the increase of the dynamic response of a foot bridge is due to the resonant vibration caused by pedestrian traffic as the primary structure stiffness is commonly in the range of

frequency is 1-2Hz making it prone to small frequency excitation sources; it was decided to study the effectiveness of these systems to the control vibrations.

In the following sub-sections, the basic mathematical equations that govern the TMDs behavior are presented. The rules and design criteria commonly used aiming the optimization of these kind of devices are also discussed. One of these criteria was programmed in MATLAB, and a comparison between its results and those from other well-known equations was performed. Apart from that, the classical case of Frahm's Vibration Absorber Device is introduced. This device differs from the TMD as there no exists damper on the linkage between the masses. Simple expressions to achieve an optimal design for a TMD with vanishing structural damping, derived by Den Hartog and Ormondroyd (Hartog, 1947), are also presented.

4.2 Frahm's Vibration Absorber

To explore the concept of a tuned mass damper system, let us start by introducing the case of Frahm's dynamic absorber, patented by Frahm (1911).This simple system is composed of an undamped mass, $\mathbf{m_S}$, linked through a spring with stiffness $\mathbf{k_S}$ to an undamped structure of mass $\mathbf{m_P}$ and stiffness $\mathbf{k_P}$,as schematically represented on Figure 4.1. Frahm's dynamic absorber is presented here with the purpose of introducing the behavior of such a simple system, identifying some of the parameters that govern its performance. In strict sense, Frahm's dynamic absorber cannot be entitled as tuned mass damper, since no damping element is present; however, in this work the general term TMD is used in a broad sense, representing a secondary mass system linked to the primary system by a spring without the presence of a damper element.

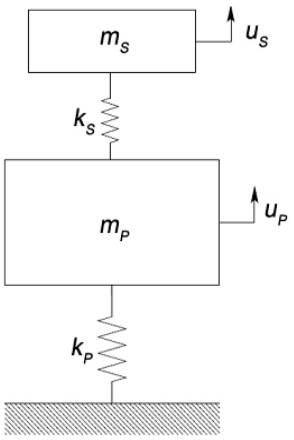

Figure 4.1-Frahm's vibration absorber

Let us consider a simple harmonic excitation force of frequency ω given by $F(t)=F_0 \sin(\omega t)$ applied in the primary mass and identify the vertical displacements as $u_P(t)$ and $u_s(t)$, respectively for the primary

and secondary masses. Hence, the governing equations of motion for the primary and secondary masses could be written as

$$m_p\ddot{u}_p(t) + \left(k_p + k_s\right)u_p(t) - k_s u_s(t) = F(t) \tag{4.1}$$

$$m_s\ddot{u}_s(t) + k_s u_s(t) - k_s u_p(t) = 0 \tag{4.2}$$

The complementary solution for the above differential equations is

$$u_p(t) = a_1 \sin(wt) \tag{4.3}$$

$$u_s(t) = a_2 \sin(wt) \tag{4.4}$$

Differentiating equations (4.3) and (4.4) twice with respect time and substituting back in to equations (4.1) and (4.2), these equations can be rewritten as

$$[a_1\left(-m_p w^2 + k_p + k_s\right) - a_2 k_s]\sin(wt) = F_o sin(wt) \tag{4.5}$$

$$[-a_1 k_s + a_2\left(-m_s w^2 + k_s\right)]\sin(wt) = 0 \tag{4.6}$$

The previous equations have to be satisfied for any time instant, t, and (non-trivial solution) thus, division by sin (ωt) can be performed in order to simplify both. In order to get a dimensionless form of equation, the following notations are introduced:

$u_{\boldsymbol{p}st} = \frac{F_0}{K_P}$ Static displacement of primary system

$w_{\boldsymbol{p}} = \sqrt{k_p/m_p}$ Natural frequency of primary system

$w_{\boldsymbol{s}} = \sqrt{k_s/m_s}$ Natural frequency of secondary system (damper)

$\mu = \frac{m_s}{m_p}$ Secondary to primary mass ratio

Substituting the above notations in equations (4.5) and (4.6), we obtain

$$a_1\left(1 - \frac{w^2}{w_p^2} + \frac{k_s}{k_p}\right) - a_2\frac{k_s}{k_p} = u_{\boldsymbol{p}st} \tag{4.7}$$

$$a_1 = a_2\left(1 - \frac{w^2}{w_s^2}\right)$$

Solving for a_1 and a_2,

$$\frac{a_1}{u_{\boldsymbol{p}st}} = \frac{\left(1-\frac{w^2}{w_s^2}\right)}{\left(1-\frac{w^2}{w_s^2}\right)\left(1-\frac{w^2}{w_p^2}+\frac{k_s}{k_p}\right)-\frac{k_s}{k_p}} \tag{4.8}$$

$$\frac{a_2}{u_{\boldsymbol{p}st}} = \frac{1}{\left(1-\frac{w^2}{w_s^2}\right)\left(1-\frac{w^2}{w_p^2}+\frac{k_s}{k_p}\right)-\frac{k_s}{k_p}} \tag{4.9}$$

It can be noted from equation (4.9) that when the excitation frequency (w) equals the frequency of the secondary system (w_s), the amplitude a_1 of the primary mass is zeroed while the amplitude of the secondary system a_2 reduces into

$$a_2 = -\frac{k_p}{k_s} u_{\boldsymbol{p}st} = -\frac{F_o}{k_s} \tag{4.10}$$

Equation (4.10) shows that with primary system having zero amplitude of vibration, the secondary system displaces in opposite direction to the sense of force. But, it is clear that the dynamic absorber is usefulness if restricted to conditions in which the primary system is in resonance with excitation or close to it. If this particular case of resonance is only considered,

$$w_p = w_s = \frac{k_p}{m_p} = \frac{k_s}{m_s} \Leftrightarrow \frac{k_s}{k_p} = \frac{m_s}{m_p} = \mu \tag{4.11}$$

Hence, equations (4.8) and (4.9) become

$$\frac{a_1}{u_{\boldsymbol{p}st}} = \frac{(1-\frac{w^2}{w_s^2})}{(1-\frac{w^2}{w_s^2})(1-\frac{w^2}{w_p^2}+\mu)-\mu} \tag{4.12}$$

$$\frac{a_2}{u_{\boldsymbol{p}st}} = \frac{1}{(1-\frac{w^2}{w_s^2})(1-\frac{w^2}{w_p^2}+\mu)-\mu} \tag{4.13}$$

For the case where any type of damping is considered in both systems, the design of the absorber passes only by choosing the values of the secondary mass ratio to the primary one and the stiffness of the absorber system. The natural frequencies of the new two degree-of-freedom system correspond to the values of ω_S that make the denominator of the two previous equations null is given by

$$\frac{w}{w_s} = \pm\sqrt{\left(1+\frac{\mu}{2}\right) \pm \sqrt{(\mu+\frac{\mu^2}{4})}} \tag{4.14}$$

Hence, the two degree-of-freedom system will have two frequencies, one lower and other greater than the original one. By including secondary mass system, the dynamic behavior of the primary system is modified, being possible, when no type of damping is considered, to cancel out the motion of the primary system, which corresponds to set the numerator of equation (4.12) to zero, obtaining

$$1-\frac{w^2}{w_s^2} = 0 \Leftrightarrow 1 = \frac{w^2}{w_s^2} \Leftrightarrow w_s = w = \sqrt{\frac{k_s}{m_s}} \tag{4.15}$$

Consequently, when the frequency of the absorber equals the frequency of excitation it is possible to completely suppress the primary mass motion. However, the range of frequencies that the excitation could assume, in order to avoid resonant behavior is narrow, as can be seen in Figure 4.2 where the modulus of the displacement transfer function for the primary system, $\left|G_P(r_p)\right| = \left|\frac{u_p}{u_{Pst}}\right|$, is represented for the case where no dynamic absorber is present and for the case where its mass ratio is equal to 0.05. The transfer function could alternatively be defined as the ratio between the response and force amplitudes, $\left|G'_P(r_p)\right| = \left|\frac{u_p}{F_0}\right| = \left|\frac{G_P(r_p)}{K_P}\right|$. Notice that r_P is defined as the ratio of the external excitation and primary system frequencies, as follows

$$r_p = \frac{w}{w_p} \tag{4.16}$$

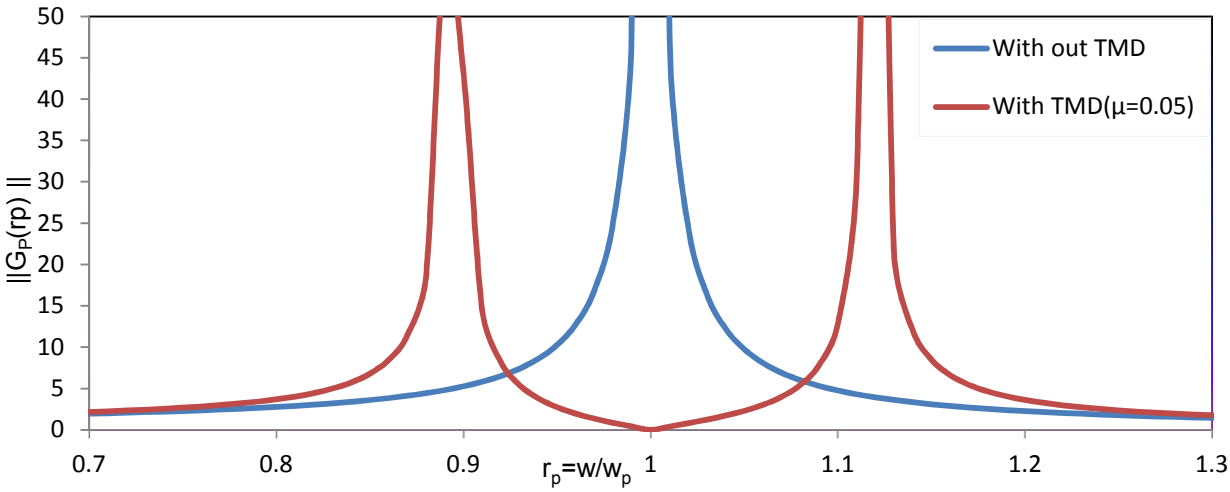

Figure 4.2-Amplitude of transfer function with TMD (μ=0.05) and without TMD

As expected, one can observe that the inclusion of a secondary mass generates two different new frequencies centered at the original natural frequency, and for an excitation with a frequency equal to the natural frequency of the primary system the motion of the primary mass is totally cancelled.

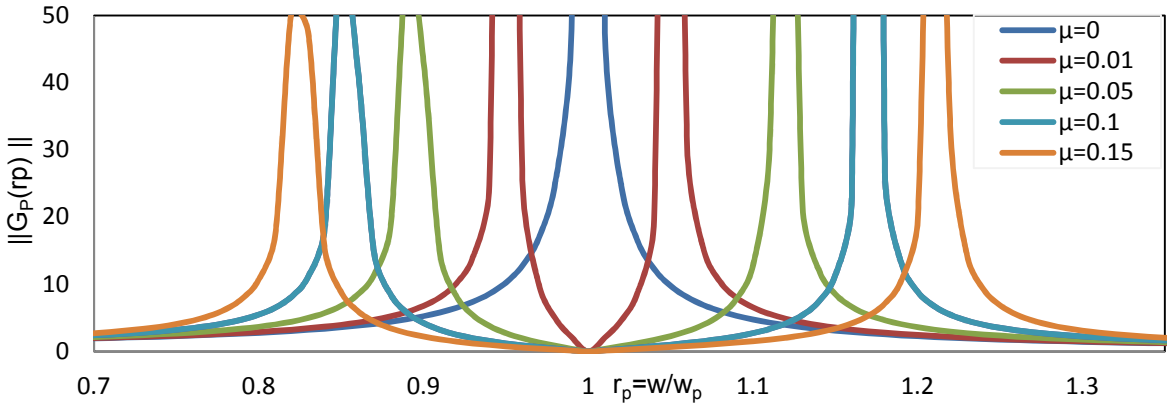

Figure 4.3-Amplitude of displacement transfer function for different mass ratios

Noting at the mass ratio effect on the system performance, through observation of Figure 4.3 one can conclude that with the increase of the mass ratio, the gap between the two new frequencies become larger improving the absorber effectiveness since the expected range of non-excitation frequencies is larger, which is not the case in pedestrian traffic. The ratio, q, is defined as follows

$$q = \frac{w_s}{w_p} \tag{4.17}$$

Thus the governing equation becomes

$$\frac{w}{w_p} = q\sqrt{\left(1+\frac{\mu}{2}\right) \pm \sqrt{\left(\mu+\frac{\mu^2}{4}\right)}} \tag{4.18}$$

Therefore, one can state that, if it was possible to create a system with total absence of damping, the mass ratio should be chosen in order to create a distance between the two new frequencies larger than the range of possible excitation frequencies. A system with these characteristics could be effective only when the frequency of the excitation force is nearly constant, as happens in the case of machinery directly coupled to synchronous electric motors or generators (Hartog, 1947). Obviously, that is not the case of footbridges subjected to a random vibration of constantly varying pedestrian traffic, where the excitation is not expressed by sum of harmonic forces.

Demonstration of frequency splitting is also done on FEM software, SAP2000, by considering a simply supported beam discretized in to 4 masses (half being at supports) as shown Figure 4.5, the total mass of the beam being 2 tons with the span masses located with quarter span spacing. And the same beam model is constructed in other SAP2000 file equipped with vibration absorber, the absorber being modeled with a linear spring link and mass at its end. The linear link is designed to have stiffness equivalent to first vertical mode of vibration of the beam without damper and free to move only in Uz (vertical axis) i.e. frequency of vibration absorber is set to 1st vertical mode (mode required to be suppressed).This is done by acquiring the fundamental vertical frequency and setting the mass of TMD as a ratio to the primary beam mass.

The demonstration of frequency splitting is also done on FEM software, SAP2000, by considering a simply supported beam discretized in to 4 masses (half being at supports) as shown Figure 4.4, the total mass of the beam being 2 tons with the span masses located with quarter span spacing. And the same beam model is constructed in other SAP2000 file equipped with vibration absorber, the absorber being modeled with a linear spring link and mass at its end. The linear link is designed to have stiffness equivalent to first vertical mode of vibration of the beam without damper and free to move only in Uz (vertical axis) i.e. frequency of vibration absorber is set to 1st vertical mode (mode required to be suppressed).This is done by acquiring the fundamental vertical frequency and setting the mass of TMD as a ratio to the primary beam mass. The mass of the absorber is set to a number of mass ratios (μ) to the simple beam mass as 10%, 15% and 20% one after the other and comparison between the amplitudes of vibration observed is presented in Table 4.1. As can be depicted from Figure 4.5, the first vertical mode is suppressed and it disappears in the modes list. The stiffness Ks is set as: $Ks = (2\pi * 6.715)^2 * m_s$, where m_s is percentage modal mass of primary structure.

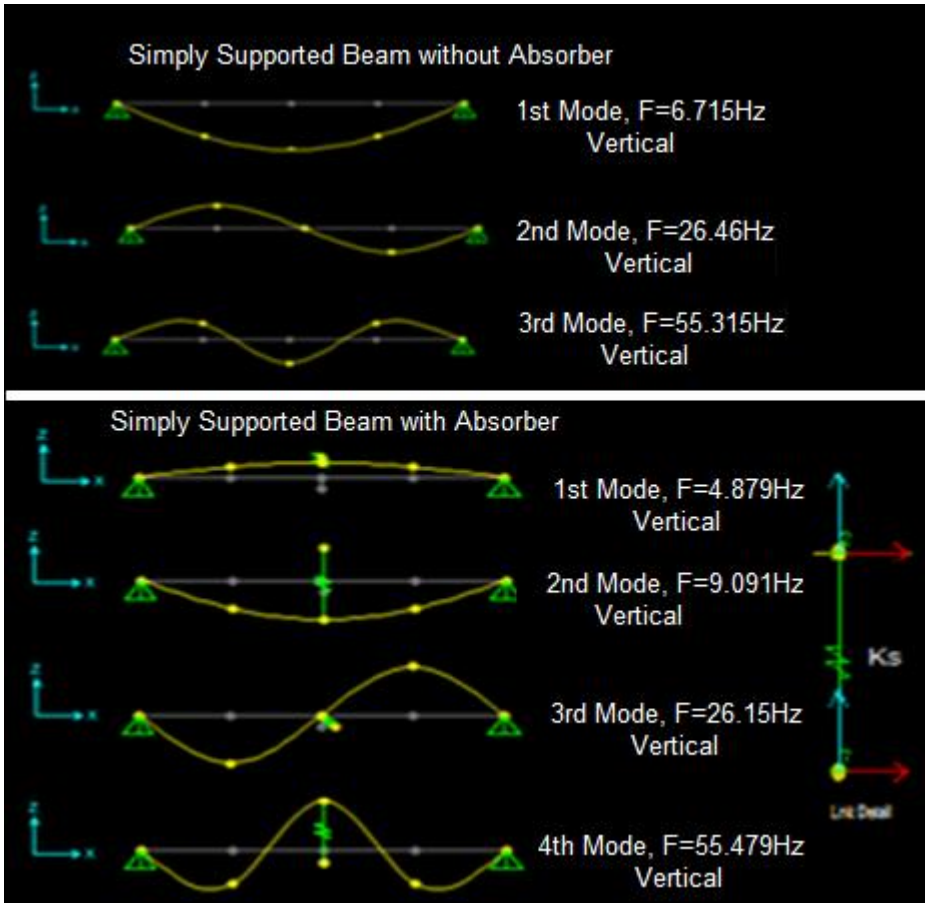

Figure 4.4-FEM model of a simply supported beam with absorber (bottom) and without absorber (top)

Table 4.1-simply supported beam FEM model with vibration absorber results

	1st Mode	2nd Mode	3rd Mode	4th Mode	|Max. Amplitude|	|Max. Relative displacement|
μ=0.2	4.879Hz	9.091 Hz	26.15 Hz	55.479 Hz	1.2715	1.707
μ=0.15	5.3367 Hz	9.63382 Hz	26.23 Hz	55.48 Hz	1.318	1.947
μ=0.1	5.8313 Hz	10.797 Hz	26.309 Hz	55.487 Hz	1.78	2.358

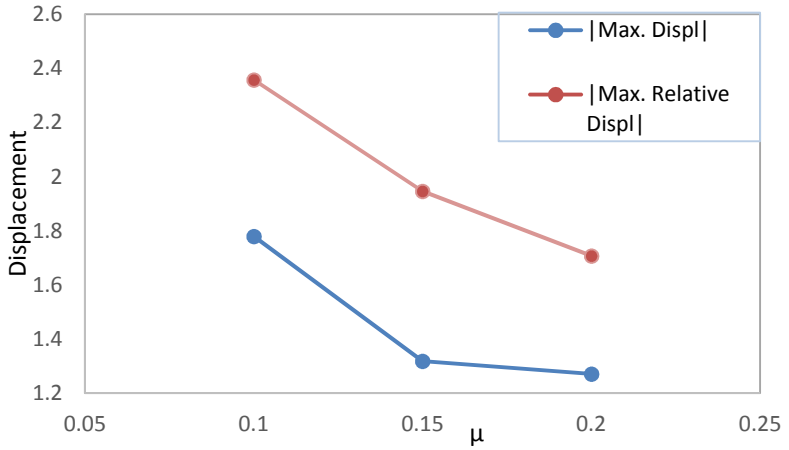

Figure 4.5-FEM beam model maximum displacement versus mass ratio of vibration absorber

It can be noted from Figure 4.5 and Table 4.1 with increase of mass ratio both maximum absolute displacement of the primary structure and absolute maximum relative displacement decreases. However, the mass ratio is always restricted by the structural capacity of the primary structure to support the additional mass and its gradient of change in reducing amplitude of vibration. More detailed explanation will be presented in the next sub-sections.

4.3 Equations of the Passive TMDs

Using the concept introduced through Frahm's Vibration Absorber, the governing equations of a general SDOF damped system associated to a tuned mass damper, represented in Figure 4.6, are now derived,

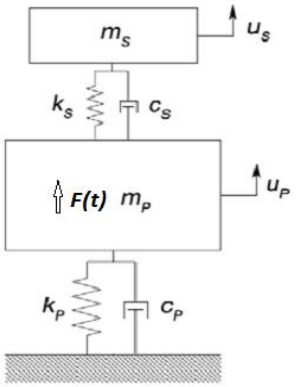

Figure 4.6-Frahm's vibration absorber

As with the case of undamped absorber, consider the system is subjected to a simple harmonic excitation of frequency ω expressed by F(t) = $F_0 e^{-it\omega}$, governing equation can be obtained by applying Newton's second law to each of the masses that make-up the system, leading to the following equations

$$m_p\ddot{u}_p(t) + (c_p + c_s)\dot{u}_p(t) - c_s\dot{u}_s(t) + (k_p + k_s)u_p(t) - k_s u_s(t) = F(t) \quad (4.19)$$

$$m_s\ddot{u}_s(t) + c_s\dot{u}_s(t) - c_s\dot{u}_p(t) + k_s u_s(t) - k_s u_p(t) = 0 \quad (4.20)$$

Above equations are for the primary and secondary systems respectively, where, $\ddot{u}_p(t)$, $\dot{u}_p(t)$ and $u_p(t)$ represent the vertical displacement, velocity and acceleration of the primary mass system, respectively, while $\ddot{u}_s(t)$, $\ddot{u}_s(t)$ and $u_s(t)$ represent the analogous variables of the secondary system.

In the case of a linear and time invariant system, the steady-state response is given by

$$u_p = u_{po}e^{-iwt} \quad (4.21)$$

$$u_s = u_{so}e^{-iwt} \quad (4.22)$$

Thus, replacing these expressions in equations (4.19) and (4.20) and simplifying, equations can be written as

$$[(-w^2m_p + (k_p + k_s) + iw(c_p + c_s)]u_{po} - (k_s + iwc_s)u_{so} = F_o \quad (4.23)$$

$$-(k_s + iwc_s)u_{po} + (-w^2m_s + iwc_s + k_s)u_{so} = 0 \quad (4.24)$$

Hence, solving the previous equations yields the solutions for the amplitudes of the primary and secondary masses, u_{P0} and u_{S0}, which respectively, can be expressed by

$$U_{po} = \frac{F_o}{D}(-w^2m_s + iwc_s + k_S) \quad (4.25)$$

$$U_{so} = \frac{F_o}{D}(iwc_s + k_S) \quad (4.26)$$

Where D is given by

$$D = \left[(k_p + k_s) - w^2m_p + iw(c_p + c_s)\right](-w^2m_s + iwc_s + k_S) - (iwc_s + k_S)^2 \quad (4.27)$$

The mass ratio of secondary to primary system, damping co-efficient of primary and secondary systems are defined as

$$\mu = \frac{m_s}{m_p} \tag{4.28}$$

$$\xi_p = \frac{c_p}{2w_p m_p} \tag{4.29}$$

$$\xi_s = \frac{c_s}{2w_s m_s} \tag{4.30}$$

Leading to the transformation of equations (4.25) and (4.26) in to

$$U_{po} = \frac{F_o}{m_p} \frac{(w_s^2 - w^2 + 2i\xi_s w_s w)}{(w_p^2 - w)(w_s^2 - w) - \mu w_s^2 w^2 - 4\xi_s \xi_p w_s w_p w^2 + iw\{2\xi_p w_p (w_s^2 - w^2) + 2\xi_s w_s [w_p^2 - w^2(1+\mu)\}} \tag{4.31}$$

$$U_{so} = \frac{F_o}{m_p} \frac{(w_s^2 + 2i\xi_s w_s w)}{(w_p^2 - w)(w_s^2 - w) - \mu w_s^2 w^2 - 4\xi_s \xi_p w_s w_p w^2 + iw\{2\xi_p w_p (w_s^2 - w^2) + 2\xi_s w_s [w_p^2 - w^2(1+\mu)\}} \tag{4.32}$$

In order to write equations (4.31) and (4.32) in a non-dimensional form, the variables r_P and q previously defined are substituted, transforming equations (4.31) and (4.32) into the following ones, respectively,

$$\frac{U_{po}}{F_0/K_p} = \frac{(q^2 - r_p^2) + 2i\xi_s q r_p}{(1-r_p^2)(q^2 - r_p^2) - \mu r_p^2 q^2 - 4\xi_s \xi_p q r_p^2 + i r_p \{2\xi_p (q_s^2 - r_p^2) + 2\xi_s q [1 - r_p^2 (1+\mu)\}} \tag{4.33}$$

$$\frac{U_{so}}{F_0/K_p} = \frac{q^2 + 2i\xi_s q r_p}{(1-r_p^2)(q^2 - r_p^2) - \mu r_p^2 q^2 - 4\xi_s \xi_p q r_p^2 + i r_p \{2\xi_p (q_s^2 - r_p^2) + 2\xi_s q [1 - r_p^2 (1+\mu)\}} \tag{4.34}$$

Similarly, the transfer function for the relative displacement can be written as the difference of the two above quantities, i.e $U_r = U_{so} - U_{po}$

$$\frac{U_r}{F_0/K_p} = \frac{q^2}{(1-r_p^2)(q^2 - r_p^2) - \mu r_p^2 q^2 - 4\xi_s \xi_p q r_p^2 + i r_p \{2\xi_p (q_s^2 - r_p^2) + 2\xi_s q [1 - r_p^2 (1+\mu)\}} \tag{4.35}$$

Which represent the non-dimensional complex displacement transfer functions for harmonic excitation of primary and secondary systems respectively and their amplitudes are given as follows

$$\left|G_P(r_p)\right| = \left|\frac{u_{po}}{F_O/K_P}\right| = \sqrt{\frac{(q^2 - r_p^2)^2 + (2i\xi_s q r_p)^2}{[(1-r_p^2)(q^2 - r_p^2) - \mu r_p^2 q^2 - 4\xi_s \xi_p q r_p^2]^2 + 4r_p^2 \{\xi_p (q_s^2 - r_p^2) + \xi_s q [1 - r_p^2 (1+\mu)\}^2}} \tag{4.36}$$

$$\left|G_s(r_p)\right| = \left|\frac{u_{so}}{F_O/K_P}\right| = \sqrt{\frac{q^4 + (2i\xi_s q r_p)^2}{[(1-r_p^2)(q^2 - r_p^2) - \mu r_p^2 q^2 - 4\xi_s \xi_p q r_p^2]^2 + 4r_p^2 \{\xi_p (q_s^2 - r_p^2) + \xi_s q [1 - r_p^2 (1+\mu)\}^2}} \tag{4.37}$$

$$\left|G_r(r_p)\right| = \left|\frac{U_r}{F_0/K_p}\right| = \sqrt{\frac{q^4}{[(1-r_p^2)(q^2 - r_p^2) - \mu r_p^2 q^2 - 4\xi_s \xi_p q r_p^2]^2 + 4r_p^2 \{\xi_p (q_s^2 - r_p^2) + \xi_s q [1 - r_p^2 (1+\mu)\}^2}} \tag{4.38}$$

4.4 Transfer Functions for Various External Excitations

The aforementioned equations (4.36) and (4.37) are the non-dimensional complex transfer functions, $G(r_p)$, derived considering harmonic excitations. Therefore, it is necessary to consider situations when it is desirable to find the optimal parameters of the TMD system to suppress the dynamic displacement of the structure (primary system). Following the procedure above described to derive the transfer function considering the displacement of the structure, similar expressions for other dynamic responses can be obtained. Table 4.2 presents some of these functions for harmonic excitations through the definition of A_k and B_k. Note that these non-dimensional complex transfer functions can be generally written as the ratio between two complex numbers, as follows

$$G_k(r_p) = \frac{A_k + iB_k}{C + iD} \tag{4.39}$$

Where C and D are given as

$$C = \left((1 - r_p^2)(q^2 - r_p^2) - \mu r_p^2 q^2 - 4\xi_s \xi_p q r_p^2\right) \tag{4.40}$$

$$D = r_p\{2\xi_p(q_s^2 - r_p^2) + 2\xi_s q[1 - r_p^2(1 + \mu)\} \tag{4.41}$$

The amplitude of $G_k(r_p)$ being

$$\left|G_k(r_p)\right| = \sqrt{\frac{A_k^2 + B_k^2}{C^2 + D^2}} \tag{4.42}$$

Table 4.2-Non-Dimensional Complex Transfer Functions (from Warburton, 1981)

Case	Excitation	Response parameter	$\left\|\boldsymbol{G_k(r_p)}\right\|$	$\boldsymbol{A_k}$	$\boldsymbol{B_k}$
1	$F_0 e^{-it\omega}$	u_p	$\frac{u_p K_P}{F_O}$	$q^2 - r_p^2$	$2\xi_s q r_p$
2	$F_0 e^{-it\omega}$	$\dot{u}_p$	$\frac{\dot{u}_p K_P}{F_O w_p}$	$-2\xi_s q r_p^2$	$r_p(q^2 - r_p^2)$
3	$F_0 e^{-it\omega}$	$\ddot{u}_p$	$\frac{\ddot{u}_p m_P}{F_O}$ or $\frac{\ddot{u}_p K_P}{F_O w_p^2}$	$-r_p^2(q^2 - r_p^2)$	$-2\xi_s q r_p^3$

4.5 Optimization Criteria for TMDs

Optimization, or tuning, of a TMD refers to the process of choosing the parameters that ascertains efficient operation of the system, such as the mass ratio, stiffness and damping. This procedure is important to achieve optimal performance of the structural system, since the efficient tuning of its parameters governs the dynamic response reduction capacity.

Besides the well-known and classic Den Hartog's optimal criterion for a SDOF undamped system, several other criteria have been proposed by various authors. However, most of these criteria present some

common points, all of them thrive to minimize the desired transfer functions (displacement, acceleration or velocity). Amongst these criteria, there are three common tuning approaches like the H_∞ and H_2 norm optimization and the Stability Maximization criteria. While the H_∞ and H_2 norm optimization intend to improve the steady state response of the primary system, the Stability Maximization criteria objective is the improvement of the transient vibration of the system. This is achieved through the maximization of the stability margin and robustness of the system, being a criterion suitable for situations when the input is not thoroughly known (Verdirame, 2003). In the following sections, the criterion related with the improvement of the steady-state response is briefly explained related to the nature of the case study.

4.5.1 H_∞ Optimization

The H_∞ norm tuning design is probably the most known optimization criterion, and aims to minimize the maximum response amplitude, also called as **H_∞** norm, under an external excitation.

Thus, for a SDOF system, **H_∞** optimization is achieved by determining the optimum parameters of the TMD for which the two peaks of the transfer function have the same height and, for which that height is the minimum possible.

Mathematically, the **H_∞** norm is defined by (Weber et al., 2006):

$$\left\|G_P(r_p)\right\|_\infty = \max(r_p)\left|G_P(r_p)\right| \tag{4.43}$$

H_∞ norm represents the maximum amplitude of the absolute value of the transfer function. The objective of this optimization criteria is to find the frequency ratio, q, and the damping ratio, ξ_S, for the TMD that minimizes $\left\|G_P(r_p)\right\|_\infty$ value:

$$\min(r_p,\xi_s)\left\|G_P(r_p)\right\|_\infty = Min(r_p,\xi_s)\max(r_p)\left|G_P(r_p)\right| \tag{4.44}$$

This minimum of $\left\|G_P(r_p)\right\|_\infty$ exists only if two local maxima exist, and both possess exactly the same amplitude. Den Hartog's fixed-points method (Den Hartog (1947)) for computing approximations of the optimal parameters q_∞ and ξ_∞ is based on the observation that for primary systems with vanishing damping ($\xi_P = 0$), there exist at least two frequencies $r_{p,1}$ and $r_{p,2}$ where $\left|G_P(r_p)\right|$ is invariant with respect to a variation of ξ_s,(q fixed) i,e $\frac{\left|G_P(r_{p,1})\right|}{\partial \xi_S} = \frac{\left|G_P(r_{p,2})\right|}{\partial \xi_S} = 0$.This is achieved by maximizing both points, $\left|G_P(r_{p,1})\right| = \left|G_P(r_{p,2})\right|$.This fixed points method account for the property that Den Hartog derived closed-form solutions for the case of an undamped structure. Since the derived method is based on the existence of two fixed points, without the use of the TMD damping, and this property in no longer valid in situations when the primary system is damped, as the primary damping destroys the fixed points.

Nevertheless, the expressions derived by Den Hartog could also be applied with accurate results for structures without vanishing damping, if the structural damping is small (ξ≤1%-2%, corresponding to 0.01≤μ≤0.1), as shown in section 4.6. Nevertheless, if the structural damping increases, it is necessary to

use a computational procedure to optimize the TMD parameters, or alternatively, apply other expressions (Asami et al., 2002;Asami and Nishihara, 2003; Warburton, 1982; Tsai and Lin, 1994) which gives exact closed form solutions for H∞. Their method is based on the observation of a function $\mathrm{H}(r_p) = \mathrm{h} - \left|G_P(r_p)\right|$ has two real roots $r_{p,1}\ and\ r_{p,2}$ of multiplicity of two if and only if,

$\mathrm{h} = \mathrm{h}_\infty = \min(r_p, \xi_s)\left\|G_P(r_p)\right\|_\infty$, where h is an arbitrary real constant.

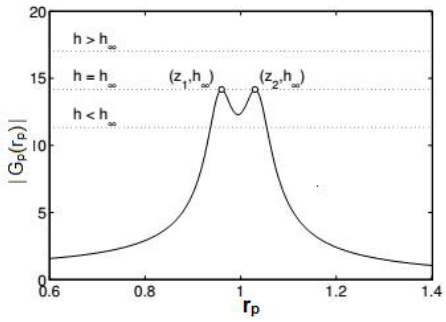

Figure 4.7-H∞ Optimization Criteria [Den Hartog]

The formulas are obtained by simplifying the exact solutions by using a rational functions approximation technique. The error of the formulas with respect to the exact solutions is smaller than 1% for μ≤ 0.1.

4.5.2 H_2 Optimization

The H_2 norm optimization criteria aim at the minimization of the total vibration energy in the system. If the system is subjected to a random, white noise excitation, the H_2 norm of the transfer function $G_P(r_p)$ is directly related to the variance of the output associated to the transfer function. That is in other words, to the minimization of the variance to a random white-noise excitation. Therefore, this criterion can be defined as (Weber et al, 2006)

$$\left\|G_P(r_p)\right\|_2 = \sqrt{\int_{t=-\infty}^{t=\infty}(\mathrm{G_p(t)})^2 \mathrm{dt}} \quad = \sqrt{\frac{1}{2\pi}}\sqrt{\int_{r_p=-\infty}^{r_p=\infty}\left|\mathrm{G_p(r_p)}\right|^2 \mathrm{dr_p}} \tag{4.45}$$

Which represents a measure of the area comprised between the square of the absolute value of the transfer function, $\left|\mathrm{G_p(r_p)}\right|^2$, and the horizontal axis, r_P. Notice that, for this reason, when the H_2 norm optimization is considered, there exists only one maximum of the transfer function and not two as for the H∞ norm optimization criterion. Generally, closed form expressions of $\left\|G_P(r_p)\right\|_2$ can be obtained by evaluating the integral in equation 4.45(Crandall and Mark (1963)) or by computing the observability grammian of the linear system described by the transfer function $G_P(r_p)$.

H_2 norm optimization criterion aims at the determination of the frequency ratio, q, and the damping ratio, ξ_S, for the TMD that minimizes $\left\|G_P(r_p)\right\|_2$, and is obtained from

$$\min_{q,\xi_s} \left\|G_P(r_p)\right\|_2 = \min_{q,\xi_s}\sqrt{\frac{1}{2\pi}}\sqrt{\int_{r_p=-\infty}^{r_p=\infty}\left|\mathrm{G_p(r_p)}\right|^2 \mathrm{dr_p}} \tag{4.46}$$

Minimization of $\left\|G_P(r_p)\right\|_2$can be achieved by

$$\frac{\partial \|G_P(r_p)\|_2}{\partial q} = 0 \; and \; \frac{\partial \|G_P(r_p)\|_2}{\partial \xi_s} = 0 \tag{4.47}$$

These conditions are usually sufficient and yields two nonlinear equations defining the optimal parameters q_2 and $\xi_{s,2}$.

Exact closed form solutions have been obtained for systems with vanishing structural damping (ξ_p) which can be used under different excitation sources. For primary systems with structural damping, accurate closed form expressions can be obtained in form of a power series with respect to the damping ratio ξ_p. In general, the optimal parameters with respect to the H_2 norm are less sensitive to structural damping ξ_p than the optimal parameters with respect to the H_∞ norm. For small mass ratios, the optimal damping ratio $\xi_{s,2}$ which minimizes the variance of the displacement of the primary system with respect to the H_2 norm is virtually independent of the structural damping.

Finally, several optimization procedures are available from several authors who developed numerical, power series or exact solutions for optimization of dynamic systems with respect to the H_2 norm.

4.6 Single Degree-of-Freedom Systems with TMDs

4.6.1 TMD linked to an Undamped System and optimized tuning of TMDs

For structural damping $\xi_P \leq 1\%$-2%, one can approximately consider that no structural damping exists, disregarding thus its contribution to the dynamic analysis of the system. Results will indicate that for structures with small damping the error here introduced is negligible. As shown later, in this case and contrary to what happens with Frahm's Vibration Absorber, the motion of the primary system could not be completely suppressed, but only reduced. However, it presents the advantage of avoiding the possibility of peak motion amplitudes during resonance conditions as happens for the case where no damping in the TMD is considered.

For the case studied in this section, the amplitude of the transfer function of the SDOF system displacement, as derives in the previous section, subjected to a harmonic excitation can be written as follows

$$\left|G_P(r_p)\right| = \left|\frac{u_{po}}{F_O/_{K_P}}\right| = \sqrt{\frac{(q^2-r_p^2)^2+(2\xi_s q r_p)^2}{[(1-r_p^2)(q^2-r_p^2)-\mu r_p^2 q^2]^2+4r_p^2\{\xi_s q[1-r_p^2(1+\mu)\}^2}} \tag{4.48}$$

This function depends on four variables, q, μ, ξ_S and r_P, previously defined. Figure 4.8 represents the amplitude of the transfer function of the primary system displacements versus the ratio of the excitation frequency to primary mass natural frequencies, r_P, and the damping ratio, ξ_S, for μ = 0.2 and q = 0.90. Similarly, Figure 4.9 presents the same function but for q =0.8.The observation of such plots shows that the optimal value for the frequency ratio, for a given mass ratio, that minimizes the amplitude of the transfer function values varies between q = 0.90and q = 0.8 (which can be noted from a graph showing the variation of the amplitude of the primary mass displacement function reaching maximum value at $r_p \approx 0.76$, as shown in Figure 4.8).

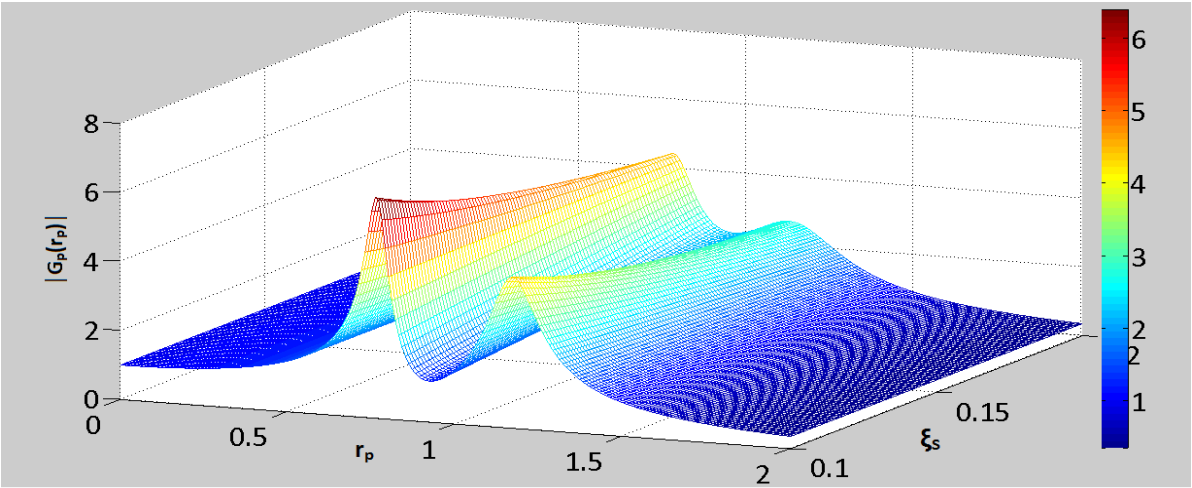

Figure 4.8-Displacement Transfer Function for q=0.9 and μ = 0.2 (ξ_p=0).

It is important to point out that for a given value of q all the lines cross each other on the same points, independently of the value of ξ_S, which not obvious in Figure 4.8, so, two-dimensional representations of the amplitude of the displacement transfer function for several damping ratios are plotted as a function of r_P as shown in Figure 4.10. Plot (a) is for q = 0.9 while in plot (b) q = 0.8. This well-known characteristic of fixed points P and Q independently of the damping was the basis for the derivation of Den Hartog's optimum tuning conditions for TMD devices linked to undamped structures. A concise explanation about the procedure followed by this author to derive the optimal parameters is here referred. For a more detailed explanation, reader is advised to refer the comprehensive book (Den Hartog, 1947).

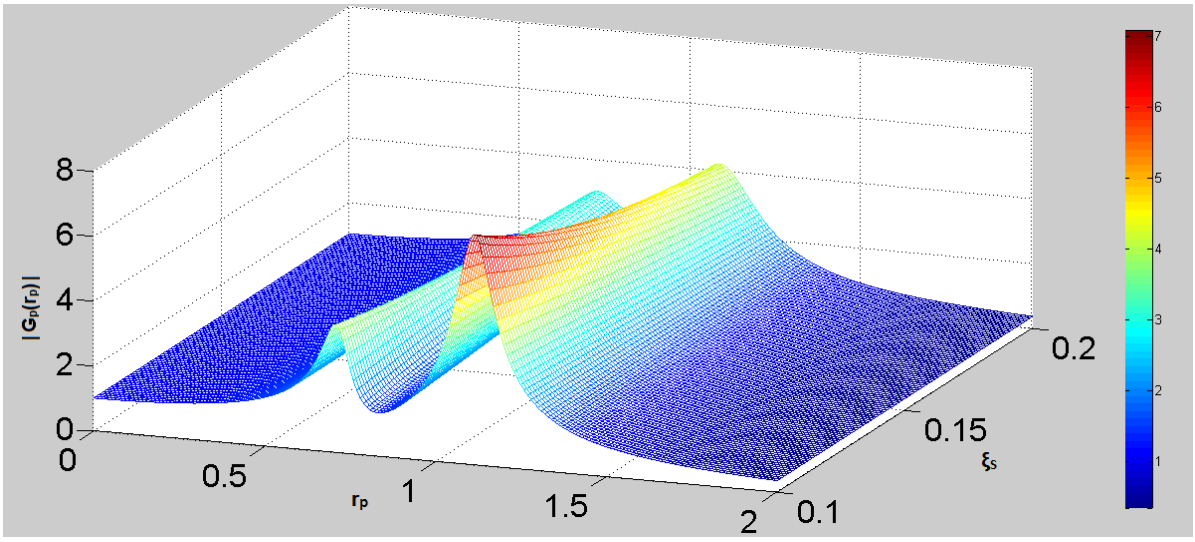

Figure 4.9-Displacement Transfer Function for q=0.8 and μ = 0.2 (ξ_p=0).

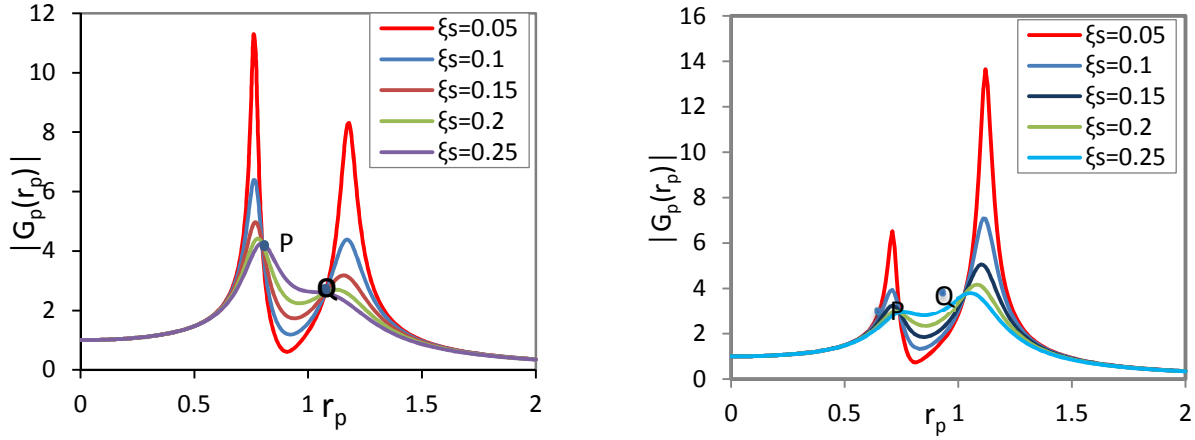

Figure 4.10-Transfer Function for undamped system (a) q=0.9 and (b)=0.8 for various of ξ_S

To find the optimum parameters that minimize the response of the combined system, it is necessary to start with a proper choice of the frequency ratio, q, setting thus the two fixed points to the same height, independently of the damping coefficient, ξ_S, and, subsequently, to select the damping coefficient that makes the curve pass with a horizontally tangent through one of them. Notice that, rigorously, if the two fixed points possess the same ordinate, the curve must pass with a horizontally tangent on both points

Implementing the above described procedure according to Den-Hartog, one can present the optimum parameters for a TMD associated to an undamped system,

$$q_{opt} = \frac{1}{1+\mu} \tag{4.49}$$

$$\xi_{opt} = \sqrt{\frac{3\mu}{8(1+\mu)}} \tag{4.50}$$

But according to Den Hartog's textbook (Hartog, 1947), the optimum damping ratio is defined as

$$\xi_{opt}^{DH} = \sqrt{\frac{3\mu}{8(1+\mu)^3}} \tag{4.51}$$

However, for this author the damping ratio is established as the ratio between the effective damping and the critical damping, defined as

$$c_c^{DH} = 2m_s w_p \tag{4.52}$$

Where as in this dissertation context the critical damping is assumed as $c_c = 2m_s w_s$, being thus only dependent of TMD properties.

We know that $\xi^{DH} = \alpha\xi$, where $\alpha = {}^{w_s}/_{w_p} = q$ and $\xi = {}^{c_s}/_{2m_s w_s}$ .Therefore, it can be verified that,

$$\xi_{opt}^{DH} = \alpha_{opt}\xi_{opt} = q_{opt}\xi_{opt} = \frac{1}{1+\mu}\sqrt{\frac{3\mu}{8(1+\mu)}} = \sqrt{\frac{3\mu}{8(1+\mu)^3}} \tag{4.53}$$

Given the above optimum parameters and considering resonance condition, the amplitude of the transfer function is obtained by

$$\left|G_P(r_p)\right| = \sqrt{\frac{2+\mu}{\mu}} \tag{4.54}$$

Figure 4.11 shows the transfer function for the primary mass displacement for a mass ratio of 0.20(very high for practical purposes), where the optimum parameters have been determined through Den Hartog's optimal criterion discussed above. In order to emphasize the optimization effect on the effectiveness of TMDs, on the same plot, curves for other non-optimal frequency ratios but with optimal damping are also represented.

It can be noted that with a variation of ±5% around *qOPT*, the maximum amplitude of the transfer function increase about 30% or more. Moreover, for frequency ratios different from the optimum value, the peaks of the amplitude of transfer function are considerably different from each other, one of them being higher than the other. Furthermore, this increase is more severe as the drift from *qOPT* is larger, which leads to a great loss on the efficiency of this passive system. Therefore, it is essential that a correct tuning of frequency should be made.

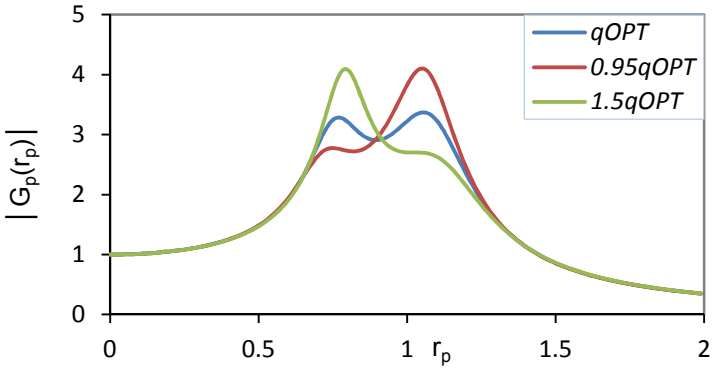

Figure 4.11-Transfer Function for *qOPT*, *0.95qOPT* and *1.05qOPT* (ξ_p=0)

In the previous plot, the optimum characteristics were defined according with expressions developed by Den Hartog, which consists on an approximate H_∞ norm optimization. Nevertheless, Den Hartog expressions do not lead to the exact H_∞ norm optimum design, as long as the ordinate of the two fixed points is not the same which is prevalent in damped primary system.

The sensitivity of this system to the TMD damping ratio (ξ_S) drift from the optimum value is also analyzed for the same value of the mass ratio. Figure 4.12 represents this variation and it can be deduced that effectiveness of the TMD is not as sensitive to variations in this parameter as to variations in the frequency ratio. Thus less importance is given to de-tuning related to damping issues.

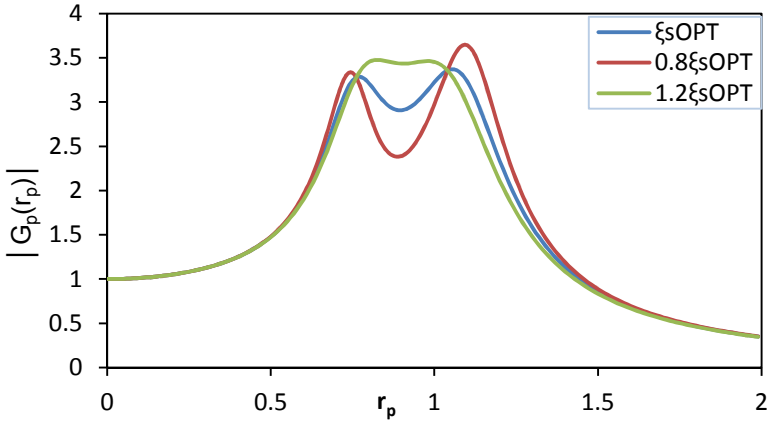

Figure 4.12-Transfer Function for $\xi_{S,OPT}$, $0.80\xi_{S,OPT}$, and $1.20\xi_{S,OPT}$(ξ_p=0)

Actually, if the damping ratio increases considerably, the transfer function presents only one peak, disappearing the local minimum, shown above, which is expected to happen, if one takes into account the physical meaning of the damping ratio leading to a conclusion that as this ratio goes extremely large, the TMD loses its efficiency as it vibrates in association with the structure as a SDOF system with a total mass equal to the sum of the two systems, losing thus the concept that is introduced by this system.

Similarly, trying to investigate the importance of the mass ratio, μ, variation impact on the transfer function, it can be clearly seen that mass ratio plays an important role which is shown in the Figure 4.13.

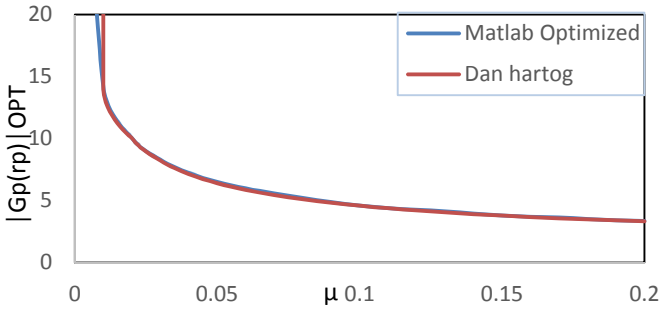

Figure 4.13-Amplitude of the Transfer Function variation with mass ratio μ (ξ_p=0).

Figure 4.13 shows that that the transfer function decreases significantly with increasing mass ratio and Comparison between the MATLAB programmed optimized values and Dan Hartog's recommendation is done, it can be seen from the Figure 4.13 that the two methods yield almost the same results with minor difference for small values of mass ratios, μ, implying that Den Hartog optimized parameters expression for TMD attached to undamped primary structure can be used with sufficient accuracy. Increase of TMD mass is efficient in the range of 0.02-0.05 mass ratios while further increase has less relevance in reducing the response as it can be depicted from Figure 4.13. Tabular comparison is provided at the end of this topic.

The increase with increasing mass ratio is particularly strong for small structural damping. In the range of practically realizable mass ratios, a TMD provides good performance only for lightly damped structures ($\xi_p \leq 0.01$).The observation of the Figure 4.13 leads to the conclusion that for small mass ratios the effective range of applicability of the TMD is limited for two reasons. The first is due to the impossibility to adapt to structural frequencies changes and the second is the impracticality to accommodate the TMD displacements in the available space within the structure (may go excessive). Nevertheless, this parameter is not usually chosen through any type of the optimizations described in section 4.5, but by evaluating the bridge capacity supplemented by economic considerations.

Table 4.3-Comparison between optimized values from Den Hartog criteria and MATLAB program

Undamped ($\xi_P \approx 0\%$)	**Dan Hartog criteria**			**Numerically Optimized solution**		
μ	q_{OPT}^{DH}	ξ_{OPT}^{DH}	$\left\|G_P(r_p)\right\|_{DH}^{OPT}$	q_{OPT}^{DH}	ξ_{OPT}^{DH}	$\left\|G_P(r_p)\right\|_{\infty}^{OPT}$
0.02	0.9803	0.08575	10.049	0.990	0.090	10.065
0.05	0.9523	0.13363	6.4031	0.950	0.140	6.449
0.1	0.9090	0.18463	4.5825	0.910	0.210	4.596
0.15	0.8695	0.22116	3.7859	0.870	0.250	3.795
0.2	0.8333	0.25000	3.3166	0.830	0.290	3.365

4.6.2 TMD Attached to a Damped System and optimized tuning of TMDs

The displacement transfer function of the primary structure for the case when the structure has non-vanishing damping was derived in previous section. The correspondent amplitude is given by

$$\left|G_P(r_p)\right| = \left|\frac{u_{po}}{F_O/K_P}\right| = \sqrt{\frac{(q^2-r_p^2)^2+(2\xi_s q r_p)^2}{[(1-r_p^2)(q^2-r_p^2)-\mu r_p^2 q^2-4\xi_s\xi_p q r_p^2]^2+4r_p^2\{\xi_p(q_s^2-r_p^2)+\xi_s q[1-r_p^2(1+\mu)\}^2}} \quad (4.55)$$

As in the case of an undamped structure, the frequency ratio and the mass ratio of the TMD are the most important parameters on the TMD design procedure, leaving its damping ratio to a secondary role, since differences in the damping ratio in relation to the optimal value do not lead to important variations on its effectiveness.

Analogous to the previously presented description of undamped structure, the frequency ratio, q, and the mass ratio of the TMD, μ, are the most important parameters on the TMD design procedure, its damping ratio being less important, since differences in the damping ratio in relation to the optimal value do not lead to significant variations on its effectiveness. It should be noted here that the ultimate use of damping in TMD is mainly to reduce its displacement as a result of the energy transferred from the structure.

Hence, the available space allowed for installation of TMD will govern the amount of TMD damping coefficient that should be adopted, but without greatly affecting the response of the primary system. Also, substituting one TMD mass by several smaller masses may result in increased TMD displacement.

In a similar manner the modulus of the transfer function is plotted on a grid mesh for μ=0.2, ξ_s=0.2 and q=0.9.

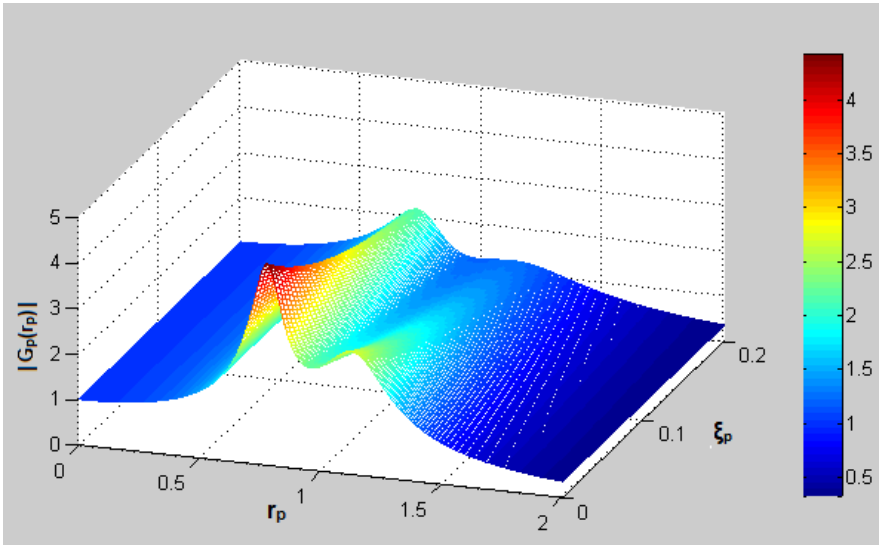

Figure 4.14-Modulus of the Transfer Function as function of ξ_P

When non-vanishing structural damping is considered, the concept of fixed points used by Den Hartog to derivate optimum criterion is not valid anymore. Nevertheless, in the range of small structural damping ratios, these expressions could be applied without loss of accuracy as mentioned above. To illustrate this amplitude of the displacement transfer function of for a structural damping ratio ξ_P of 1% and 5%, respectively, is plotted with different TMD damping ratios. It is evident that, when ξ_P=1% the various curves almost appear to cross each other on the same point, while for ξ_P = 5% curves move away from each other which indicates, we can fairly consider primary damping ratios below 5% as that of undamped structural system simplifying the problem.

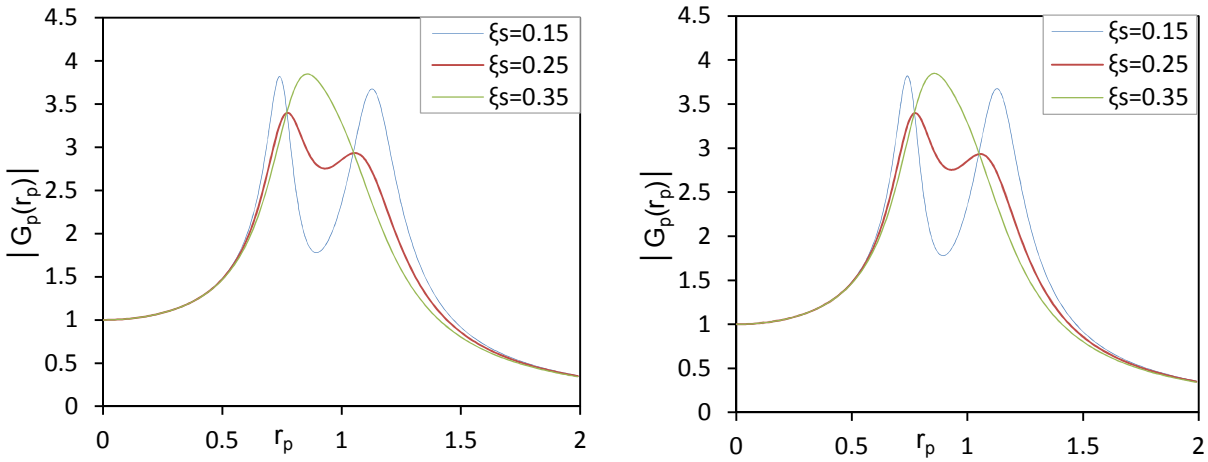

Figure 4.15-Amplitude of the Transfer Function (left) for ξP=1% and (right) for ξP=5% (μ = 0.2)

Furthermore, to check the range of applicability of Den Hartog's optimum criterion derived for vanishing structural damping, a comparison was performed between the values obtained by those expressions and those calculated through the numerical procedure programmed in MATLAB.

Through analysis of Table 4.4 and Table 4.5, one can conclude that with the increase of the structural damping ratio, the difference between the values determined by Den Hartog's expressions and those calculated numerically rises. Nevertheless, for small structural damping ratios the difference is small, and, therefore, these expressions could be applied without significant loss of accuracy.

Table 4.4-Comparison between Den Hartog and Numerically optimized values for ξP=1%

ξP=1%	**Den Hartog criteria**			**Numerically Optimized solution**		
μ	q_{OPT}^{DH}	ξ_{OPT}^{DH}	$\left\|G_P(r_p)\right\|_{DH}^{OPT}$	q_{OPT}^{DH}	ξ_{OPT}^{DH}	$\left\|G_P(r_p)\right\|_{\infty}^{OPT}$
0.02	0.9803	0.08575	8.6890	0.98	0.09	8.695
0.05	0.9523	0.13363	5.8690	0.95	0.15	5.802

0.1	0.9090	0.18463	4.3370	0.91	0.22	4.596
0.15	0.8695	0.22116	3.6350	0.87	0.26	3.367
0.2	0.8333	0.25000	3.2120	0.83	0.30	3.173

Table 4.5-Comparison between Den Hartog and Numerically optimized values ξ_P=5%

ξ_P=5%	**Den Hartog criteria**			**Numerically Optimized solution**		
μ	q_{OPT}^{DH}	ξ_{OPT}^{DH}	$\lvert G_P(r_p)\rvert_{DH}^{OPT}$	q_{OPT}^{DH}	ξ_{OPT}^{DH}	$\lvert G_P(r_p)\rvert_{\infty}^{OPT}$
0.02	0.9803	0.08575	5.6275	0.97	0.10	5.140
0.05	0.9523	0.13363	4.4076	0.94	0.16	4.212
0.1	0.9090	0.18463	3.5598	0.89	0.23	3.359
0.15	0.8695	0.22116	3.1168	0.85	0.27	2.953
0.2	0.8333	0.25000	2.8320	0.81	0.32	2.664

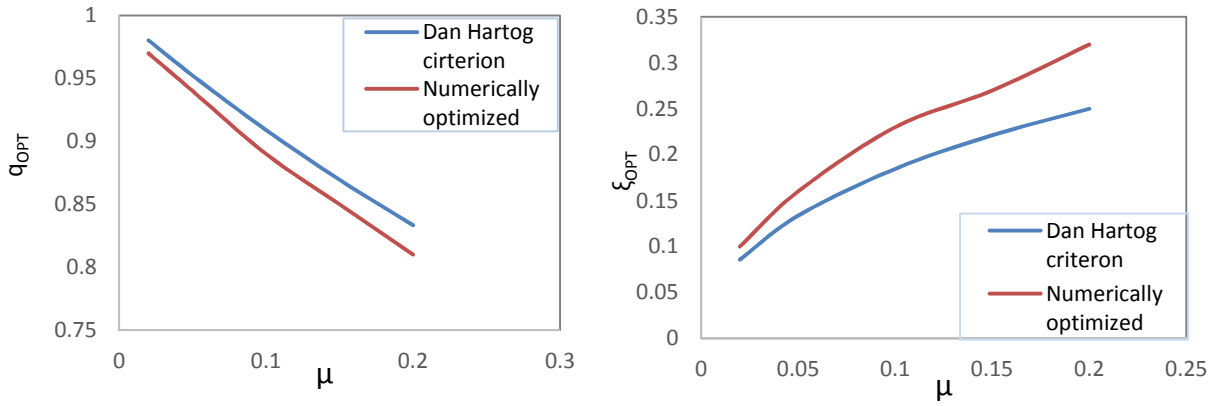

Figure 4.16-Den Hartog versus Numerical solution comparison for optimized values a) frequency ratio, b) damping ratio

Table 4.4 and 4.5 clearly shows the effect of increased damping of a structure on the accuracy of Den Hartog criterion. Thus, for structures with damping higher than 5% Den Hartog method is not recommended.

To conclude, the numerically optimized parameter for Damping is higher than that of the Den Hartog criterion. In the other hand, Den Hartog criterion for optimization demands a bit higher stiffness of TMD as compared to numerical solution.

4.7 Multi Degree-of-Freedom Systems with TMDs

SDOF structure assumption for the primary structure is a simplification by considering the mass to be concentrated on one point which is not the real case. Thus, TMD attached to MDOF can be considered in order to actually simulate the distributed mass of primary system. [According to João Francisco, IST, 2007].

Nevertheless, since the TMD is designed to work properly only to a specific vibration mode of the structure, being thus effective in a narrow frequency band, its concept can easily be extended to MDOF structures making it possible to design independent TMDs in which each TMD will mitigate the vibration of a specific vibration mode. Note that this consideration can only be applied if the structure yields well-spaced natural frequencies and, of course, if the structure presents a linear elastic behavior.

A procedure similar to the one followed in a general SDOF system can be applied to achieve the equilibrium equations for a N degree-of-freedom structure to which a TMD is attached to the nth degree-of-freedom, resulting thus in N dynamic equilibrium equations, that can be written as follows

$$\boldsymbol{M_p}\ddot{U}_p(t) + \boldsymbol{C_P}\dot{U}_p(t) + \boldsymbol{K_P}U_p(t) = \boldsymbol{F}(t) + \left(c_s\left(\dot{u}_s(t) - \dot{U}_{p,K}(t)\right) + k_s(u_s(t) - U_{p,K}(t))\right)\boldsymbol{E_K} \quad (4.56)$$

$$m_s\ddot{u}_s(t) + c_s\dot{u}_s(t) - c_s\dot{U}_{p,K}(t) + k_s u_s(t) - k_s U_{p,K}(t) = 0 \quad (4.57)$$

where $\boldsymbol{M_p}$, $\boldsymbol{C_P}$ and $\boldsymbol{K_P}$ denotes the mass, damping and stiffness matrices of the structure respectively, and $\boldsymbol{E_K}$ stands for the column vector filled with zeros, but with a unitary value in the kth row. The acceleration, velocity and displacements vectors of the structure are designated by $\ddot{U}_p$, $\dot{U}_p$ and U_p respectively, while $\dot{U}_{p,K}$ and $U_{p,K}$ represents the velocity and displacement of the structure of the kth degree-of-freedom of the structure (where the TMD is placed) and $\ddot{u}_s$, $\dot{u}_s$ and u_s stands for the acceleration, velocity and displacements vectors of the TMD. Finally, the force vector is designated by **F**.

It can emphasize here that the need for consideration of relative movement between the two systems as it defines the efficiency of the TMD in alleviating the vibratory motion. Thus,

$$u_r(t) = u_s(t) - U_{p,K}(t) \quad (4.58)$$

$u_r(t)$ being the relative displacement of the TMD mass with respect to the displacement of the kth degree-of-freedom of the structure .Therefore equations (4.56) and (4.57) can be rearranged as

$$\boldsymbol{M_p}\ddot{U}_p(t) + \boldsymbol{C_P}\dot{U}_p(t) + \boldsymbol{K_P}U_p(t) = \boldsymbol{F}(t) + \left(c_s(\dot{u}_r(t)) + k_s(u_r(t))\right)\boldsymbol{E_K} \quad (4.59)$$

$$m_s\ddot{u}_s(t) + c_s\dot{u}_r(t) + k_s u_r(t) = 0 \quad (4.60)$$

The solution to the above problem can be attained by superposition method of modal analysis given by

$$U_p(t) = \sum_{i=1}^{N} \phi_i \, u_i(t) = \boldsymbol{\phi} u_p \tag{4.61}$$

Where φ is a matrix of dimension N×N that contains N spatial vectors which are independent of time and each column vector represents the mode shape in each mode. Pre-multiplying equation (4.60) by the φ^T and substituting equation (4.61) in to equation (4.60), we arrive at

$$\boldsymbol{m_p}\ddot{u}_p(t) + \boldsymbol{c_P}\dot{u}_p(t) + \boldsymbol{k_P}u_p(t) = \boldsymbol{\phi}^{\mathrm{T}}\boldsymbol{F}(t) + \left(c_s(\dot{u}_r(t)) + k_s(u_r(t))\right)\boldsymbol{\phi}^{\mathrm{T}}\boldsymbol{E_K} \tag{4.62}$$

where $\boldsymbol{m_p} = \boldsymbol{\phi}^{\mathrm{T}}\boldsymbol{M_p}\boldsymbol{\phi}$, $\boldsymbol{c_P} = \boldsymbol{\phi}^{\mathrm{T}}\boldsymbol{C_p}\boldsymbol{\phi}$ and $\boldsymbol{k_P} = \boldsymbol{\phi}^{\mathrm{T}}\boldsymbol{K_p}\boldsymbol{\phi}$

Moreover equation (4.60) can be written as a function of relative displacements which enables us to express in terms of stroke of the TMD.

$$m_s\ddot{u}_r(t) + c_s\dot{u}_r(t) + k_s u_r(t) = -m_s\ddot{U}_{p,K}(t) \tag{4.63}$$

Substituting $\ddot{U}_{p,K}(t) = E_K^T \boldsymbol{\phi}\ddot{u}_p$(t) in to equation (4.63),

$$m_s\ddot{u}_r(t) + c_s\dot{u}_r(t) + k_s u_r(t) = -m_s\boldsymbol{E_K^T}\boldsymbol{\phi}\,\ddot{u}_p(\mathrm{t}) = -m_s\,\boldsymbol{\phi_k}\ddot{u}_p(\mathrm{t}) \tag{4.64}$$

As stated in the previous sections a passive TMD is designed to be effective only for a specific mode of vibration of the structure. As far as a single TMD can only be tuned to a single mode shape of the structure, if it is intended to control the *i*th mode shape of the structure and considering only the contribution of the *i*th mode shape can be expressed since each multi–degree freedom is decoupled in to NSDOF equations Thus, the SDOF equation of motion at i^{th} degree of freedom can be written as

$$\boldsymbol{m_{p,i}}\ddot{u}_{p,i}(t) + \boldsymbol{c_{P,i}}\dot{u}_{p,i}(t) + \boldsymbol{k_{P,i}}u_{p,i}(t) = \boldsymbol{f_i}(t) + \left(c_s(\dot{u}_r(t)) + k_s(u_r(t))\right)\boldsymbol{\phi_{k,i}} \tag{4.65}$$

Where
$$\boldsymbol{f_i}(t) = \boldsymbol{\phi_i}^{\mathrm{T}}\boldsymbol{F}(t) \tag{4.66}$$

$$m_s\ddot{u}_r(t) + c_s\dot{u}_r(t) + k_s u_r(t) = -m_s\,\boldsymbol{\phi_{k,i}}\ddot{u}_{p,i}(\mathrm{t}) \tag{4.67}$$

Where $\boldsymbol{f_i}(t)$ represents the force at *i*th degree of freedom and $\boldsymbol{\phi_{k,i}}$ identifies the displacement of $\mathbf{k^{th}}$ degree of freedom due to *i*th mode.

Normalizing the vector $\boldsymbol{\phi_i}$ by the mass matrix it presents a unitary value on the $\mathbf{k^{th}}$ row, $\boldsymbol{\phi_{k,i}} = \mathbf{1}$, allowing equations (4.65) and (4.67) to be written, respectively, as:

$$\boldsymbol{m_{p,i}}\ddot{u}_{p,i}(t) + \boldsymbol{c_{P,i}}\dot{u}_{p,i}(t) + \boldsymbol{k_{P,i}}u_{p,i}(t) = \boldsymbol{f_i}(t) + c_s(\dot{u}_r(t)) + k_s(u_r(t)) \tag{4.68}$$

$$m_r\ddot{u}_s(t) + c_s\dot{u}_r(t) + k_s u_r(t) = -m_s\,\ddot{u}_{p,i}(\mathrm{t}) \tag{4.69}$$

Hence the dynamic equilibrium equation for the ith mode shapes of the structure with the contribution of the TMD is attained which is equivalent to the equations of a SDOF system. Therefore, it is possible to establish an analogy between the SDOF system presented in the previous subsection and the MDOF structure, if modal coordinates are used$(eg. u_p)$. Therefore, the procedure described to design TMDs for SDOF system may be used to optimize the design TMDs to control vibrations for a specific mode shape in a MDOF structure.

Moreover, multiple TMDs attached to the primary MDOF structure can be implemented using the equilibrium equation (4.68) and (4.69) at each TMD; each TMD being tuned to a specific mode shape enabling us to control vibrations of, even, the higher modes which commonly are less relevant.

4.8 Case study Footbridge withTMDs tuned to the same Frequency

The North foot-bridge understudy, Property of the Energias de Portugal (EDP), is proposed to be equipped with two TMDs tuned to the same frequency. The TMDs proposed by the company, OZ Lda, involved in the design check for dynamic behaviour of the foot-bridge, are located to be around the center span, where the amplitude of the fundamental mode of vibration is maximum. As shown in Figure 4.17 the TMDs are placed in N14-N15 and N15-N16 Grid lines.

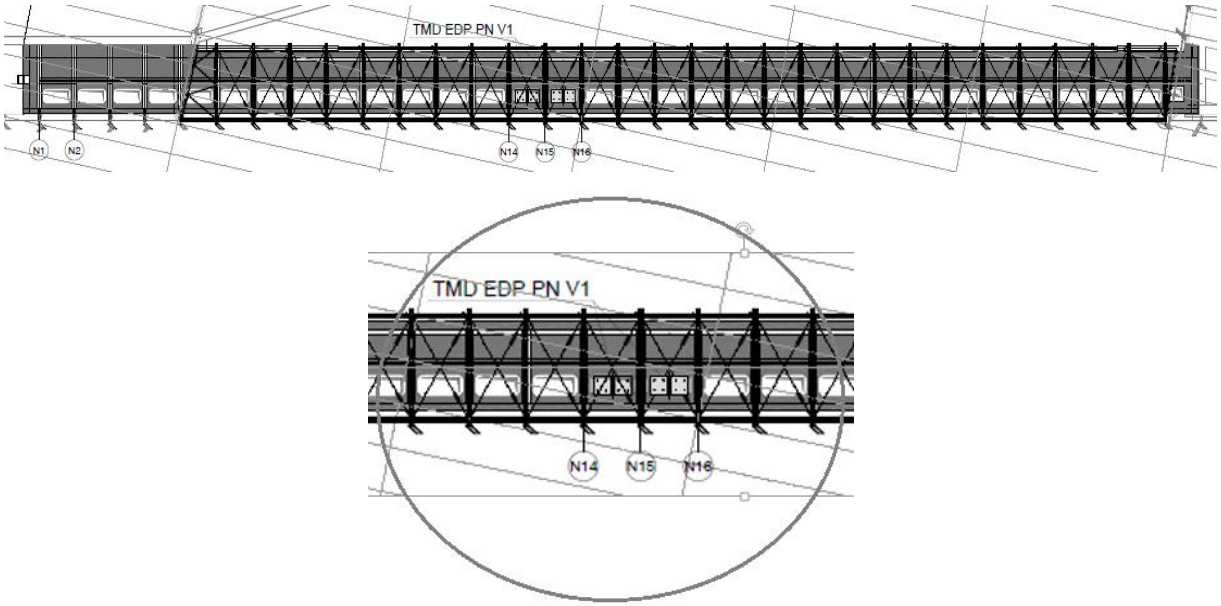

Figure 4.17-TMDs location in the North Footbridge-plan view

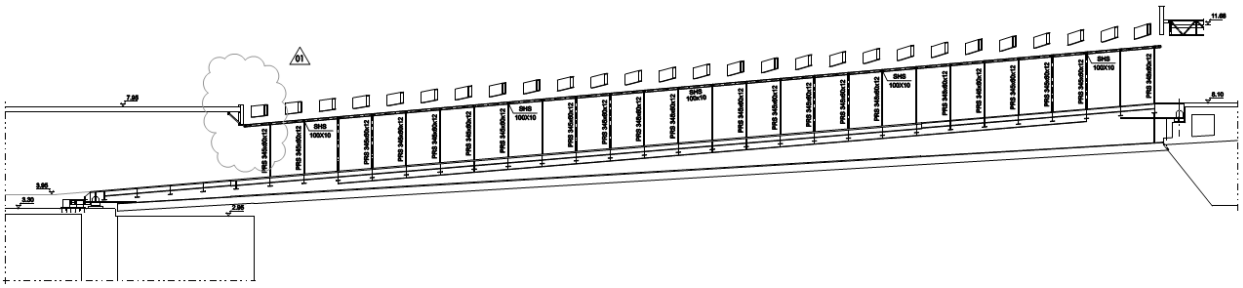

Figure 4.18-North Footbridge side view

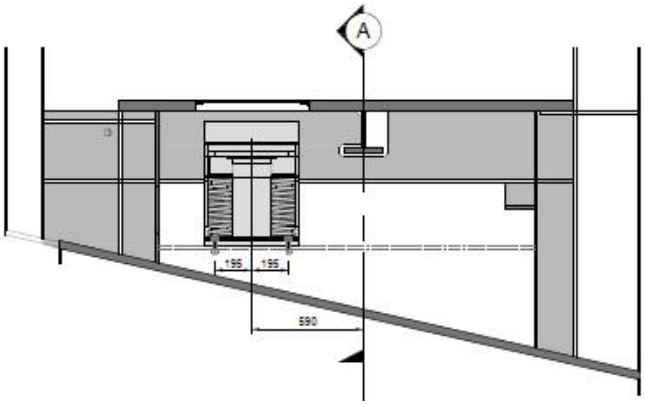

Figure 4.19-North Foot bridge sectional view at TMD location

According to the company involved in fabricating the TMDs, the following properties are reported:

Table 4.6-Properties of TMDs in North Footbridge

	Units	North bridge
Quantity	-	2
Mass	M [kg]	1241
Stiffness	K [N/m]	55948
Damping	C [Ns/m]	1401
Frequency	f [Hz]	1.07
Amplitude	[mm]	120

It can be deduced from Table 4.6 that the North foot bridge TMDs are tuned to 1.06Hz frequency, with a damping ratio 8.406% obtained from the classical equation $\xi = \frac{c}{c_c} = \frac{c}{2\sqrt{KM}}$.These inherent properties will be used to define or verify the efficiency of tuning of the TMDs. It should be brought to notice that, the TMDs are built with adjustable mass with layers of metal plates which allows to add or reduce the mass of TMDs. This might be important to alter the frequency tuning of TMDs during initial installation case or prolonged time; for example, the results of FEM model and actual ambient vibration test results may not agree, and thus the initial design of TMDs which had been done on the basis of FEM analysis and hence, by changing the mass of the TMDs, the TMDs may be tuned to the actual desired frequency. More over after long time service the foot bridge may loss some of its stiffness leading to detuning of the TMDs which can be corrected by adjusting the mass(additional mass in this case) of TMDs provided initial consideration was done for structure capacity to resist the additional mass.

The maximum displacements permitted by the TMD's are within ± 60 mm, resulting in a maximum amplitude of 120 mm. Thus, the maximum displacements recorded between the mass of the TMD and the structure should be less than the threshold.

In order to assess the property actual condition of the North foot bridge-a case of two identical TMDs linked to the primary structure at same location-the development of equation of motion done in Frahm's vibration absorber by using two TMDs as the second degree of freedom can be done.

Mainly, the excitation forces of the foot-bridge are expected to be from pedestrian induced vibration, vertical, lateral and longitudinal, and wind loads. Seismic action can be considered to play paramount effect on the dynamic performance of the foot-bridge, while wind loads could be less important with regard to location, Lisbon(less magnitude of wind pressure).The pedestrian periodic loading developed in chapter 3 will be used to throughout the development of equations in the sub-sequent sections.

Let us consider a simple harmonic excitation force of frequency ω given by $F(t)=F_0 \sin(\omega t+\Phi)$ applied in the primary mass and identify the vertical displacements as $u_P(t)$ and $u_S(t)$, respectively for the primary and secondary masses. With the two TMDs moving in the same direction (in phase), the expression derived assuming undamped (vanishing damping) structure in previous sub-section can be used. It should be noted here that the case where the two TMDs moving opposite to each other will introduce no effect on the primary structure and the governing equation will be only that of the original equation of motion of the primary structure. The governing equations of motion for the primary and secondary masses will be equally similar to the transfer functions developed in equations (4.36 - 4.38).

4.9 Design consideration

The concept for designing passive TMDs has been established using equations of motion in the previous sub-sections. When designing a TMD, the first decision concerns the method that will be used to achieve its optimization. The first step is to address the type of excitation force that causes the structural response. In the case of pedestrian footbridge with people walking, rarely running, the force exerted in vertical, lateral and longitudinal should be assessed with some established norms. A through discussion about the pedestrian load modeling is presented in chapter 3. It may be considered that the excitation force can be modeled as a periodic load (expresses as a sum of average component and a series of sinusoids) with varying frequency in direction of application of force. Therefore, an optimization with respect to the H_∞ norm is more appropriate for this case owing to narrow range of resonance frequencies.

Secondly, identification of the structural mode shapes whose contribution is aimed to be reduced by the TMD can be done. Using the shape of this mode, an equivalent single-degree-of-freedom model of the structure is generated by computing the associated modal mass and stiffness accordingly. For obtaining a scaling of the modal mass that is compatible with equation of motion involving damper, the amplitude of the mode shape at the position where the TMD is attached to the primary structure has to be chosen equal to

unity in the direction of action of the TMD. The modal stiffness is estimated using the modal mass and the natural frequency of the vibration mode. As already mentioned, inaccurate frequency tuning reduces significantly the effectiveness of a TMD. Although much less critical as the natural frequency, the structural modal damping should also be determined by field tests or estimated conservatively based on experience (Weber et al., 2006).

The third decision concerns the optimization criteria of the TMD. For a given damping ratio of the primary structure, ξ_P, mass ratio, μ, determines the optimum damper parameters, $\xi_{S,OPT}$ and q_{OPT} including the response of the structure .The mass ratio is chosen to satisfy the acceptable response level of the structure. The maximum acceptable response level may be given by codes, guidelines, provisions or generally accepted rules.

Beyond a mass ratio of μ= 0.05, a further increase of TMD mass results only in a relatively smaller further reduction of the response of the primary system. TMD is only effective when properly tuned to a specific natural frequency or, equivalently, to a specific vibration mode. Thus, if multiple mode shapes are aimed to be controlled, MTMDs can be used where each TMD is tuned to a specific mode shape. As long as each mode shape refers to a given natural frequency, coupling of TMD is not possible, and thus the previously developed expression for TMD attached to MTMDs can be utilized.

The relative displacement of the TMD with the primary structure is an important aspect in design of TMDs since there is a need that the relative movement should be accommodated in the available space. If there exist constraints in the space available to meet the requirements for design, the mass of the TMD can be increased, or if the latter is not feasible, the damping ratio, ξ_s, can be increased. Failure to do so might result in reduction of effectiveness of the TMD.

In existing structures, the mass of the TMD may be restricted by the load bearing capacity of the structure and the installation of a single TMD may require a strengthening of the structure. A design with multiple TMDs having smaller masses may avoid the required strengthening. However, the effectiveness decreases if not all TMDs can be installed at the locations with maximum amplitude of the mode shape. Furthermore, because of the smaller mass, the TMDs will exhibit a larger relative displacement and hence require more space than a single TMD.

Natural frequency and damping ratio of structures may change because of the effect of live loads (e.g. pedestrians on footbridges) or environmental parameters (e.g. temperature). Since the effectiveness and response of TMDs are very sensitive to an incorrect frequency tuning, changes of natural frequencies have to be considered in the design. Bad frequency tuning increases the response of the structure as well as the relative displacement of the TMD. Adjustable mass TMDs can be recommended in such cases.

5

OPERATIONAL MODAL ANALYSIS APPLICATION TO THE EDP's NORTH FOOTBRIDGE

5.1 Description of the Footbridge

EDP (Energias de Portugal), which is the electric supplying company in Portugal, recently built a composite structure building in Cais do Sodré, Lisbon. The new building have two compartment buildings parallel to each other on the east-west direction and connected by two slender housed steel footbridges with aesthetically appealing glass panels. The main function of the two pedestrian steel bridges is to allow to and fro movements of pedestrians (customers or employees in this case) between the two buildings facing each other. The footbridges are designed in such a way that one is rising and other one is descending in the west to east direction. Due to the similarity of the footbridges in terms of geometry, location and excitation forces, the North footbridge is chosen as a case study to be investigated. The footbridges are also decided to be equipped with TMD's which makes the, work rather interesting, in an effort to control pedestrian induced vibrations and guarantee safety levels recommended by various European researches done on footbridges including the HIVOSS and SYNPEX.

The footbridge has two plate girders inside a trapezoidal hollow steel box which tappers as the bridge descends. The steel plate box house the TMDs and it can be accessed from the footbridge deck by simply opening metal plate movable covers beneath wool carpets which makes it easy to for surveillance of TMDs, thermocouples and other structural monitoring devices installed inside it. The footbridge is 49.87m in length and 2.925m in width. Figure 5.1 presents the external and internal features of the north footbridge under study.

Figure 5.1-a) side view under construction and b) internal view after completion of the North footbridge

The footbridge is made of steel elements interconnected with each other through welding and bolts and 4 simply supported conditions, two at each end. More over the footbridge is simply supported on the roof at the west end of the span. The roof is made of an assembly of RHS members with wire stel grate ceiling, and it is connected laterally by flexible ceramic finished RHS members. As aforementioned the vibration control devices (TMDs) are installed around the mid-span composed of adjustable mass of bundled metal plates, springs of desired stiffness and damping device. The two TMDs are placed only separated by one floor panel which is uncommon practice as TMDs are preferred to be placed in points of higher displacements with each TMD suppressing a given mode of vibration which leads to a different dynamic behaviour. Nevertheless the objective of designer is that the two TMDs suppress the same fundamental mode. The positioning of TMDs in the width and its components are elaborated in Figure 5.2.

Figure 5.2-TMDs location in the span of the bridge and details of TMD

5.2 Ambient records of the footbridge with and without TMDs installed

Systematic and planned data collection is very crucial during vibration records as failure to do so leads to biased and erroneous estimation. Reduction of harmonic and noise sources like electric cable interference should be taken carefully. During construction stage, records were taken before the installation of TMDs and glass panels, but with all structural elements already built. The aim of these records was to determine the dynamic behavior of the footbridge without TMDs, but unfortunately, the footbridge was not completed (meaning the entire mass of the structure was not in place) which could affect the natural frequency of the system. Even though the condition was not satisfactory records were taken and preliminary operational modal analysis was carried out; the data collected is used in chapter 2 as an example to illustrate the abstract mathematical models of operational modal analysis algorithms.

During this first site visit, two Etna tri-axial accelerometers (1/5 and 2/5) with 3 channels from Kinemetrics Inc. were used to measure the ambient vibration response of the structure. The accelerometers were placed

on different positions in the footbridge and records are triggered through PC equipped with Kinemetrics Quick Talk monitoring software. And the records were trimmed for synchronization effect using strong motion analyst software which allows also preliminary Fourier transformation and power spectra functions. Calibration and proper functioning of these instruments was ascertained by confirming its calibration in terms full-scale setting of the sensor jumper following the user guide of the devices provided by the manufacturer. Proper functioning of sensors was also checked in IST.

After Signal conditioning modal estimation was performed on the records. Modal parameters estimated using the MATLAB programmed EFDD program and ARTeMIS are presented in Table 5.3 and Table 5.4 respectively using singular value plot shown in Figure 5.3 and Figure 5.4. It is produced, as described in chapter 2, with no decimation and 1024 sampling points (resolution =100/513=0.1949, high but allows full view of modes and modes are separately distributed).

.

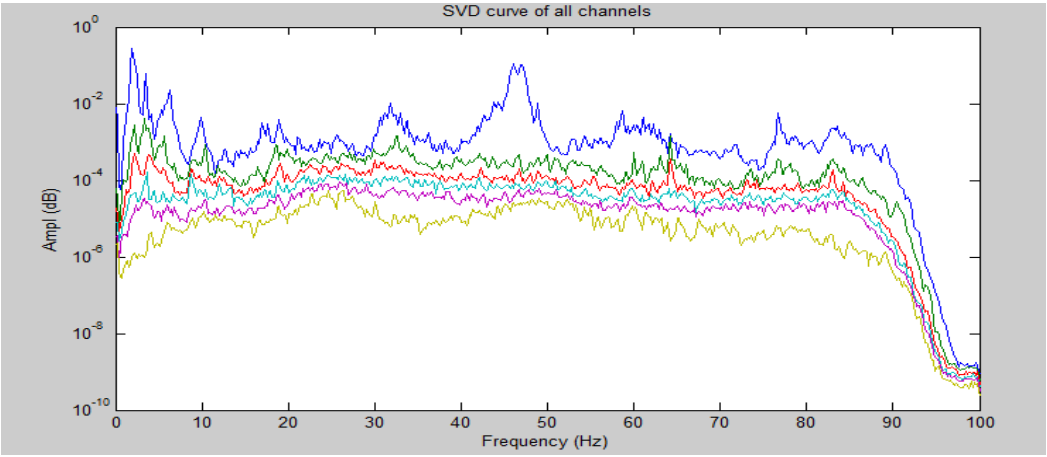

Figure 5.3-MATLAB program singular value plot of records during construction and TMDs not installed

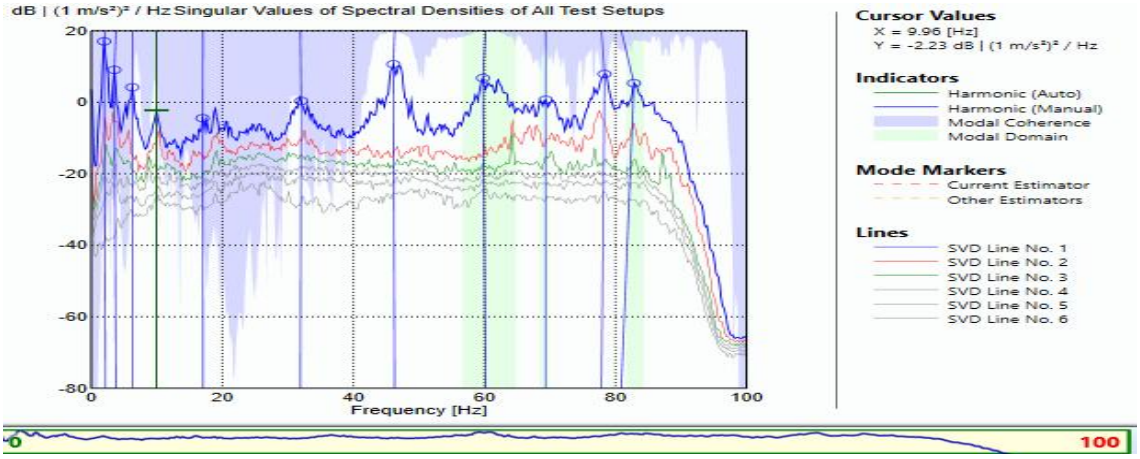

Figure 5.4-ARTeMIS singular value plot of footbridge records during construction and TMDs not installed

After completion of the footbridge and mounting of TMD devices, once again, records were taken using uni-axial accelerometers which are meant for the long-term structural health monitoring task, three at each point in orthogonal directions, supported on a mounting device as shown in Figure 5.5. Hence, the 6

available uni-axial accelerometers and two mounting devices were used to perform the task. The central span with three accelerometers supported on one of the mounting devices is left in position as a reference point and the other three uni-axial accelerometers were used to take measurements by roving at 8 different points totally making up 8 sets of records. Due to shortage of instrumentation, only 6 channels exist at each setup representing two sampling points, the overall mode shape of the structure cannot be attained from each setup. Thus, to solve this problem, modal superposition using scaling factor of the common sampling point (reference point) of all the setups is used and the mode shape along the stretch of the footbridge can be found by using those 8 points at each mode of vibration. The data collection sensor layout and pattern with two points of measurement each consisting of 3 sets of uni-axial accelerometers supported on a single mounting device, as shown in Figure 5.5, is presented in table 5.1.

Table 5.1-Data collection sensor layout of the North footbridge

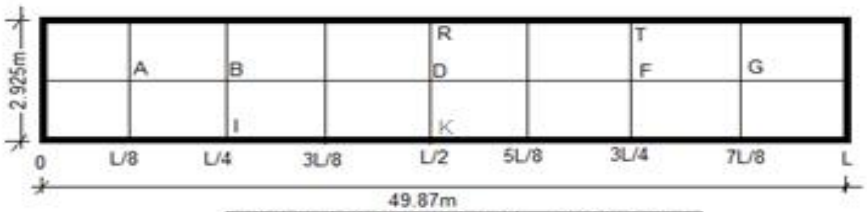

Test no.	Reference point	Roving point
1	D	F
2	D	B
3	D	A
4	D	I
5	D	G
6	D	T
7	D	TMD at midspan
8	R	K

The duration of each record is chosen to be 5minutes for adequacy to produce smooth average spectra matrix by overlapping of given number of sampling points.

Figure 5.5-Ambient vibration records after completion of the footbridge

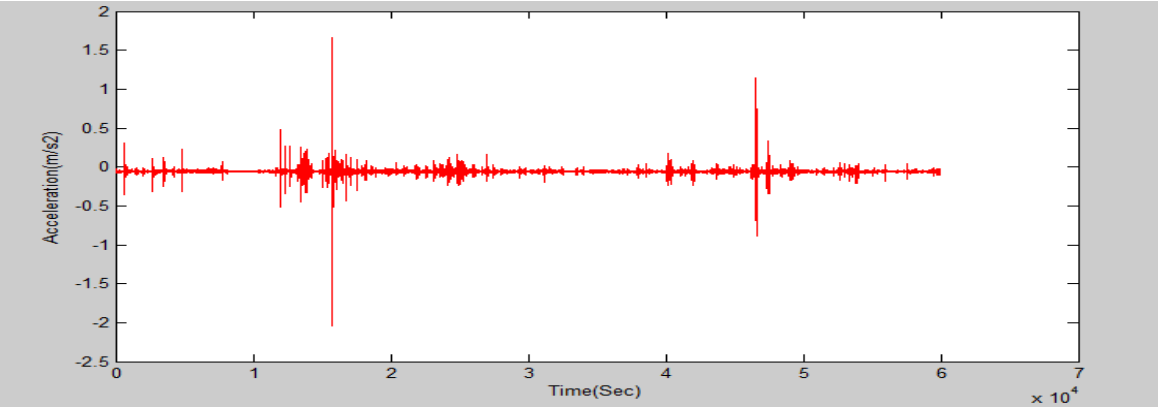

Figure 5.6-Typical ambient vibration record at Mid-span in vertical direction after completion of footbridge

5.2.1 Reduction of errors from records

As records are signals they are prone to errors and the need for error reduction is emphasized when frequency domain methods are employed. In this case study leakage and aliasing errors are considered. Each record in each setup is treated to reduce the aforementioned errors.

5.2.1.1 Aliasing error, choice for Nyquist Frequency

Aliasing errors are errors which arise due to which the chosen sampling frequency become inadequate enough to depict the natural frequencies of the system. This can be avoided by restricting the half of the sampling frequency (Nyquist frequency) not to fall below the maximum (or desired frequency range) natural frequency of the system understudy. In this context, it is necessary to have the feeling of the expected natural frequency range of the system so as to set the sampling frequency. In this project, sampling frequency of 200Hz is used which makes it possible to encompass all the expected frequencies to be determined. Initially, rough analysis of expected natural frequencies from previous works done on related projects was referred and low frequencies of vibration are found to be prevalent in such structures.

Further, after employing decimating process, there is a tendency of the data to aliases, thus it should be treated by anti-aliasing filter. In this project, the decimated data ('r' being decimation ratio) is treated with lowpass Chebyshev Type I IIR filter of order 8 and end results reduce to a sampling frequency of [0.8*fs /(2*r)]. A decimation ratio of 4 is adopted in this case, as the frequency range of importance is 0-20 Hz.

5.2.1.2 Leakage, windowing and de-trending

Leakage error is a very demanding error and can only be reduced, but cannot be completely eliminated from the system. Leakage is a phenomena where the power (energy) of one frequency, most importantly natural frequency, leaks to other frequencies in the proximity reducing the power at that frequency. Several windows, Hann, Hamming and Rectangular, are devised to reduce leakage errors depending on the accuracy desired in terms of frequency and amplitude precision. The collected records were treated with

Hann window which is a bell curve trimming down the response to zero at extremities and multiplies the response by the bell curve function. Figure 5.7 illustrates the Hann window treatment.

Finally, decimated and windowed data is de-trended to remove any linear trend or mean value from the data for FFT and spectra matrix determination. A mat lab command de-trend is used to perform the task.eg. setup_2_5=detrend(SETUP_2(:,5)); plot(setup_2_5,'r').

5.2.2 Enhanced Frequency Domain decomposition (EFDD) estimation

5.2.2.1 EFDD implementation using MATLAB programmed algorithm

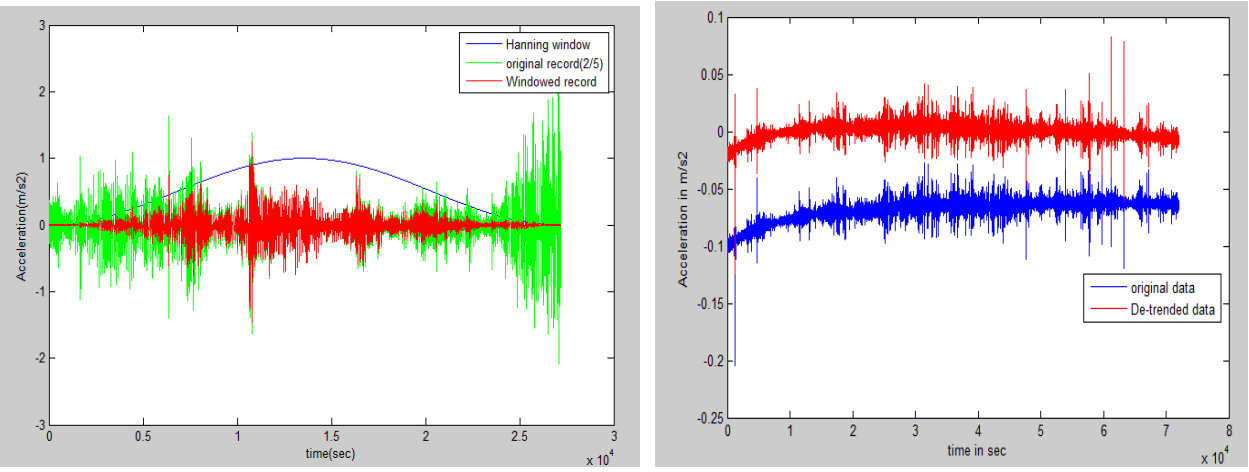

(a) (b)

Figure 5.7-(a) Application of Hann window; (b) Application of de-trending to records

Frequency domain method of modal estimation program written in MATLAB was employed to determine the modal parameters. The Enhanced frequency domain decomposition method (EFDD) is preferred in order to have full information including the damping ratio. Apart from that, scaled mode shapes (in terms of mode shapes of sampling points around the natural frequency whose MAC values exceed the criteria set) can be found as well with a corrected natural frequency through zero crossing of the correlation function.

Before modal estimation there is a need to create a 3D spectra matrix which can serve as an input the EFDD program. Hence to perform this task a separate function was developed in MATLAB to prepare 3D spectra matrix by the name *FDD spectra matrix* and output variables from this function serve as direct input to the EFDD program. Detailed description of the MATLAB programs can be found in the Annex.

The EFDD program first displays the singular value plot of all the channels or selected channels, and one peak at a time is selected and its corresponding frequency is supplied to the command prompt requesting for input frequency. Finally the program displays the results of modal estimation consisting of MAC value plot, SDOF bell curve and bell curve in 1Hz frequency range, free decay plot (correlation of SDOF bell

curve), curve fitted damping estimation plot, zero crossing and curve fitted natural frequency estimation plot all together at the same time.

The 8 setups are processed through EFDD and the respective estimated modal parameters are collected, compared and modal shape calibration for each mode is done using the aforementioned method of scaling mode shapes method. Figures 5.8 – 5.10 shows the sample results for the analysis pertaining to setup 4. It should be noted that, the estimated parameters are highly dependent on the data collection methodology and sensor layout, thus proper care should be taken and maximum number of points should be employed during the for estimation so as to avoid rank deficiency of the spectra matrix.

An important aspect to be considered during the estimation task is to set the MAC criterion properly. If the data collection is not reliable, not dependable enough, higher MAC criterion should be set to eliminate possible noise from the response. In order to eliminate noise, as the data collected is not dependable enough in our case due to lack of instrumentation, a higher MAC Criterion value is set i.e. MAC=0.9. But comparison of estimates from 0.8 and 0.9 MAC criteria is done.

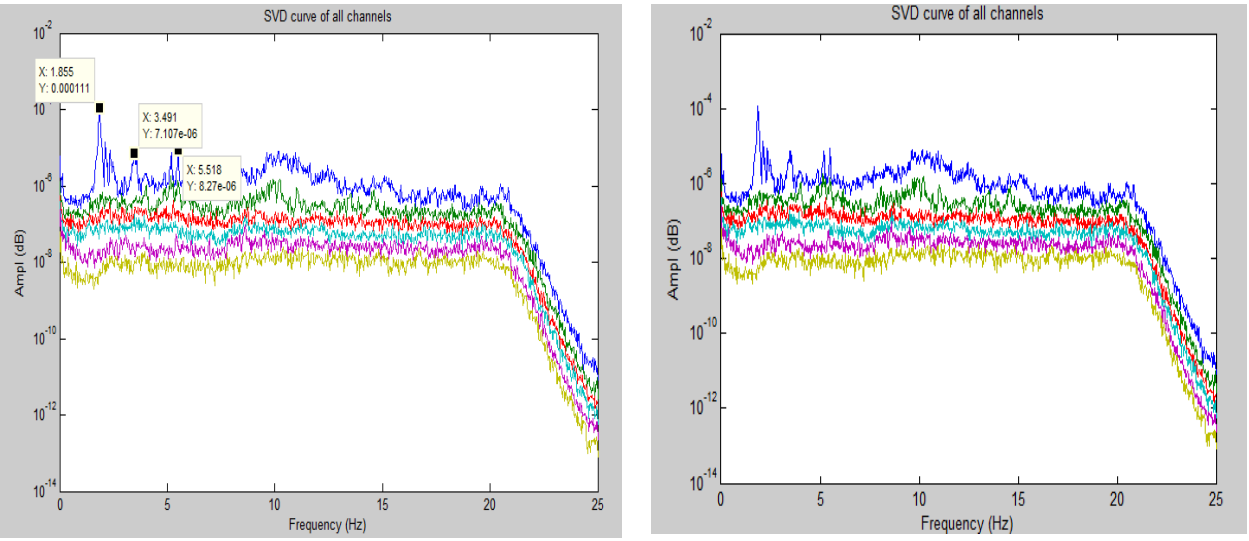

(a) (b)

Figure 5.8-singular value plot for (a) MAC=0.9 and (b) MAC=0.8 [setup 4]

The modes of vibration are not evident except the fundamental mode of vibration at 1.86Hz and lateral mode at 3.46Hz.Thus, it is necessary to use a more complex method, other than pick-peaking, e.g. EFDD, to find modal parameters and other modes of vibration.

Figure 5.8 presents the same singular value plot for both cases for obvious reasons; Figure 5.9 in other hand presents the distinction before the two categories of MAC. In Figure 5.9(b) the SDOF bell curve has extra sample points on the right side as compared to SDOF bell curve for MAC=0.9 .It can be concluded that, by reducing the MAC value the number of Sampling points that make up the SDOF bell curve increases. This can be interpreted, as the number of sample points increase the noise introduced in to the estimation also increases which can only be done under data collected with higher caution and precision

(called clean data). As expected, the damping estimation of the two criteria should vary leading to different damping ratio values. It can be seen in the Figure 5.10, the correlation plot of the peaks deviates at the tail (end), by using lower MAC value, from the typical linear pattern manifesting the inclusion of noise in to the estimation procedure. However, the damping estimation is based on normalized correlation values in the range of 0.95-0.3 (marked with red in the central plot of Figure 5.10) which avoids the inclusion of noise to the curve fitting determination of logarithmic decrement value for modal damping. Hence, the two criteria lead to the same modal results. The case is similar with natural frequency estimation because they are computed from the same normalized correlation function in the range of 0.95-0.3.

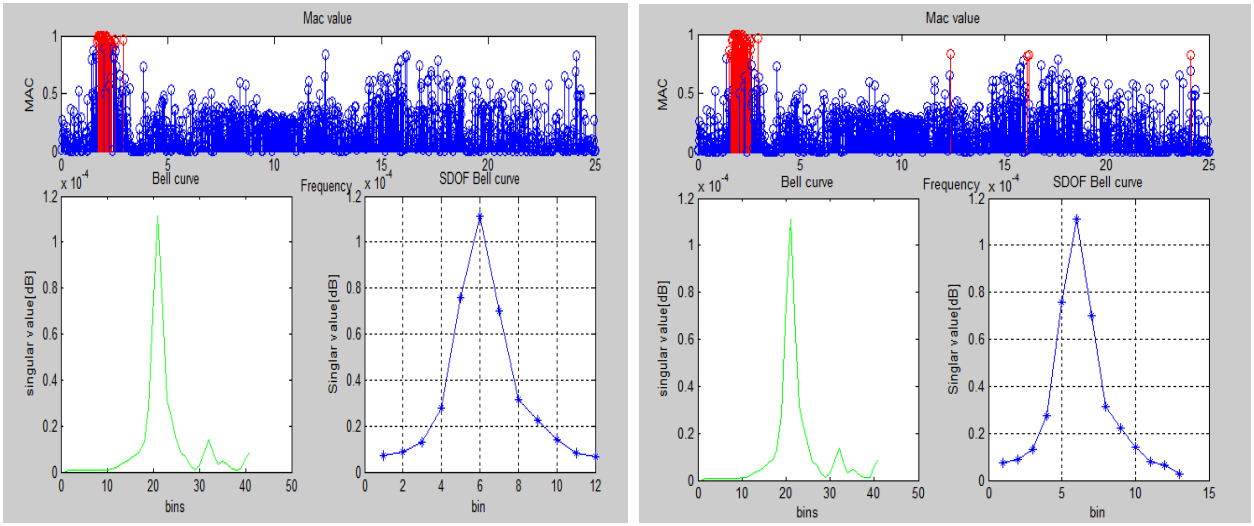

(a) (b)

Figure 5.9-MAC plot and SDOF bell curve for (a) MAC=0.9 and (b) MAC=0.8

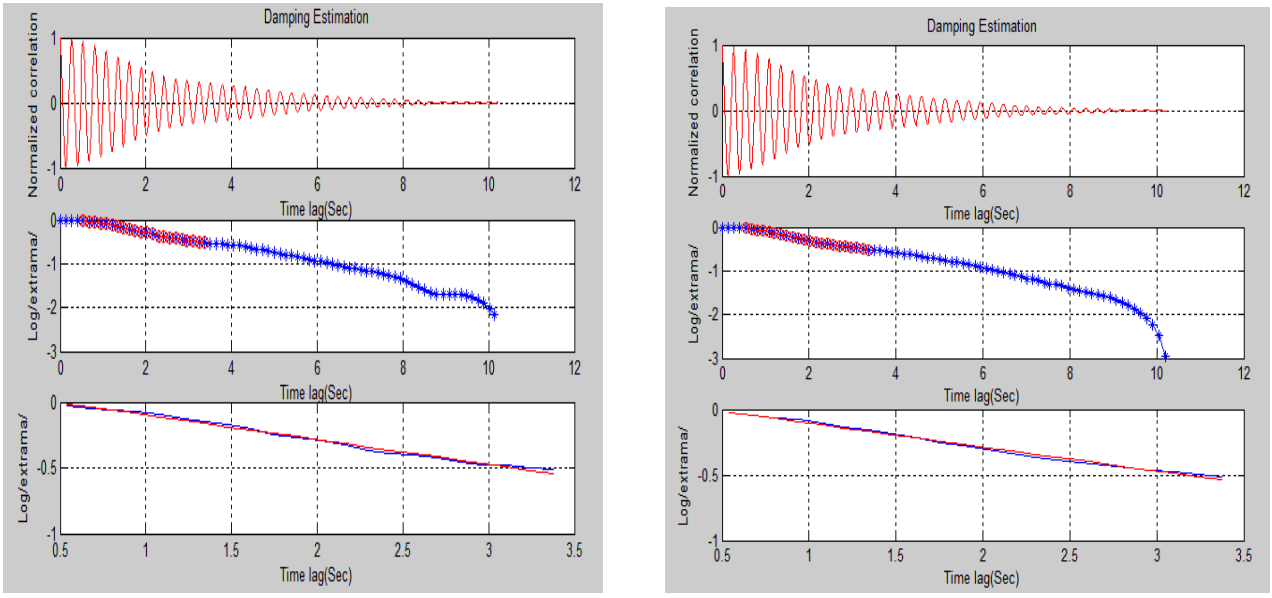

(a) (b)

Figure 5.10-Free decay curve and damping estimation plot for (a) MAC=0.9 and (b) MAC=0.8

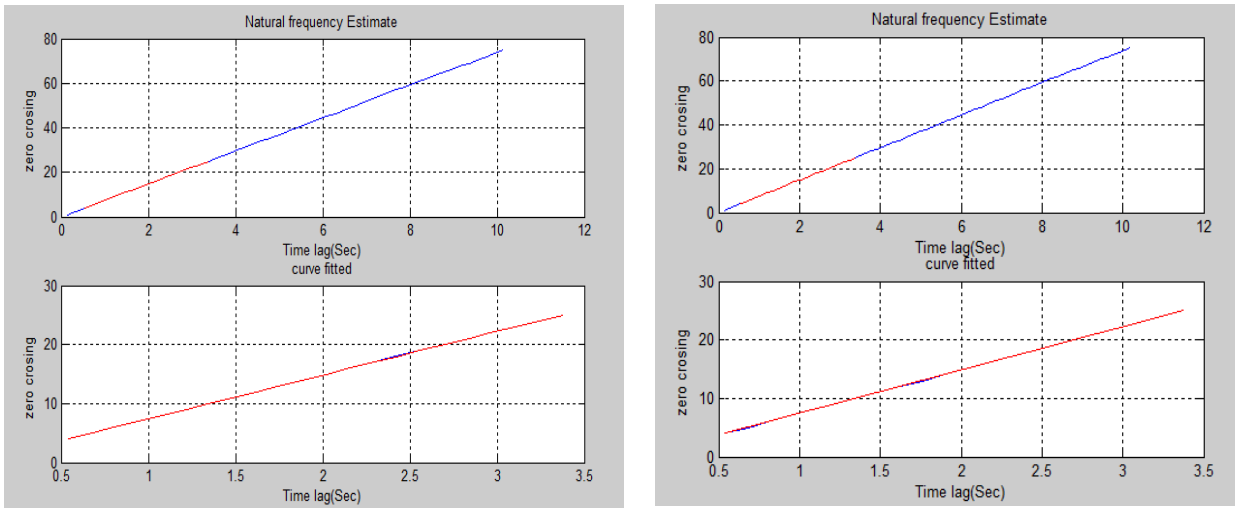

(a) (b)

. Figure 5.11-Zero crossing times and corrected natural frequency estimation plot for criterion (a) MAC=0.9 and (b) MAC=0.8

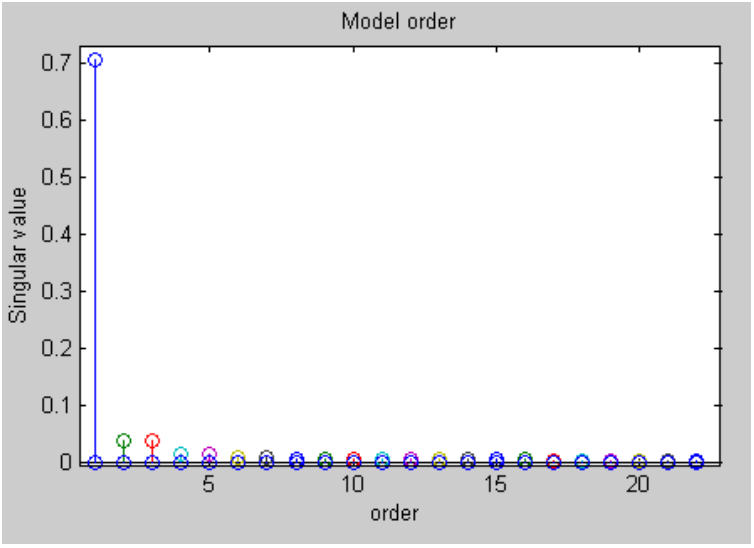

Figure 5.12-Model order computed using SSI-DATA algorithm for ambient vibration records after completion of footbridge [setup 4]

SSI-DATA algorithm programmed in MATLAB produce the model order of the ambient vibration records after completion as shown in Figure 5.12. The main objective of this demonstration is to determine the number of singular values which are important in the estimation of modal parameters. A large drop between 1 and 2 singular values is observed as depicted from graph implying that the system is characterized with low model order implying the forfeit higher model order checks. Also concluded, the effect adopting smaller MAC value may have less effect on damping estimation if the correlation range is restricted to 0.3-0.95 which may not be true for other cases. So, the correlation peaks curve should be studied carefully.

5.2.2.2 EFDD implementation using ARTeMIS modal software

ARTeMIS Modal is the leading software for Operational Modal Analysis (OMA). The modal analysis software is applicable for a vast number of cases where it is preferred not to control or measure the loading which is typical with civil engineering cases. It is developed by Structural Vibration Solution A/S, a world-renowned supplier and developer of the software for Operational Modal Analysis. The software can be used in:

- Operating machinery or other mechanical structures with or without rotating components
- Large civil engineering structures like bridges, dams and buildings subjected to ambient loads
- Structures with rotating components such as wind turbines, stream turbines, engines and gas compressors
- Maritime structures like ships and offshore structures
- Automotive, trucks, trains and vehicles and sub parts systems
- Aerospace structures such as launch vehicles and aircrafts

The standard modal ARTeMIS 3.6 software is used for this project capable of performing FDD (Frequency domain decomposition), EFDD, CFDD (Curve fit frequency domain decomposition) and ODS (Operating deflection shapes) methods of estimation. Its benefits are:

- Handles single or multiple Test Setups in exact same way. Through the use of the powerful statistical harmonics detection modal parameters can be extracted in the presence of deterministic (harmonic) signals from e.g. rotating machinery.
- Peak-picking can be made manually or automatic.
- EFDD and CFDD methods provide estimates of damping ratios as well as improved estimates of natural frequencies and mode shapes.

5.2.2.2.1 Creating geometry, importing, managing records and analysis

Geometry of the structure or mechanical element can be easily created in the prepare geometry option of the software. Geometry can be drawn using points, lines and surface, or pre-defined 2D and 3D shapes are available. It allows also automatic meshing (dividing one element into desired regular number of

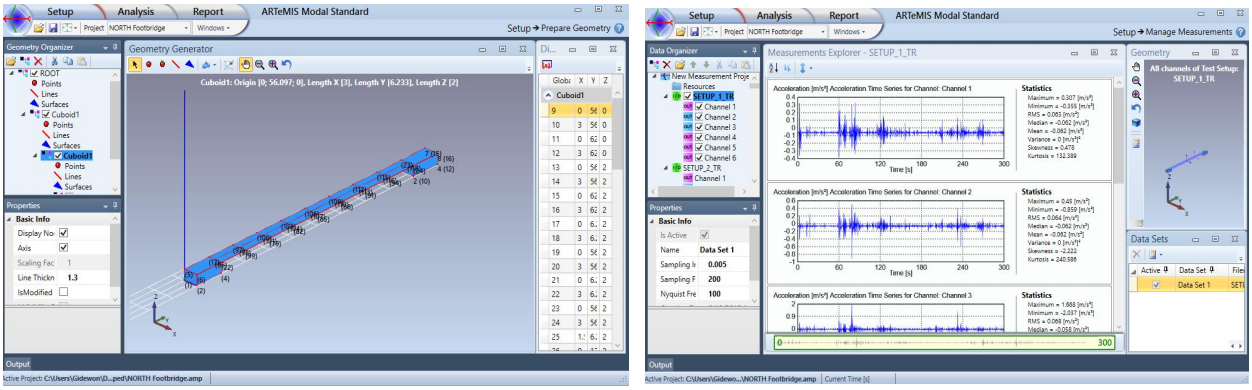

Figure 5.13-Geometry creation (left); Manage Measurements window (right) of ARTeMIS standard v.3.6

elements). As shown in Figure 5.13 the footbridge geometry was constructed using cuboid element and meshing was applied to locate sensor locations.

Each setup Measurements is imported by clicking the folder import icon shown in Figure 5.13(b) and the imported channels are displayed in the central screen field including its statistical information. The geometry along with previously applied channels is also displayed in the top right hand side of the manage measurements display menu for visual information.

In this dialog page, one set-up can only be connected to the structure, while the other imported setups remain inactive, if the channels don't share a reference sensor, otherwise many setups can be connected with same reference channel which enables the overall mode-shape determination particularly if enough sensors are not available to cover the necessary points to produce overall mode shape, and thus same reference sensor position is used in all the setups and connected all at the same time in ARTeMIS to produce the overall-shape mode shape. This is case in this project because the available sensors were not sufficient (only two sensors setup used) enough to produce the desired mode shapes. Also in this dialog page, the sampling frequency/Nyquist frequency is set.

Assigning channels to their respective points, location (necessary to get correct configuration of mode shape), was done by picking each channel from the top left hand location in Figure 5.14(a) and dropping it on its location point in the central geometrical figure where the position (point) to be assigned will be marked by a red dot before dropping it. In this case reference sensor position is the center span and all reference channels are automatically assigned to blue color while roving sensors are green colored.

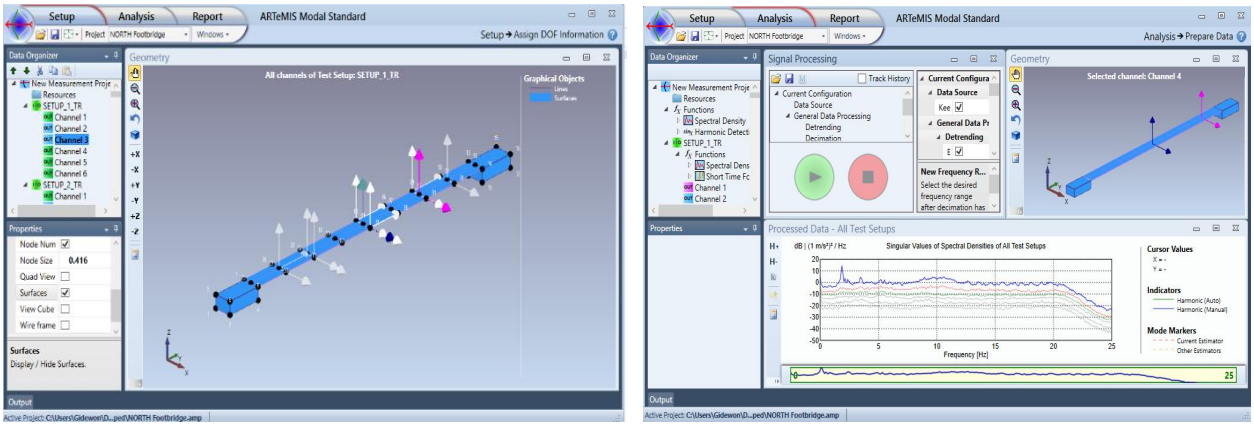

Figure 5.14-Channel assignment (left); Analysis options (right) window ARTeMIS standard v. 3.6

The analysis option allows user to choose analysis parameters in the current configuration field section which includes use of previously processed data, de-trending, decimation, filters of several types, number of sampling points, number of projection channels to be used for analysis (elimination of redundant channels for reduced processing time) and harmonic detection(fast and extended). In this project; de-trending of applied; data is decimated to 0-25Hz (other decimation factor results are also computed and

compared); no filtering is applied as anti-aliasing filter is automatically applied after decimation; sampling points (varying between 256 and 1024) are chosen followed by averaging. Projection channels was set to 6 as the available channels were small enough to cause delayed processing and, finally, harmonic detection was set to fast as the this method is proven to be efficient for channels more than two in a given setup. Green button shown in Figure 5.14(b) runs the analysis and singular value plot is displayed right after the analysis.

5.2.2.2.2 Modal estimation

In order to determine damping along with frequency estimate, the EFDD command estimation was employed, however all the other methods of analysis (FDD & CFDD) results comply with it. As shown in Figure 5.13 three modes are depicted, one lateral and two vertical modes. Damping and natural frequency estimates of the modes were also validated as presented in Figure 5.15 and Figure 5.16. Detailed results will be presented for all available setups in the proceeding sub-section.

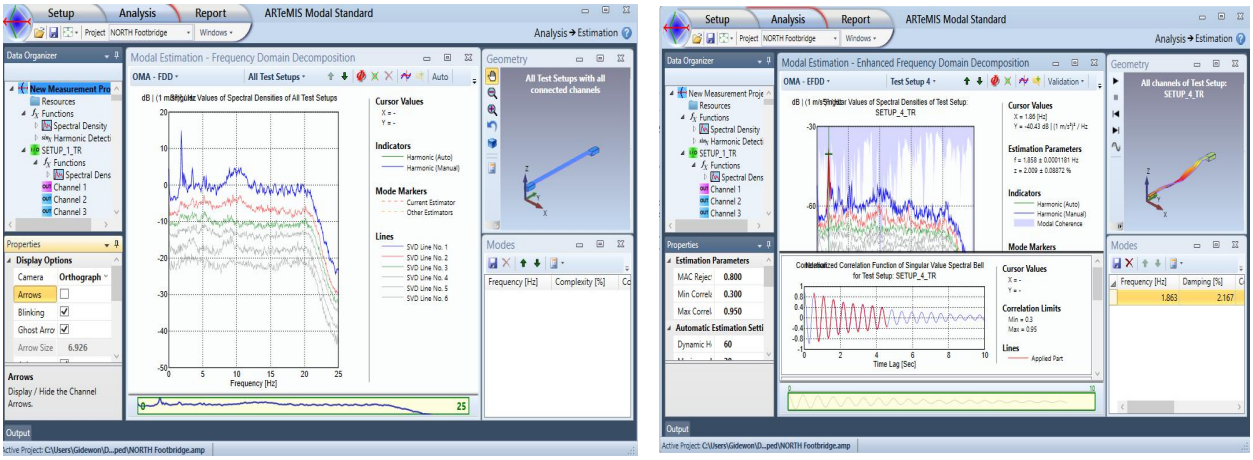

Figure 5.15-Estimation window of ARTeMIS (left); Damping validation using Free-decay(right)

Validation among different modes from the same estimation method is done to identify the relation between the modes of vibration (MAC value close to zero indicates the modes are entirely different and values close to unity, in the other hand, indicates that the modes are similar), and validation of the same mode from different estimation methods was also performed to compare the results from different algorithms to determine the credibility of estimated modal parameters using different algorithms. Detailed results of modes and corresponding modal parameters are presented in tables 5.2-5.4.

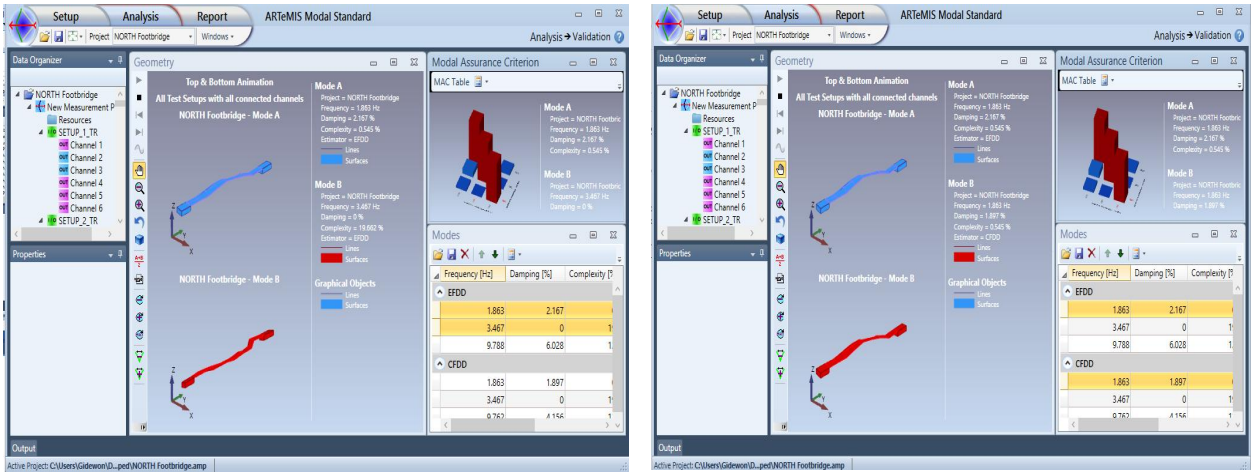

Figure 5.16-MAC validation between Modes in one method, EFDD, (left); between EFDD and CFDD of the same mode (right)

Figure 5.16 shows one of the important tools in assessing the validity of estimated mode shapes. Determination of MAC values between different modes of the same estimation method assist in validating the uniqueness of each mode identified. Validation of the same mode of vibration from different algorithms also helps to determine consistency of the mode of vibration which, in some cases, some algorithms may lead to erroneous singular results. Validation through complexity, shown in Figures 5.16 & 5.17, measures the credibility of estimated mode, complexity values close to zero are best estimates of modes of vibration. Some modifications in terms of sampling points and decimation is done to reduce the complexity values observed e.g. 2nd and 3rd mode.

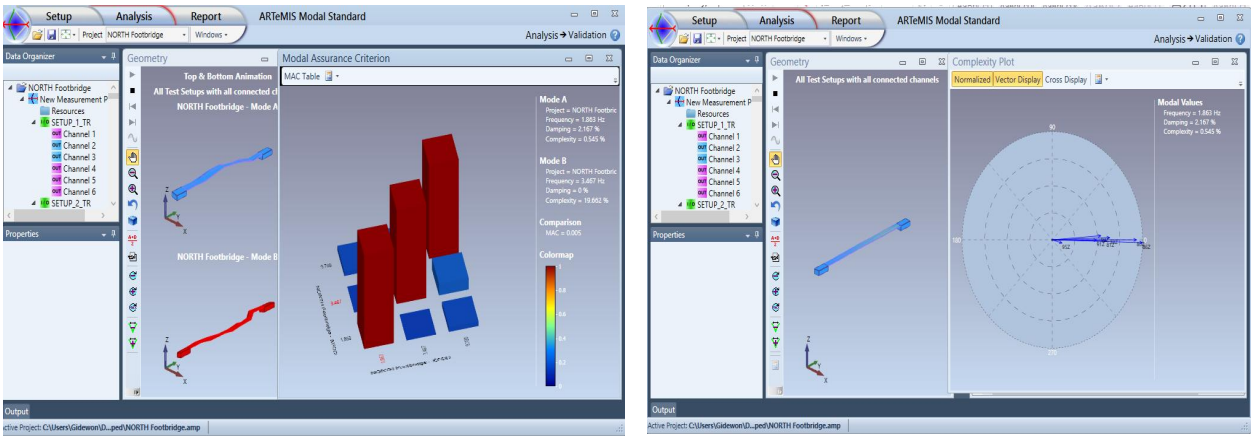

Figure 5.17-MCF validation of first two modes from EFDD (right); MAC validation for first two modes in EFDD (left)

Table 5.2-EFDD/CFDD modal estimates during construction and before TMDs installation using ARTeMIS standard.v.3.6 [V-Vertical, L-Lateral and Tor-Torsional]

ARTeMIS

Mode	Freq.(Hz)	St.Deviation	Damping (%)	St.Deviation	Mode shape
1	1.97	0.01149	1.8298	0.21872	1^{ST} V
2	3.49	0.00227	0.7421	0.29250	1^{ST} T
3	6.23	0.26749	1.6268	2.13218	Tor
4	9.92	0.02000	1.3900	0.10000	2^{ND} T+'weak'Tor
5	17.17	0.02677	0.3550	0.44599	2^{ND}V+3^{RD}T
6	46.3	0.39193	0.6691	0.60993	Local
7	62.99	0	0.6300	0	Local
8	78.61	0.00386	0.1868	0.06895	Local
9	83.12	0.01000	0.5070	0.12000	Local

Table 5.3-MATLAB EFDD program modal estimates during construction and before TMDs installation

MATLAB Program

Mode	Freq.(Hz)	Damping (%)	Mode shape
1	1.97	2.0370	1^{ST} V
2	3.46	0.8151	1^{ST} T
3	6.25	5.8512	Tor
4	9.86	1.1077	Tor+2^{ND}T
5	18.15	0.7156	2^{ND}V+3^{RD}T
6	76.76	0.5148	Local
7	83.59	0.6020	Local

Tables 5.2 and 5.3 presents the Eigen frequencies and associated modal damping of the North footbridge during the construction stage and before TMDs installed in place. The modal estimates results in evolution of 9 modes of vibration as shown in table 5.2.The fundamental mode of vibration was found at 1.975Hz which is a vertical mode of vibration. This natural frequency exhibits a higher damping value of 1.83-2.03%. And note can be taken on the discrepancy of estimates between the approaches (ARTeMIS vs MATLAB programmed EFDD).The second mode of vibration has, in the same case, a small difference on the estimates of the two approaches, nevertheless the difference can be ignored with acceptable margin of error. Two local modes extracted in ARTeMIS cannot be depicted in the MATLAB program.

The rest of the estimated modes have a certain difference in terms of frequency estimates as well as damping ratios. It is evident that the two approaches use zero crossing method for corrected natural frequency estimate and positive time lag correlation (free decay) function for damping estimate. It is to be noted that ARTeMIS modal mode shapes estimation method is quite different as it employs MAC weighting function of the bell curve sample points. Significant discrepancy in damping estimates may be observed in tables 5.2 and table 5.3 which may arise due to different decimation and sampling used to adjust the smooth decay function in the MATLAB program.

Modal parameters estimated after the footbridge completion was done based on uni-axial data collected on the health monitoring apparatus installed. The data is found to have a certain degree of complexity. It generally arise due to:

- Non-proportional damping.
- Bad measurements or poor modal parameter estimation.
- Inconsistent data due to e.g. time variant conditions.

ARTeMIS was not able to produce modes of vibration, so modes were manually imposed and complexity was checked for every imposed mode and adjustment (reducing complexity number) was done by changing the sampling points and decimation factor until reliable results were obtained.

Table 5.4.ARTeMIS modal estimates after completion of construction and after TMDs installation

ARTeMIS

Mode	Freq.(Hz)	St. Deviation(σ)	Damping (%)	St. Deviation(σ)	Complexity (%)	Mode shape
1	1.860	0.0026	2.768	0.928	0.697	1^{ST} V
2	3.4875	0.0063	2.729	0.127	12.180	1^{ST} T
3	9.654	0.1533	6.124	2.069	11.309	2^{ND}V+2^{ND}T
4	76.840	0.024	1.3165	0.0506	4.514	Local, Mid span
5	82.49	0.6933	0.5777	0.1088	3.620	Local, L/4 span

ARTeMIS present 5 modes (vertical(V), transversal(T), dual mode and two local modes) of vibration. Similarly, MATLAB programmed EFDD detects all the modes of vibration. It is evident that all modes of vibration are identical to the modes obtained in MATLAB. Nevertheless, damping values from ARTeMIS are higher as compared to MATLAB results. More exceptional, the 3rd mode is characterized with very high damping value and it can be witnessed from the SVD plot that the bell curve is wide, Figure 5.22. Two higher modes, at 76.95Hz and 82.49Hz, are extracted in both approaches which are related to the local modes. Moreover, higher complexity is depicted in the 2nd and 3rd modes but credibility of modes is verified using MAC validation.

Table 5.5.MATLAB modal estimates after completion of construction and after TMDs installation

MATLAB Program

Mode	Freq.(Hz)	St.Devaition (%)	Damping (%)	St.Devaition (%)	Mode shape
1	1.85	0.0072	2.334	0.3620	1^{ST} V
2	3.43	0.0516	2.706	0.9580	1^{ST} T
3	9.78	0.0450	4.860	1.5510	2^{ND}V+2^{ND}T
4	76.95	0.2150	1.650	0.3450	Local, Mid span
5	85.12	0.1200	0.532	0.1030	Local, L/4 span

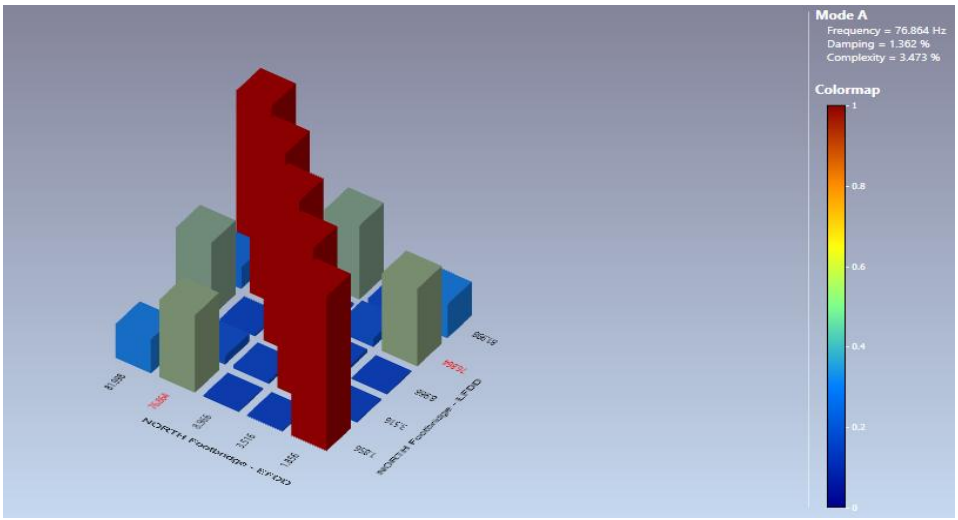

Figure 5.18-MAC value matrix shown in bar-graphs for all modes after completion of footbridge

In this context, it should be noted that the first two modes of vibration, and least probably the 3rd mode, are important for this project related to pedestrian excitation. As explained in chapter 3, the range of frequencies

for vertical and lateral pedestrian traffic do not exceed 4.6Hz (including the possibility of second harmonic pedestrian load excitation).Thus, the vibration control of the first two modes should be emphasized.

5.2.2.3 Comparison of modal estimates

5.2.2.3.1 Comparison of FEM estimates with ambient modal estimates and FEM updating

The FEM modal analysis undertaken by the design office produced a range of frequencies which are close to each other. The FEM analysis considers different traffic classes (refer chapter 3) and actions of movement in order to define the superimposed load for modal analysis load case.

Investigation presented here is related to the worst case scenario of footbridge traffic loading. Nevertheless, it is clear that the expected traffic loading is milder than a public footbridge. Accordingly, FEM modal results related to combination of loads (HIVOSS, 2007) will be only be addressed and compared with the ambient vibration results. Nevertheless, the change of Eigen values attributed to different traffic classes is almost negligible for practical purposes (verified in FEM).

FEM method yields lower magnitude of Eigen values as compared to ambient vibration test results obtained after completion of the project. The main reasons could be problems associated with modelling issues due to:

- Neglecting the stiffness contribution of some non-structural members namely glass panels;
- In accurate modelling of support conditions (capacity for rotation etc.);
- Conservative material properties.

The mode shapes obtained by analytical method and experimental method is presented in Figure 5.19.

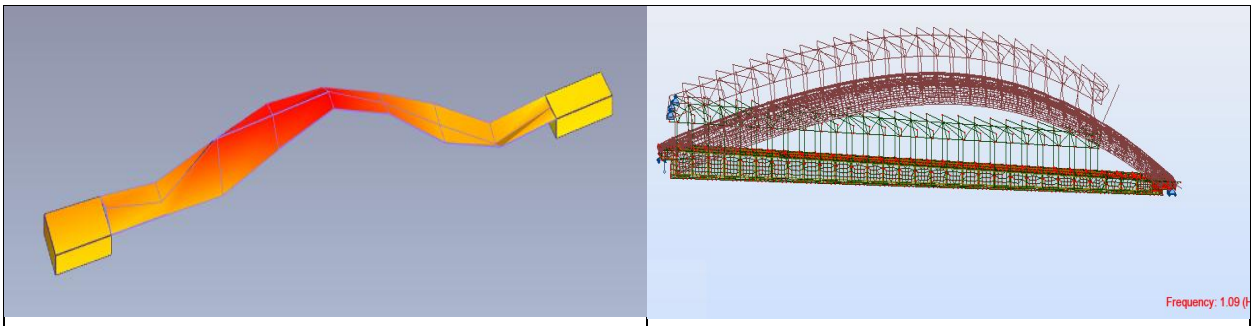

OMA	FEM
1.86Hz(1st Vertical Mode)	1.09Hz-(1st Vertical Mode)

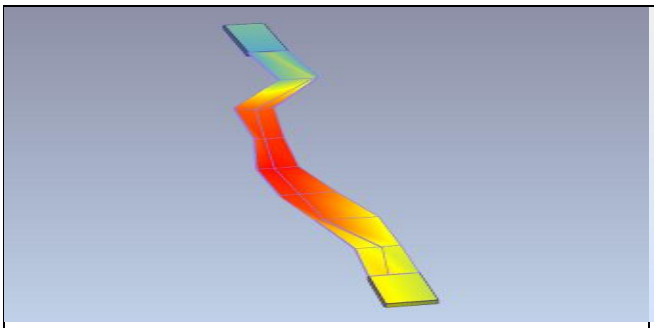	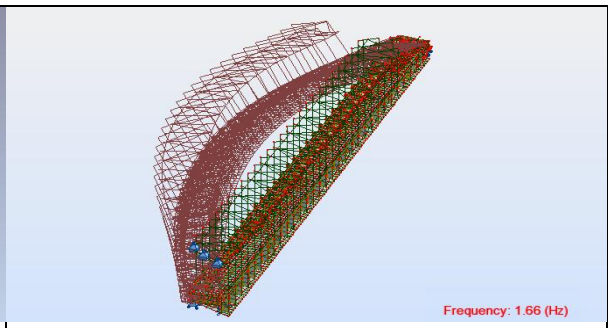
OMA	**FEM**
3.49Hz(1st Transversal Mode)	1.66Hz(1st Lateral Mode)

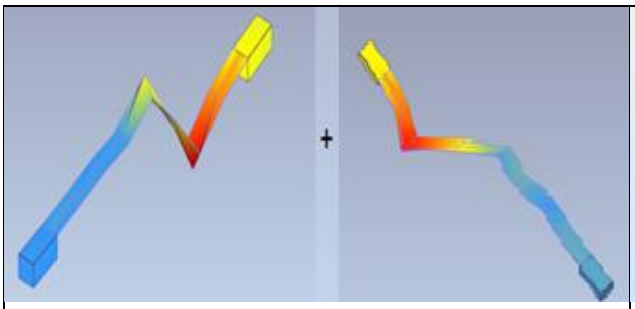	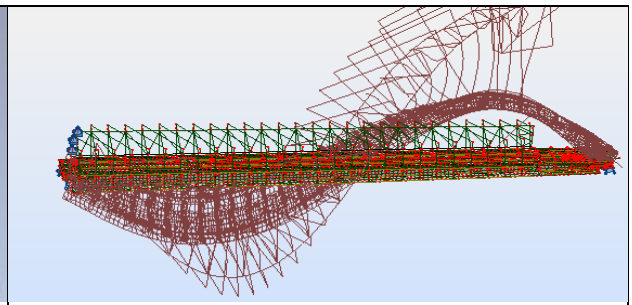
OMA	**FEM**
9.78Hz(2nd Vertical e+2nd Transversal Mode)	4.71Hz(2nd Vertical e+2nd Transversal Mode)

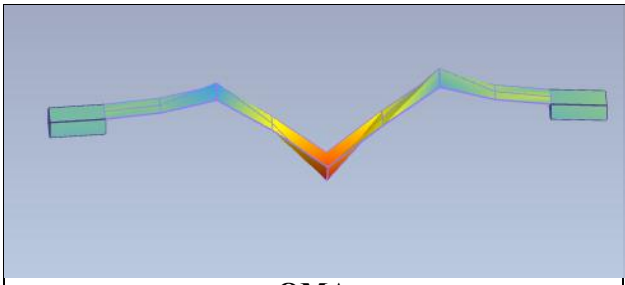	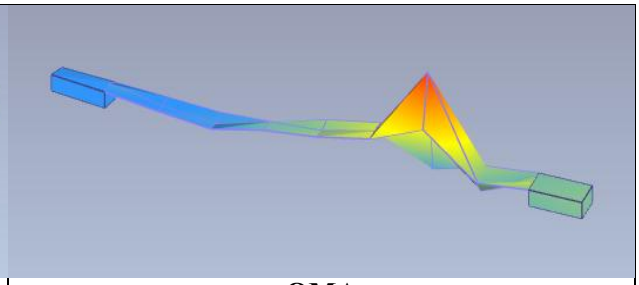
OMA	**OMA**
76.84Hz(Local Mode, Mid span)	82.15Hz(Local Mode, Quarter span)

Note: The modes shapes represented by V, T and L and represent vertical, transversal, and longitudinal respectively.

Figure 5.19-Mode shapes calculated by OMA (after completion) and Finite Element Method

Consequently, it is recommended to update the FEM model following the results obtained in OMA as the results obtained from FEM analysis are less stiff than those obtained from ambient vibration tests which is a common phenomenon owing to FEM being not suitable for representing structure behavior under low excitation forces. Three different updating mechanisms or a combination of those can be used, namely:

- Frequency residual
- Mode shape related function and
- Modal flexibility residual

Better results can be obtained by combining those methods. But, in this study detailed FEM updating techniques will not be covered as it is not the main objective, nevertheless, simple manual stiffness adjustment will be carried out. It can be noted that the vertical fundamental mode presents an error of 41.39%. Similarly, the estimate gap is higher in 2nd mode which may be attributed to laterally connected RHS lateral stiffness contribution omitted in the FEM model. Thus, simple finite element updating is applied to emphasize the end use of experimental modal estimates function in practical world.

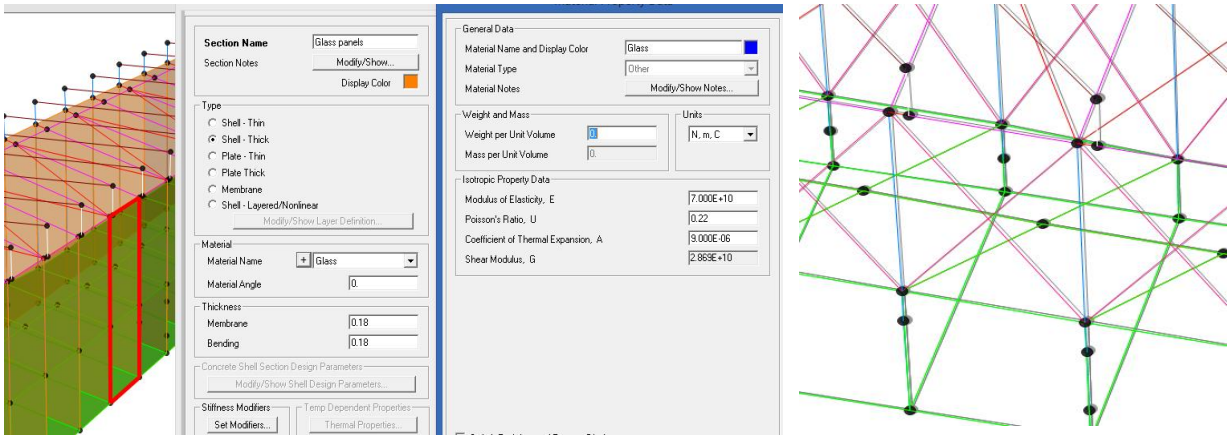

Figure 5.20-FEM updating trails, glass panel model (right) and cross bars model to simulate glass panels (left)

The model created in SAP2000 is updated to match the ambient vibration estimates. Initial trials had been done to stiffen the structure by adding steel cross beams to simulate the stiffness of the glass panels but results obtained were not realistic. Finally, Glass panels of 8mm thickness were modelled as thick shell elements with conservative mechanical properties (from Institute of Structural Engineering) as shown in Figure 5.20. Modal properties evolution is studied and the first fundamental frequency is turned out to be lateral mode and the mode of necessity, 1st vertical mode, appears as second method with a frequency of 1.6148Hz. In this case 13.18% error is registered from the ambient vibration results. As shown in the ambient mode shapes in Figure 5.19, the mode shape exhibit certain degree of restraint, i.e. rotational restraint, at the support ends. Therefore, ignoring other cause of estimation bias factors both in the FEM model and ambient vibration, the probable un-modeled stiffness of the supports is computed by determining

the rotational stiffness at supports in U2 direction which will update the model to the ambient vibration estimate. Note should be taken that all 4 supports, 2 in each end, are subject to the additional rotational stiffness. And the equivalent stiffness computed at each of the supports is found to be 275000KNm/rad equivalent to having 3% of the negative fixed end moments had the footbridge been with fixed end supports.

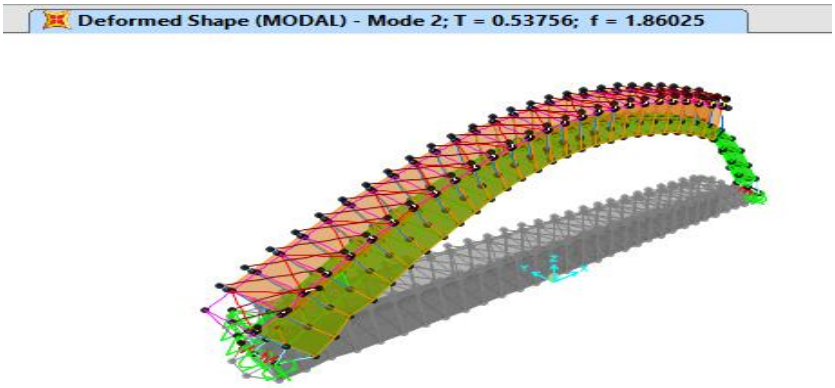

Figure 5.21-Updated model with rotational springs at support, 1st vertical Mode

5.2.2.3.2 Comparison of estimates before and after installation of TMDs

The modal estimates done for the records taken before TMD installation, uncompleted footbridge (glass panels not installed in place), and estimates done after completion of footbridge and TMDs installed were compared though the records were taken under different conditions of mass of the structure.

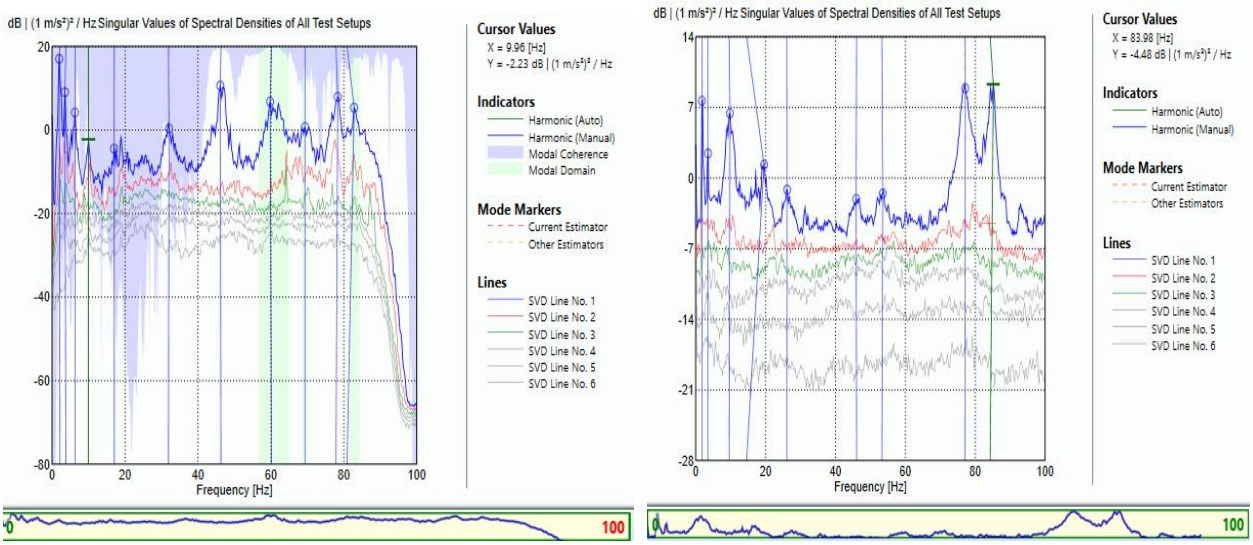

Figure 5.22-Averaged Singular value plot for all setups before (left) and after (right) completion of the project using 1024 sampling points and without decimation

The change of the fundamental frequency after the completion, from 1.975Hz to 1.86Hz, can be attributed to change of stiffness and mass, at the same time, of the structure. On the other hand, the lateral mode is fairly is constant before and after completion mainly due to less mass participation ratio attributed to this

mode which makes it less dependent on mass change of the structure. After completion modes in the range of 20-70Hz are eliminated due to high complexity

5.2.2.4 Assessment of Efficiency of TMD's in attenuating vibration

The analytical model and assessment done related to TMDs efficiency in vibration control on chapter 4 can be demonstrated by using ambient vibration tests by taking records before and after TMD installation at the same conditions of mass, stiffness and damping of the structure. Unfortunately this approach couldn't be implemented due to several administrative reasons. Hence, FEM model constructed in SAP2000 to simulate only the first mode of the original FEM model, developed in ROBOT by the design company, will be used to calibrate the effectiveness of TMDs in alleviating the serviceability vibration problems.

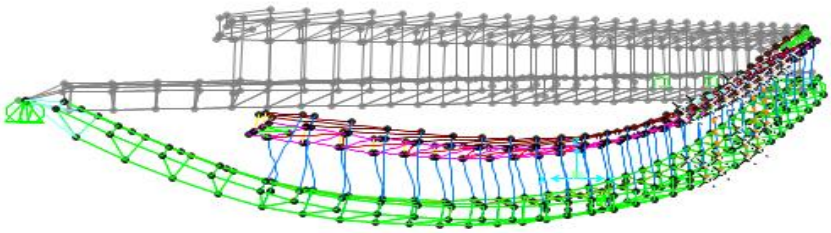

Figure 5.23-SAP2000 model to simulate only the first mode of footbridge, f=1.09Hz

TMDs are modelled with an equivalent linear spring of stiffness obtained from

$$K_{TMD} = \alpha * M_{1st\ mode} * (2\pi f_1)^2 \quad (5.1)$$

$$C_{TMD} = \beta * 2\xi * M_{1st\ mode} * (2\pi f_1) \quad (5.2)$$

Where $M_{1st\ mode}$ is the first mode modal mass, $\propto and\ \beta$ being percentages adopted for optimization and

f_1 is the fundamental mode frequency to which the TMDs are tuned

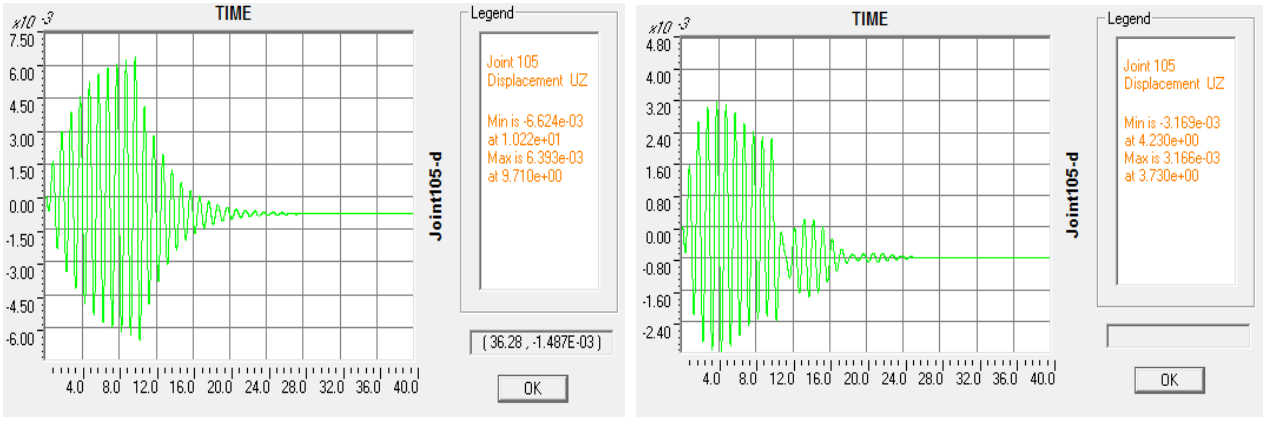

Figure 5.24-Pedestrian load Traffic class 5 (1st Harmonic) time history displacement response at Mid-Span without TMD (left) and with TMD (right) tuned to the 1st mode with a mass ratio of 2% [units in m]

Considering the worst case scenario, traffic density class 5, the pedestrian group load model is defined as explained in chapter 3. It is defined as a time history load with an excitation frequency equal to the fundamental mode of vibration.

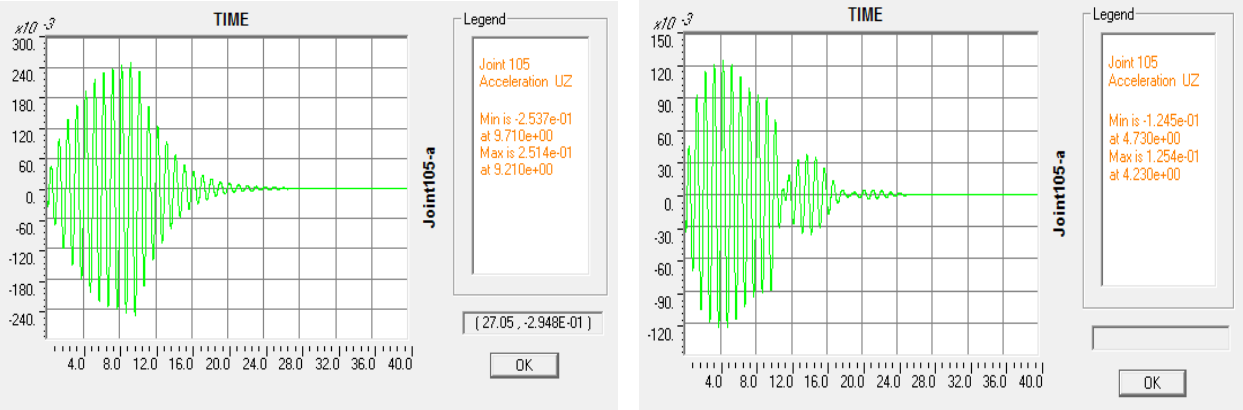

Figure 5.25-Pedestrian load Traffic class 5 (1st Harmonic) time history acceleration response at Mid-Span without TMD (left) and with TMD (right) tuned to the 1st mode with a mass ratio of 2% [units in m/s^2]

Time history of responses shown in figures 5.24 and 5.25 were obtained by setting the mass ratio to 2% of the modal mass associated with the fundamental vertical mode under undamped TMDs. The reduction of responses caused by introduction of TMD can be then measured allowing to determine the efficiency of the TMD under such excitation forces.

A 50% of reduction in the maximum acceleration response, at 2% mass, can be found owing to TMD installation and, similarly, the maximum displacement response reduction registered is 52%.The relative displacement between the TMD and footbridge was also investigated which is of paramount importance in

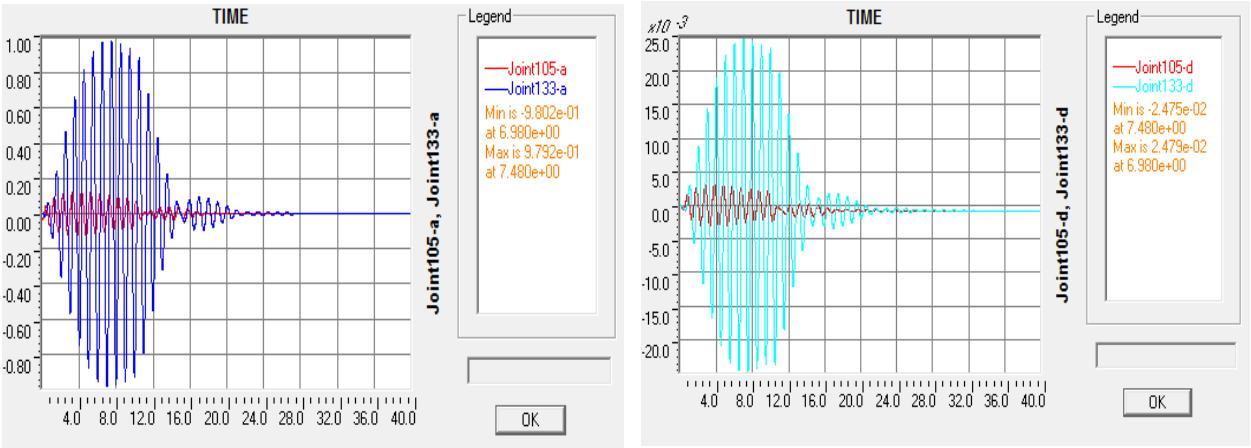

Figure 5.26-Pedestrian load Traffic class 5(1st Harmonic) Time history displacement (right) and acceleration (left) responses of TMD (joint 133) and footbridge mid-span node (joint 105) for the TMD tuned to the 1st mode with a mass ratio of 2% [units are in m and m/s^2]

relation to the available space for the TMD to displace. As mentioned, the maximum stroke of the TMDs was also fixed to $\pm$ 60mm, and the compliance of the results obtained can be confirmed referring to Figure

5.28 with TMD maximum displacement of 27.96mm. But it should be noted here that the results shown are done by considering undamped TMDs and further assessment of TMDs maximum displacement reduction under introduction of damper to TMD will be addressed.

In order to assess the change of responses reduction with varying mass ratio, the FEM model results of the maximum time history response is plotted versus mass ratio adopted under optimized frequency ratio obtained from MATLAB program. Figure 5.27 contains the aforementioned information which makes it able to make conclusions about the efficiency of undamped TMD in controlling vibration.

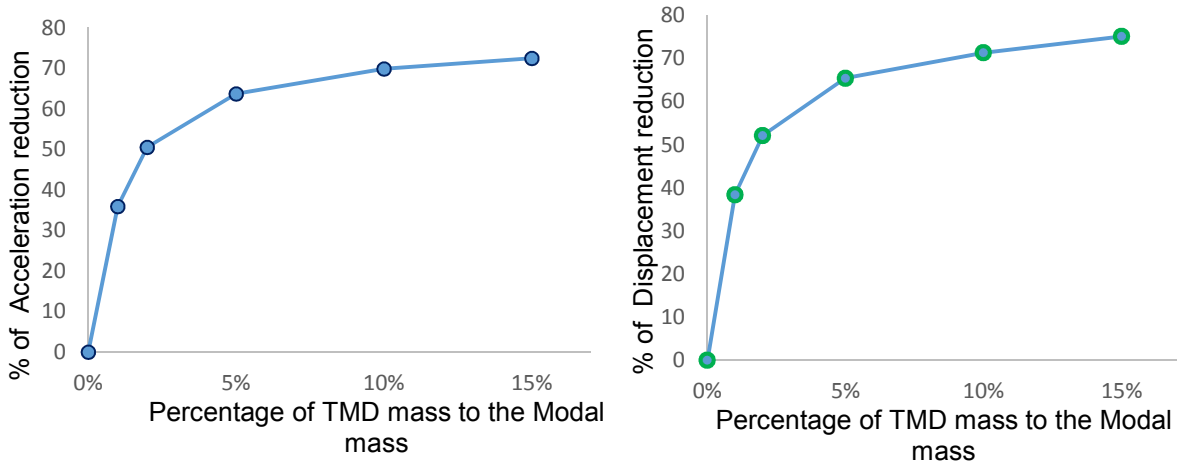

Figure 5.27-Percentage of reduction in footbridge maximum response vs TMD mass ratio owing to TMDs, Mid-span displacement (right) and Mid-span acceleration (left)

Considering the Mid-span displacement and acceleration, the maximum values across the time of harmonic excitation load is computed and the percentage of reduction in maximum acceleration and displacement by changing the mass percentage of the TMDs is investigated. Figure 5.27 is produced by taking sample mass ratios (1%, 2%, 5%, 10% and 15%) to determine the reduction of the aforementioned footbridge responses. And, it can be concluded that, the reduction of the footbridge responses beyond 5% mass are not significant which allows us to define the efficient mass ratio to control vibrations as further increase leads to an increase in the structural load carried by the footbridge.

Assuming 2% of mass the total stroke of TMD magnitude ranges 40mm as shown in Figure 5.29 which is less than the maximum allowed stroke of the TMD. Hence, it can be concluded that while choosing mass, proper assessment of available space for TMD displacement and maximum reduction of responses desired should be considered at the same time.

.

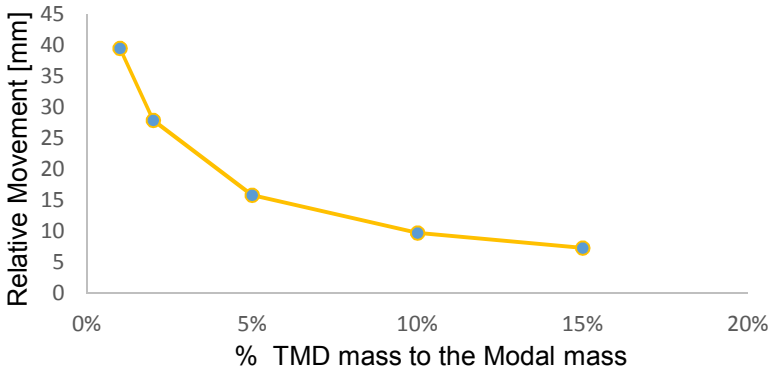

Figure 5.28-Relative displacement vs Mass of TMD

The intrinsic purpose of adding damper to TMD assembly it to reduce the displacement of the TMD due to the energy transmitted from the structure which intern assist in reducing the relative movement allowing the possibility of accommodating the TMD in a relatively smaller space for operation. As shown in Figure 5.28, a significant reduction of the TMD displacement can be achieved with effective damping coefficient up to 10% and further increase of damping merely affects the relative displacement of the TMDs.

Similarly, the choice of damping coefficient of TMDs is based mainly on the maximum displacement to which the TMDs are allowed to. Using the same SAP2000 model, non-linear time-history, the effect of varying damping coefficient on the stroke of TMD is determined under the same load case used before and the relevant conclusions can be drawn from Figure 5.29. It indicates a milder reduction of stroke of TMD with increased damping coefficient, but as discussed in chapter 4 for TMD efficiency, for a chosen mass of TMD, efficient TMD damping is computed.

Ambient vibration results show that the vertical mode presents a 2% damping and as concluded in chapter 4, Den Hartog's expression is valid for structural damping up to 5% which verifies its applicability in the case study.

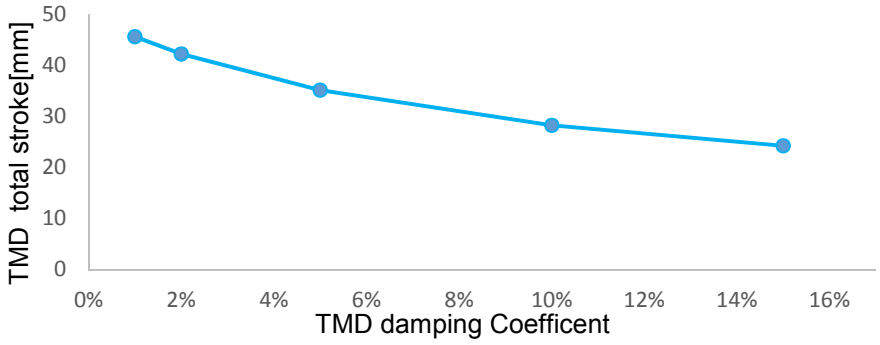

Figure 5.29-TMD stroke vs. TMD Damping coefficient for 2% mass of TMD

Case study vibration level assessment:

According to the updated model, updated also for modal damping values, with in-situ properties given by designer as shown in Figure 5.21, the model is checked for maximum levels of vibrations for comfort level defined by HIVOSS. Comfort Level of class 1 is met as shown in Figure 5.30 which is the maximum grade for serviceability purposes.[Refer Annex E, for detailed results]

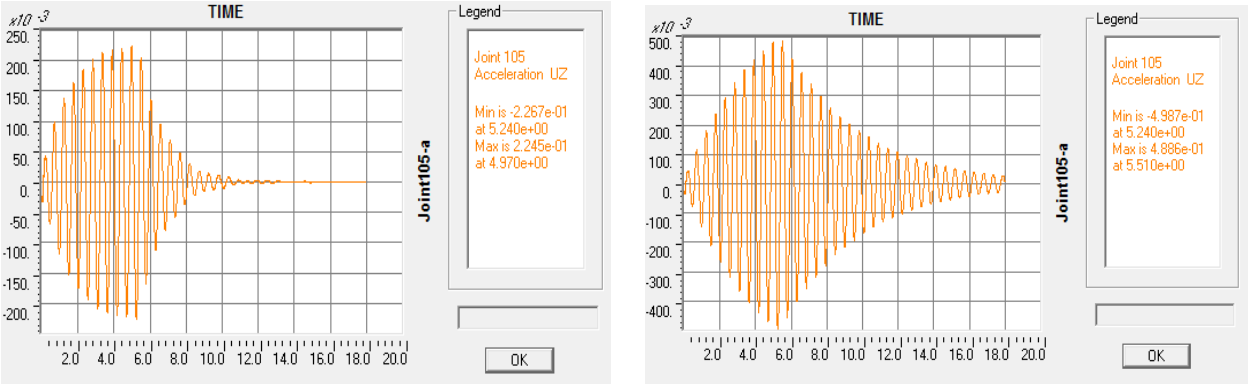

Figure 5.30-Footbridge vibration time History on final updated Model, actual TMDs and TC5 [m/s^2], with TMDs (left) and without TMDs (right)

5.2 Summary and conclusions

The implementation of operational modal analysis algorithms developed in chapter 1 was presented along with the results of FEM analysis of the model. Effective data collection advantages, error reduction methods employed, spectral calculations and modal estimates using EFDD MATLAB program and ARTeMIS were explained respectively. The main issues related to OMA, e.g. noise reduction during estimation of damping and natural frequency were explained and elaborately discussed. Comparison of modal estimates during construction and after completion as well as the estimates from ARTeMIS versus MATLAB programed algorithm were presented with probable reasoning for the evolution of results obtained.

Additionally, recommendations for FEM updating and Assessment of TMDs using the FEM model was brought forward. TMDs efficiency calibration was also done under varying mass ratio for suppressing the fundamental mode in order to reduce pedestrian induced vibrations.

6

CONCLUSIONS AND FUTURE WORKS

6.1 Conclusions

The present work was performed with the purpose of studying the operational modal analysis (ambient modal identification) of a case study, North footbridge owned by EDP, Portugal, as well as the assessing the effect of TMDs in modal parameters and its effectiveness in suppressing the vibrations induced by pedestrian traffic. In fact, with the increased trend of constructing an ever filigree and slender footbridges nowadays, mainly for aesthetical purposes, the dynamic effects caused by pedestrian traffic is required to be controlled for the fulfilment of ultimate and serviceability limit states prescribed by international design guidelines and codes.

One of the main issues concerning dynamic effects due to pedestrian traffic is the possibility of resonance between the structure and the pedestrians, vertically or laterally (lock-in), leading to a considerable increase of the dynamic effects. The reason pointed out for this resonant behaviour is the synchronization of pedestrians passing footbridge as discussed in chapter 3.Thus, to avoid the resonance effect the natural frequency of footbridge, usually low, is important not be in the frequency range of walking pedestrian traffic. In order to assess the actual modal parameters of a footbridge, ambient vibration methods are of paramount importance as to validate FEM solution.

Several approaches to ambient modal identification methods are investigated in this paper, ranging from frequency domain to time domain identification models. Non-parametric modal identification algorithms are highly stressed in the presented work as opposed to parametric methods.

The abstract algorithms of frequency domain, and to some extent in the time domain, are demonstrated using an example of ambient vibration record undertaken in the case during the construction phase and before installation of TMDs. The classic EFDD method in frequency domain and stochastic sub-space identification method in time domain are programmed in MATLAB and proper understanding of identification models is performed. The following conclusions can be drawn concerning OMA:

I) Proper data collection is an essential task towards a more realistic modal results and easy processing of sensor records. It is concluded that a systematic and planned sensor layout during data collection and use of sufficient number of sensors, so as to avoid rank deficiency during spectra computation, is recommended.
II) Lack of sufficient instrumentation needs very well studied sensor layout to find all the modes of vibration as each setup contribute to the identification of specific mode which may not be revealed

in other setups.eg. Torsional modes could be easily identified from a setup with sensors located at opposite ends of the width of footbridge;

III) Proper signal pre-processing plays a paramount role in the identification of unbiased modal parameters. As ambient vibration tests are prone to noises from different sources; cables, data acquisition apparatus, harmonic sources in the proximity (e.g. rotating machine) etc., and thus. appropriate filtering should be applied (low-pass, band-pass etc.). The introduction of decimation to reduce frequency range to range of importance, use of anti-aliasing filters and windowing of data in alleviating leakage should be all considered for clean input spectra computation. The aforementioned treatments are emphasized in frequency domain algorithms as opposed to time domain;

IV) The evolution of SDOF bell curve in EFDD represents the uncoupled SDOF mode of vibration which plays an important role in definition of weighted mode shape and damping coefficient. Thus, the MAC criterion taken should comply with the overall identification process in terms of methodology considered, precision desired and site properties.0.8 value can be considered as a starting value;

V) Enhanced frequency domain algorithms provides user to choose minimum and maximum correlation co-efficient for damping value computation and hence, co-efficient chosen have to be practically feasible depending on the overall process of modal identification. E.g. correlation range can be narrowed for a project in which the precision of the modal estimates is not highly important and/or ambient records not taken with precision and care. The pattern of a line formed by plotting the peaks of the correlation function versus time-lag should be investigated for its linearity. Non-linear pattern implies the inclusion of noise in the range of the normalized correlation function assumed;

VI) MATLAB programmed EFDD yields similar results with ARTeMIS standard EFDD estimates, but the advantage of checking the complexity percentage in ARTeMIS, in addition to MAC validation, is found helpful in distinguishing natural modes of vibration and observing the pattern of modes in the complexity circle;

Moreover, in an effort to calibrate the excitation force due to pedestrian traffic at different densities and patterns of movement, pedestrian loading is studied in brief terms. Precautions should be taken to prevent lock-in possibility by changing the modal properties of the footbridge in order that natural lateral modes of vibration does not exist in the range of the lateral frequency of pedestrian traffic. It can be concluded that:

I) Realistic pedestrian densities should be considered for design purposes as lack to do so will result in biased modal parameter estimation during FEM analysis.

Additionally, the analysis of TMDs, presented in chapter 4, was done in an effort to determine the effect of TMDs in suppressing given modes of vibrations in the footbridge. This numerical development, vibration control through TMDs, was expected to be supplemented by in-situ effect of TMDs using ambient vibration

responses pertaining to footbridge with locked and unlocked TMDs, thereby allowing the efficiency of TMDs to be determined. But, this couldn't be carried out due for many reasons.

Numerical optimization of TMDs also has been done by developing MATLAB program and results are compared to Den Hartog optimization criteria which were found to comply with it. Moreover, TMD efficiency assessment was done using FEM model of the footbridge to supplement the numerical development done on chapter 4. Note that the tuning of TMDs is done by mass ratio, frequency ratio and damping ratio and conclusions drawn are:

I) With the increase of TMD mass ratio, the ability of this device to control vibrations of the primary structure increases. Nevertheless, this increment is more evident up to a mass ratio of 0.05. Besides, higher mass ratios can lead to situations where it is impossible to allocate that mass to the structure;
II) The TMD effectiveness is highly dependent on the frequency tuning. For instance, if a variation of only 5% around *qOPT* occurs, the maximum amplitude of the transfer function increases by about 39 % in the case of an undamped primary structure;
III) Variations on the TMD optimum damping ratio did not lead to a significant variation in the TMD effectiveness. Nevertheless, in some cases as, for instance, in TMDs applied to footbridges, it is recommended to design the TMD with a slightly higher damping ratio, assuring that the transfer function has only one peak, in order to overcome the lock-in effect.

The extrapolation of the concepts here introduced concerning the behavior of these vibration control devices attached to single degree-of-freedom systems into multi degree-of-freedom structures was also briefly investigated. Since the TMD is designed to work properly only to a specific structural vibration mode, and if the cross-coupling between mode shapes can be disregarded, the considerations introduced for a single degree-of-freedom system can be readily extended to multi degree-of-freedom structures, through the concept of modal coordinates.

Design issues related to the effective implementation of these systems were also addressed. Some reasons that may lead to unfeasible implementations were pointed out:

I) The TMD mass could be extremely large and not of practical implementation due to the lack of space to accommodate this device within the structure;
II) The required space for TMD working properly may not be compatible within the available space of the structure;
III) Limited load bearing capacity of the structure may require its strengthening and, consequently, the reasons pointed out for the adoption of a TMD system may no longer exist

Concerning the high dependency on the effective structural dynamic characteristics and also the possibility of TMD fabrication errors, to assure a good design, the tuning of these devices should be

performed with in-situ vibration tests, validating its behavior and obtaining a reliable estimation of its performance.

6.2 Future Works

Based upon the work described in this dissertation, and within the scope of operational Modal analysis and vibration control, some suggestions for further research can be drawn.

Firstly, it should be remarked that many other results would be very interesting to present in this dissertation. Among these a complete set of results for modal parameter estimates for each set-up of ambient vibration tests could be presented, but the possibility of presenting all the aforementioned outputs in this document is limited.

In relation to the EFDD program developed in MATLAB, some modification could have been done in terms of the modifying the mode shape estimates. This could be carried out by weighting the mode shapes using the sample points in the SDOF bell curve definition. Moreover, automated estimation would be the second modification to the MATLAB program for automatic modal estimation.

Similarly, complete sub-space modal identification with increased efficiency could have been implemented in MATLAB and ARTeMIS Pro and compared with frequency domain estimates for validation of modes of vibration.

The assessment of damage over a period of time using structural health monitoring procedures would be the continuation of this study. In fact, the case study, EDP's North footbridge, is equipped with structural health monitoring apparatus which will run for a period of one year and the extension of this study to structural health monitoring of this footbridge would be a smooth transfer of task. Topics of interest would be damage detection, environmental effect of degradation versus structural weakness (failure), remaining life of structure etc.

The last but not the least, the assessment of TMDs in vibration control of the footbridge would be a very interesting aspect to discover there by drawing conclusion on its applicability and drawbacks. Footbridge vibration levels assessment under actual test pedestrians would be very interesting. To overcome one of the main drawbacks of TMDs, other vibration control devices may also be investigated. In fact, semi-active and active control of structures that are able to "read" the excitation and modify the properties of the control device to improve its efficiency may be in the near future one of the most important fields of research concerning the dynamic behavior of structures in controlling vibrations not only in footbridges but also in bridges.

BIBLOGRAPHY

Anders Mårtensson Martin Nilsson. “Dynamic Analysis of Pedestrian Load Models for Footbridges, A review of current load models and guidelines.” Thesis in the Master’s Structural Engineering and Building Technology by, Chalmers University of technology Goteborg, Sweden, 2014

Andrew T. Zimmerman, Michihito Shiraishi; R. Andrew Swartz, and Jerome P. Lynch. “Automated Modal Parameter Estimation by Parallel Processing within Wireless Monitoring Systems.” M.ASCE, 2008

Arnaud Guyader, Laurent Mevel. “Covariance Driven Subspace methods: input/output vs output-only.” Universite´ de Haute Bretagne and IRISA / INRIA, Campus de Villejean and Campus de Beaulieu, 35042 Rennes Cedex, France, 1997

ARTeMIS (2010). “Ambient Response Testing and Modal Identification Software.” Structural Vibration Solution A/S, Alborg, Denmark.[http://www.svibs.com/]

Bachmann, H. (1998). “Vibration Problems in Structures, Practical Guideline.” Birkhäuser Verlag, Basel.

Bendat, J.S., Piersol, A.G., 1980, “Engineering Applications of Correlation and Spectral Analysis.” John Wiley & Sons, New York, NY.

Brincker, R. Ventura, C. Andersen, P. “Damping Estimation by Frequency Domain Decomposition.” In Proceedings of IMAC XIX, Kissimmee, USA, 2001

Brown, D.L. Allemang, R.J. Zimmerman, R.D. Mergeay, M. “Parameter Estimation Techniques for Modal Analysis.” SAE Paper, No.790221, SAE Transactions 88,828-846, 1979

Butz, C., Feldmann, M., Heinemeyer, C., Sedlacek, G., Chabrolin, B., Lemaire, A. et al. 2008.“ Advanced load models for synchronous pedestrian excitation and optimised design guidelines for steel footbridges.” Research Fund for Coal and Steel, European Comission.

Caetano et al. “Footbridge vibration design.” Third International Conference, footbridge, 2008, Porto, Portugal

Caetano, E. Cunha, A. Magalhães, F. Moutinho, C. (2010a). “Studies for controlling human-induced vibration of the Pedro e Inês footbridge, Portugal. Part 1: Assessment of dynamic behaviour. Engineering Structures.” 32(4), 1069-1081.

Caetano, E. Cunha, A. Moutinho, C. Magalhães, F. (2010b). “Studies for controlling human-induced vibration at the Pedro e Inês Footbridge, Portugal. Part 2: Implementation of tuned mass dampers.” Engineering Structures, 32(4), 1082-1091

Caetano, E; Cunha, A (2004). “Experimental and numerical assessment of the dynamic behaviour of a stress-ribbon footbridge.” Structural Concrete, 5(1), 29-38.

Christian Meinhardt. “Application of tuned mass dampers for bridge decks.” Dr.-ing. Project engineer, gerb vibration control systems, essen, Germany, third international conference, footbridge 2008

Christohph Heinemeyer and Markus Feldmann. “European design guide for footbridge vibration, third international conference.” footbridge 2008, RWTH Aachen University, Aachen, Germany

Cunha, A. Caetano, E. Magalhães, F. (2007). “Output-only Dynamic Testing of Bridges and Special Structures.” Structural Concrete (Fib), 8(2), 67-85.

Felber, A. J. (1993). “Development of a Hybrid Bridge Evaluation System.” PhD Thesis, University of British Columbia, Vancouver, Canada

Felix Weber, Glauco Feltrin, and Olaf Huth, Dübendorf. “SAMCO Final Report F05, Guidelines for Structural Control.” Switzerland, 2006

Felix Weber, Glauco Feltrin, and Olaf Huth. “F05 Guidelines for Structural Control.” SAMCO Final Report, 2006

Frahm, H. (1911). "Device for Damping Vibrations of Bodies." U.S.Patent, No. 989, 958

Friswell, M.I. and Mottershead J.E. Finite Element Model Updating in Structural Dynamics. Kluwer Academic Publishers, Dordrecht, The Netherlands, 1995.

Henrik Herlufsen, Brüel & Kjær. “Identification techniques for operational modal analysis– an overview and practical experiences.” Sound & vibration measurement a/s, Denmark

Human Induced Vibration of Steel Structures, HIVOSS, RFS2-CT-2007-00033, 2007

Iemke Roos. “Human induced vibrations on footbridge, application and comparison of pedestrian load models.” master thesis study in civil engineering at Delft University of technology in the Netherlands, may 2009

J. W. Cooley and J. W. Tukey. “An algorithm for the machine calculation of complex Fourier series. Mathematics of Computation.” 1965

James Brown John, Stana Zivanovic, Aleksandar PAVIC. “Crowd Dynamic load on footbridges”, Third International Conference, footbridge, 2008, Porto, Portugal

João Francisco de Carvalho Santos Henriques. “Dynamic Behaviour and Vibration Control of High-Speed Railway Bridges through Tuned Mass Dampers.” Dissertation for the degree of Master of Science in Civil Engineering, IST, Lisboa, 2007

Karoumi, R. (1998). "Response of Cable-Stayed and Suspension Bridges to Moving Vehicles, Analysis Methods and Pratical Modeling Techinques." Ph.D. Thesis, Royal Institute of Technology, Stockholm.

Lel Zuo. “The Two-Degree-of-Freedom Tuned-Mass Damper for Suppression of Single-Mode Vibration under Random and Harmonic Excitation.” Abbott Laboratories and Samir A.Nayfeh, Massachusetts Institute of Technology, Journal of Vibration and Acoustics, FEBRUARY 2006, Vol. 128

MACEC (2011), MACEC 3.2. “A Matlab Toolbox for Experimental and Operational Modal Analysis User’s Manual, Department of Civil Engineering.” Faculty of Engineering, Katholieke Universiteit, Leuven, Belgium. [http://bwk.kuleuven.be/bwm/macec]

Magalhães, F. Costa, B. Cunha, A. Caetano E, (2006). “Experimental Validation of the Finite Element Modeling of Pinhão Bridge.” In the 3rd European Conference on Computational Mechanics: Solids, Structures and Coupled Problems in Engineering, Lisbon, Portugal.

Matsumoto, Y., Nishioka, T., Shiojiri, H. and Matsuzaki, K. (1978), ‘Dynamic design of footbridges’, IABSE Proceedings, 2, Paper P-17/78, Zurich

Mehdi Batel, Brüel & Kjær, Norcross. “Operational Modal Analysis –Another Way of Doing Modal Testing.” Georgia, sound and vibration journal (2002)

Moutinho, C. Hu, W.H. Caetano, E. Cunha, A. (2008). “Implementation of a Dynamic Monitoring System at Coimbra Footbridge.” In the Proceedings of IMAC XXVI, Orlando, Florida, USA.

Oeding D (1963) “Verkehrsbelastung und Dimensionierung von Gehwegen und anderen Anlagen des Fussgaengerverkehrs"[Traffic volume and dimensioning of footways and other facilities of pedestrian traffic]. Strassenbau und Strassenverkehrstechnik series 22.

P. Dallard et al. “The London Mileenum Beridge.”The Structural Engineer Volume 79/No 22, November 2001

P.Bukenya, P. Moyo, C. Oosthuizen. “Comparative study of operational modal analysis techniques using ambient vibration measurements of a concrete dam.” University of Cape Town, Department Civil Engineering, proceedings of ISMA2012-USD, 2012

Peeters, B. Van der Auweraer, H. (2005). “PolyMax A Revolution in Operational Modal Analysis.” In Proceedings of IOMAC, Copenhagen, Denmark.Peter Van Verschee, Bart de Moor. “Identification for linear systems theory - implementation – applications.” katholieke universiteit, Leuven, Belgium

Peeters, Bart (2000). “System Identification and Damage Detection in Civil Engineering.” PhD Thesis, Katholieke Universiteit Leuven, Leuven

Proença, J., Azevedo, J. (1999). “Identificação Dinâmica de Sistemas Estruturais.” Apontamentos da Disciplina de Dinâmica e Engenharia Sísmica de Mestrado em Engenharia de Estruturas, IST

Prof. Dr. Eleni Chatzi. “Identification method for structural systems.” Lecture 9 - 23 April, 2 013

Rainieri, Carlo, Fabbrocino, Giovanni. “Operational Modal Analysis of Civil Engineering Structures, an Introduction and Guide for Applications.” 2014

Randall J. Allemang. “The Modal Assurance Criterion –Twenty Years of Use and Abuse.” University of Cincinnati, Cincinnati, Ohio, sound and vibration journal (2003)

Sétra. “Assessment of vibrational behavior of footbridges under pedestrian loading.” Technical Guide to Footbridges, October 2006

SYNPEX Guidelines. “European Project on Advanced Load Models for synchronous Pedestrian excitation and Optimized Guidelines for Design of Steel Footbridges.” 2007

Wei-Hua Hu. “Operational modal analysis and continuous dynamic monitoring of footbridges.” Dissertation presented to the faculty of engineering of the University of Porto for the degree of doctor in civil engineering, 2009

Welch, Peter D. “The use of fast Fourier Transform for the Estimation of Power Spectra: A method based on Time Averaging over Short Modified Periodograms.” IBM Watson Research Center, Yorktown Heights, N.Y., 1967

Wiesław Fiebig. “Reduction of Vibrations of Pedestrian Bridges Using Tuned Mass Dampers (TMD).” Wroclaw University of Technology, Institute of Machine Design, Łukasiewicza, Poland (May 19, 2010)

Živanović, S., Pavić, A. and Reynolds, P. (2005). “Vibration serviceability of footbridges under human-induced excitation: a literature review.” Journal of Sound and Vibration, Vol. 279, No. 1-2

“Pedestrian Loads and Dynamic Performances of Lively Footbridges, an Overview.” CSHM – 2 Workshop, 28th September – 1st October 2008, Taormina

The Institute of Structural Engineers. “Structural Use of Glass in Buildings.” SETO, London, 1999

Annex A

MAT LAB algorithm for undamped two degree of freedom TMD optimization

```
for i=1:200;                % assigns 'a' vector with zeros except the first term
   if i==1
      a(i)=1000000;
   else
      a(i)=0;
   end
end
min1=a+zeros(200,1);   %assignment of vectors min1, min2 and max for looping
min2=a+zeros(200,1);
max=zeros(200,1);
count3=1;
% maximizing Gp under various excitation frequencies, followed by two minimization 'for loops' aiming to
minimize Gp under several TMD damping ratios and several structure to TMD frequency ratio respectively
for q=0:0.01:1              % 'q' represents the frequency ratio
       count2=1;
   for x=0:0.01:0.5         % 'x' refers to the damping ratio
            count1=1;
       for y=0:0.01:2       % 'y' indicates the excitation frequency ratio and Gp is displacement transfer
                            function
          Gp = sqrt(((q^2-y.^2).^2+(2*q.*x.*y).^2)./(((1-y.^2).*(q^2-y.^2)-0.2*q^2.*y.^2).^2+4.*y.^2.*(q.*x*(1-
(1+0.2).*y.^2)).^2));
                             % maximizing g under several 'y's
 if Gp > max(count1,1)
     max(count1+1,1)= Gp;
 else
     max(count1+1,1)=max(count1,1);
 end
      count1=count1+1;
       end
 %assigning the maximum Gp for a given damping ratio and frequency ratio to the next term of
'min1'minimizing vector
    min1(count2+1,1)= max(202,1);
% minimizing loop for damping ratio
       if min1(count2+1,1)< min1(count2,1)
    min1(count2+1,1) = min1(count2+1,1);
      else
   min1(count2+1,1)= min1(count2,1);
      end
  count2=count2+1;
   en
%assigning the minimized maximum Gp under a given frequency ratio to the next term of 'min2'
minimizing vector
   min2(count3+1,1)= min1(52,1);
 % second minimizing loop for frequency ratio
 if min2(count3+1,1) < min2(count3,1)
   min2(count3+1,1) = min2(count3+1,1);
 else
    min2(count3+1,1)=min2(count3,1);
 end
 count3=count3+1;
end
```

```
disp(min(min2(1:count3,1)));       % displays the optimized displacement transfer function
count4=0;
% looping to find the optimized frequency ratio
for i=1:length(min2)-1
    if min2(i+1)==min2(i)
        i=length(min2)-1;
    else
      count4=count4+1;
    end
end
% displays the frequency ratio of TMD to the primary structure
    disp('Fs/Fp=');
    disp((count4-1)*0.01);
    count5=0;
% looping to find the optimized damping ratio
    for j=1:length(min1)-1
     if min1(j+1)==min1(j)
        j=length(min1)-1;
    else
        count5=count5+1;
     end
    end
% displays the damping ratio of the TMD
disp('Damping=');
    disp((count5-1)*0.01);
```

Annex B

MATLAB algorithm for damped two degree of freedom TMD optimization

```
for i=1:200;                % assigns 'a' vector with zeros except the first term
   if i==1
      a(i,1)=1000000;
   else
      a(i,1)=0;
   end
end
%definition of optimization parameters (structural damping and TMD to structure mass ratio)
structure_damping=0.05;
mass_ratio=0.02;
%assigment of vectors min1, min2 and max for looping
min1=a+zeros(200,1);
min2=a+zeros(200,1);
max=zeros(200,1);
count3=1;
% looping for 'Min-max' optimization, using one internal 'for loop' for  maximizing Gp under various
excitation frequencies, followed by two minimization 'for loops' aiming to minimize Gp under several TMD
damping ratios and several structure to TMD frequency ratio respectively
for q=0:0.01:1              % 'q' represents the frequency ratio
       count2=1;
   for x=0:0.01:0.5         % 'x' refers to the damping ratio
           count1=1;
       for y=0:0.01:2       % 'y' indicates the excitation frequency
% Gp, displacement transfer function
              Gp =sqrt(((q^2-y.^2).^2+(2*q.*x.*y).^2)./(((1-y.^2).*(q^2-y.^2)-mass_ratio.*q^2.*y.^2-
4*structure_damping.*x.*q.*y.^2).^2+4.*y.^2.*(structure_damping.*(q.^2-y.^2)+q.*x*(1-
(1+mass_ratio).*y.^2)).^2));
 % maximizing Gp under several 'y's
  if Gp > max(count1,1)
    max(count1+1,1)= Gp;
  else
     max(count1+1,1)=max(count1,1);
  end
      count1=count1+1;
 end
%assigning the maximum Gp for a given damping ratio and frequency
%ratio to the next term of 'min1'minimizing vector
      min1(count2+1,1)= max(202,1);
% minimizing loop for damping ratio
      if min1(count2+1,1)< min1(count2,1)
   min1(count2+1,1) = min1(count2+1,1);
      else
          min1(count2+1,1)= min1(count2,1);
      end
      count2=count2+1;
    end
%assigning the minimized maximum Gp under a given frequency ratio to the next term of 'min2'
minimizing vector
   min2(count3+1,1)= min1(52,1);
% second minimizing loop for frequency ratio
 if min2(count3+1,1) < min2(count3,1)
   min2(count3+1,1) = min2(count3+1,1);
```

```
 else
     min2(count3+1,1)=min2(count3,1);
 end
 count3=count3+1;
end
disp(min(min2(1:count3,1)));       % displays the optimized displacement transfer function
% looping to find the optimized frequency ratio
count4=0;
for i=1:length(min2)-1
    if min2(i+1)==min2(i)
        i=length(min2)-1;
    else
        count4=count4+1;
    end
end
    disp('Fs/Fp=');
    disp((count4-1)*0.01);
% looping to find the optimized damping ratio
    count5=0;
    for j=1:length(min1)-1
     if min1(j+1)==min1(j)
        j=length(min1)-1;
    else
        count5=count5+1;
     end
    end
disp('Damping=');           % displays the damping ratio of the TMD to the structure
    disp((count5-1)*0.01);
```

Annex C

MATLAB algorithm for EFFD (Enhanced Frequency Domain Decomposition)

I) HALF SPECTRA MATRIX ALGORITHM

```
% input in to for spectra matrix formulation are tri-axial acceleration
% records from two locations (FK and IC), decimation rate r and nfft window
% length defined by nfft
function [F,Syy]=FDD_spectra(fs,r,FK,IC,nfft)
[J1,K1]=size(FK);
%decimation of records
for i=1:K1
  j=i;
    FKi(:,j)=decimate((FK(:,i)),r);
    ICi(:,j)=decimate((IC(:,i)),r);
end
decimated_data=[FKi ICi];          %assemble decimated data into one matrix
[H1,L1]=size(decimated_data);   %de-trending the decimated matrix
for i=1:L1
detrended_data(:,i)=detrend(decimated_data(:,i));
end
%defining the frequency range from DC to Nyquist frequency
l=0:H1-1;
b=ceil(H1/2);
F=fs/r*l/H1;
F=F(1:b);
for j=1:L1
for k=1:L1
%overlap length of spectral calculation is set to default value
[Syy{j,k},F]=cpsd(detrended_data(:,j),detrended_data(:,k),hann(nfft),[],nfft,fs/r);
end
end
end
```

II) MODAL ESTIMATION USING SINGULAR VALUE DECOMPOSITION METHOD

```
%Syy is the auto-spectra and cross-spectra, each spectra being stacked in each cell in the Syy matrix as
vertical vectors
%F presents the frequency range,0 to fs/2,in Hz units
%Fn is a text variable for frequency peak, done by peak picking %creating function for call with 3 inputs
variables
function [S,Mode1,MAC1,Damp,Nat_freq] = MYFDD1(Syy,F,nfft,r,fs)
Li=length(F);                %Length of the frequency domain
%size of the cross-power spectra (n*n) depending on the number of simultaneous records
[J1,K1]=size(Syy);
%formation of 3D spectra matrix (n*n*Li) floor by floor with (n*n) floor %matrix by extracting the individual
elements of each spectra cell in %orderly manner
for z=1:Li
for j=1:J1
for k=1:K1
Gi(j,k)=Syy{j,k}(z);
end
end
%application of singular value decomposition of each floor matrix formed at %respective floor level
(Gauged by 'z')
```

```
[Ui,Si,Vi]=svd(Gi);
for j=1:J1
for k=1:J1
%singular vector matrix assignment as a 3D stack with each slice gauged %by 'z'
Uj{j,k,z}=Ui(j,k);
%singular value matrix with each cell of matrix vertically ordered values (reproducing the same Si)
Sj{j,k}(z,1)=Si(j,k);
end
end
end
%formulation of the diagonal singular value matrix and transposing
for j=1:J1
S(:,j) = Sj{j,j};
end
%plotting singular values
figure
if nargin==5
subplot(6,1,[1 6])
semilogy(F,S)
else
semilogy(F,S)
xlabel('Frequency (Hz)')
end
title('SVD curve of all channels')
xlabel('Frequency (Hz)')
ylabel('Ampl (dB)')
% Finding peak frequency with 1Hz band width centered at the specified freq.
%input of modal frequency by peak-picking from the SVD displayed already
prompt='Modal Frequency[Fn]:';
Fn=input(prompt);
figure
semilogy(F,S)
hold on
plot([Fn,Fn],[min(S(:,6)),max(S(:,1))],'o')
d1=round(nfft*Fn*r/fs)+1;
if nargin==5
Fn = num2str(Fn,'%6.4f');
minF = str2num(Fn)-0.5;
maxF = str2num(Fn)+0.5;
con=0;
for k = 1:Li
if F(k,1)>=minF && F(k,1) <= maxF
con = con +1;
%assignment of singular value to Sssi
Ssi(con,1) = (S(k,1));
%assignment of the reference singular vector for MAC computation over the 1Hz freq. width
VecFi(:,con) = real(cell2mat(Uj(1:J1,1,k)));
end
end
%Reference singular vector 'VecF' definition by using the maximum absolute singular value
First Sssi variable is maximum term, as singular values are %arranged in descending order
con2=0;
for i=1:con
   if abs(Ssi(i,1))==max(abs(Ssi))
      VecF(:,1)= VecFi(:,i);
      break;
```

```
    else
        con2=con2+1;
    end
 end
figure
subplot(3,2,[3,5])
plot(Ssi,'g')
title('Bell curve')
xlabel('bins')
ylabel('singular value[dB]')
Mode1=VecF;
%MAC value calculation through MAC function and plotting
for k=1:Li
VecF1(:,k) = real(cell2mat(Uj(1:J1,1,k)));
X=VecF;
Y=VecF1(:,k);
GL=size(X,2);
for i=1:GL
for j=1:GL
R=(X(:,i)'*Y(:,j))^2/(((X(:,i)'*X(:,i))*(Y(:,j)'*Y(:,j))));
end
end
MAC(k,1)=R;
end
subplot(3,2,[1,2])
%plotting MAC value across frequency range, separating the values of those below and above MAC=0.9
for i=1:Li
        if MAC(i,1)>=0.9
stem((i-1)*fs/nfft/r,MAC(i,1),'r')
    else
 stem((i-1)*fs/nfft/r,MAC(i,1),'b')
hold on;
        end
 end
title('Mac value')
xlabel('Frequency')
ylabel('MAC')
% evaluation of MAC1 at the modal frequency, usually unity
MAC1=(X(:,1)'*X(:,1))^2/(((X(:,1)'*X(:,1))*(X(:,1)'*X(:,1))));
else
Modos1=0;
title(['Fn=', Fn, ' Hz'])
MAC1=0;
end
%SDOF bell and evaluation of damping value(MAC rejection criterion used) by taking back the singular
value
%to time domain by Inverse Fourier transform, thus the correlation function will be obtained
% MAC criterion check on the right-hand of the bell curve formed centered at Fn
SDOF_I=zeros(Li,1);
j=d1;
 for i=1:d1
      if MAC((d1-i+1),1)>=0.9
          SDOF_I(j)=S((d1-i+1),1);
          j=j-1;
      else
           break;
```

```
        end
end
% MAC criterion check on the left-hand of bell curve formed centered at Fn
SDOF_r=zeros(Li,1);
for i=d1:Li
    if MAC(i+1,1)>=0.9
        SDOF_r(i+1)=S((i+1),1);
    else
        break;
    end
end
%combining right hand and left hand singular values centered at Fn selected by MAC rejection criteria
defined
SDOF_bell=SDOF_l+SDOF_r;
%plotting the SDOF bell curve for each modal frequency, Fn
subplot(3,2,[4,6])
index=find(SDOF_bell);
plot(SDOF_bell(index),'-*b')
title('SDOF Bell curve')
xlabel('bin')
ylabel('Singlar value[dB]')
grid on
%computing correlation function of singular values included in the SDOF definition
corr_fun=real(ifft(SDOF_bell));
%normalizing the correlation function
Normalized_corr_fun=corr_fun./corr_fun(1,1);
len=length(corr_fun);
b=ceil(len/2);
n=0:b-1;
time_lag=r/fs*n;
figure
subplot(3,2,[1,2])
%plotting the normalized correlation function
plot(time_lag,Normalized_corr_fun(1:b),'r')
xlabel('Time lag(Sec)')
ylabel('Normalized correlation')
title('Damping Estimation')
grid on
%defining the limits of correlation
min_corr=0.3;
max_corr=0.95;
%collecting correlation values of extrema points from the entire correlation function
SDOF_corr1(1,1)=Normalized_corr_fun(1,1);
for i=1:len/2
   if (abs(Normalized_corr_fun(i+1,1))-abs(Normalized_corr_fun(i,1)))>0
&&(abs(Normalized_corr_fun(i+1,1))-abs(Normalized_corr_fun(i+2,1)))>0
      SDOF_corr1(i+1,1)=Normalized_corr_fun(i+1,1);
    end
end
% plotting the SDOF correlation function
ind1=find(SDOF_corr1);
ind2=ind1-1;
time_lag=ind2.*r/fs;
subplot(3,2,[3,4])
plot(time_lag,log10(abs(SDOF_corr1(ind1))),'-*');
%collecting correlation values of extrema points defined by maximum and minimum correlation values
```

```
for i=0:length(SDOF_corr1)-1
    if abs(SDOF_corr1(i+1,1))>=min_corr && abs(SDOF_corr1(i+1,1))<=max_corr
       SDOF_corr(i+1,1)=SDOF_corr1(i+1,1);
     end
end
ind=find(SDOF_corr);
ind3=ind-1;
time_lag1=ind3.*r/fs;
hold on;
%plotting the logarithmic scale of the absolute value of SDOF correlation function
plot(time_lag1,log10(abs(SDOF_corr(ind))),'-or')
xlabel('Time lag(Sec)')
ylabel('Log/extrama/')
grid on
subplot(3,2,[5,6])
plot(time_lag1,log10(abs(SDOF_corr(ind))),'b')
xlabel('Time lag(Sec)')
ylabel('Log/extrama/')
grid on
%linear regression for damping calculation
p=polyfit(time_lag1,log10(abs(SDOF_corr(ind))),1);
fit=polyval(p,time_lag1);
hold on
plot(time_lag1,fit,'r')
xay=log(max_corr/min_corr)*2/length(ind)/sqrt((p(1))^2+4*(pi)^2);
Damp=abs(xay*100);
% Natural frequency Estimation determination of damped frequency
cross_time1(ind(1,1),1)=1;
for i=1:length(ind1)-1
    cross_time1(ind1(i+1,1),1)=cross_time1(ind1(i,1),1)+1;
end
cross_time(ind(1,1),1)=cross_time1(ind(1,1),1);
for i=1:length(ind)-1
    cross_time(ind(i+1,1),1)=cross_time(ind(i,1),1)+1;
    end
index2=find(cross_time1);
index3=index2-1;
time_lag3=index3.*r/fs;
index4=find(cross_time);
index5=index4-1;
time_lag4=index5.*r/fs;
p1=polyfit(time_lag4,cross_time(index4),1);
fit1=polyval(p1,time_lag4);
figure
subplot(2,2,[1,2])
plot(time_lag3,cross_time1(index2),'b')
hold on
plot(time_lag4,cross_time(index4),'r')
xlabel('Time lag(Sec)')
ylabel('zero crossing ')
title('Natural frequency Estimate')
grid on
subplot(2,2,[3,4])
plot(time_lag4,cross_time(index4))
hold on
plot(time_lag4,fit1,'r')
```

```
xlabel('Time lag(Sec)')
ylabel('zero crosing ')
title('curve fitted')
grid on
Nat_freq=p1(1)/4/sqrt(1-(xay)^2);
end
```

Annex D

MATLAB algorithm for (SSI) STOCHASTIC SUBSPACE IDENTIFICATION METHOD

```
function [dampin,frqz] = ssi_t(FK1,Syy,F,fs,r)
%algorthim to draw the singular value plot as background to the stabilization diagram.
Li=length(F);
%size of the cross-power spectra (n*n) depending on the number of simultaneous records
[J1,K1]=size(Syy);
%formation of 3D spectra matrix (n*n*Li) floor by floor with (n*n) floor
%matrix by extracting the individual elements of each spectra cell in orderly manner
for z=1:Li
for j=1:J1
for k=1:K1
Gi(j,k)=Syy{j,k}(z);
end
end
%application of singular value decomposition of each floor matrix formed at respective floor level
(Gauged by 'z')
[Ui,Si,Vi]=svd(Gi);
for j=1:J1
for k=1:J1
%singular vector matrix assignment as a 3D stack with each slice gauged by 'z'
Uj{j,k,z}=Ui(j,k);
%singular value matrix with each cell of matrix vertically ordered values (reproducing the same Si)
Sj{j,k}(z,1)=Si(j,k);
end
end
end
%end of integration
%formulation of the diagonal singular value matrix and transposing
for j=1:J1
S(:,j) = Sj{j,j};
end
%plotting singular values
figure
semilogy(F,S)
xlabel('Frequency (Hz)')
hold on
%it should be noted that this does not have anything to do with the %subspace algorithm

                    %-----------------------------end of singular value plot---------------------------------
%start of sub-space identification
%identification of model order by looking at the singular value vs model %order
h=FK1; [r,c]=size(h);
n2=r;n1=20;
d=2000;
%definition of frequency and damping values
%the hankel matrix is 2*n1*c * (n2-2*n1)
for j=1:n2-2*n1
   for i=1:2*n1
      hankel1(c*(i-1)+1:c*i,j)=h(i+j-1,:)       % generate Hankel matrix
   end
end
hankel1= hankel1/n2^0.5;                    % generate Hankel-matrix from R-matrix
yp=hankel1(1:c*n1,:);                       % past matrix (top half of the hankel matrix)
```

```
yf=hankel1(c*n1+1:c*2*n1,:);                % future matrix (bottom half of the hankel matrix)
yp1=hankel1(1:c*(n1-1),:);                  %one row shifted at end of past matrix
yf1=hankel1(c*(n1-1)+1:c*2*n1,:);           % one row shifted at the start of future matrix
%projection of row space future matrix in to row space past matrix
pref=yf*yp'*pinv(yp*yp')*yp;                % projection of the original matrices
pref1=yf1*yp1'*pinv(yp1*yp1')*yp1;          % projection of the shifted matrices
%SVD of the projection matrix to find kalman states
[u1 s1 v1]=svd(pref);
[ud1 sd1 vd1]=svd(pref1);
[r1 c1]=size(s1);
%collecting the diagonals of the singular value matrices and finding out the non-zero diagonal elements
for i=1:r1
   ss1(i)=s1(i,i);
   ssd1(i)=sd1(i,i);
end
   n=find(ss1);
   nd=find(ssd1);
   n=max(n);
   nd=max(nd);
%collecting the non-zero singular values and corresponding singular %vectors
for i=1:n
u11(:,i)=u1(:,i);                           % for upshifted matrix
s11(i,i)=s1(i,i);                           % for upshifted matrix
v11(:,i)=v1(:,i);                           % singular values transposed
end
for j=1:nd
u1d(:,j)=ud1(:,j);                          % for row shifted matrices
s1d(j,j)=sd1(j,j);                          % for row shifted matrices
end
figure
stem(s11);
prompt='Model order:';
order=input(prompt);
            %-----------------------------end of Model order identification---------------------------------
```

Annex E

Table 1-Pedestrian traffic load

Load	d [p/m^2]	n [P]	n' [P/m^2]	f_s [Hz]	l_p [m]	v [m/s]	$\Psi_{vert/long}$	P[KN/ m^2]
TC2_H1	0.2	19.4	0.022	2.25	0.8	1.8	0.25	4.599
TC2_H2	0.2	19.4	0.022	2.25	0.8	1.8	0.0625	1.149
TC3_H1	0.5	48.6	0.035	2	0.75	1.5	1	29.091
TC3_H2	0.5	48.6	0.035	2	0.75	1.5	0.25	7.272
TC4_H1	1	97.2	0.188	1.75	0.7	1.23	1	42.889
TC4_H2	1	97.2	0.188	1.75	0.7	1.23	0.25	10.722
TC5_H1	1.5	145.8	0.23	1.7	0.6	1.02	1	52.528
TC5_H2	1.5	145.8	0.23	1.7	0.6	1.02	0.25	13.132

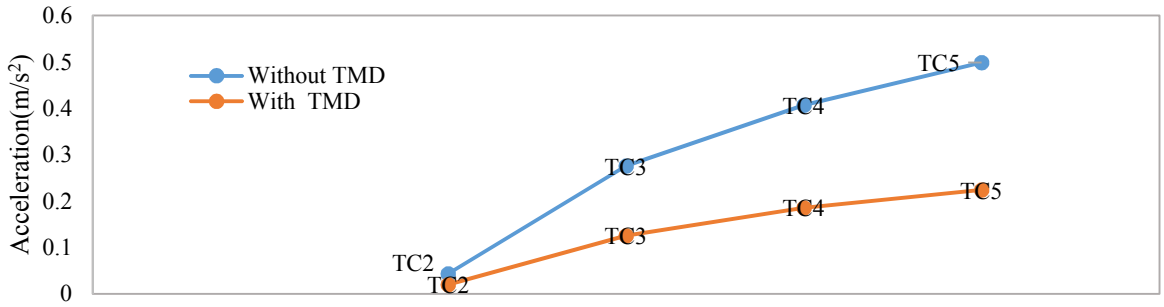

Figure 1-1st Harmonic resonant vertical vibrations of footbridge, updated model

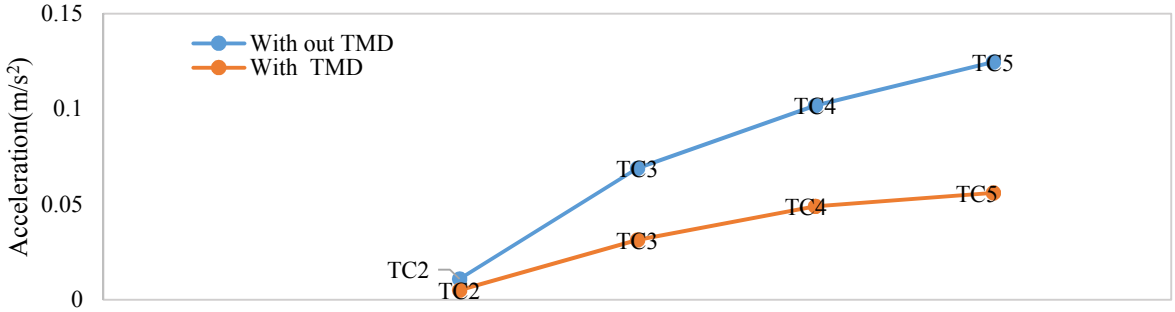

Figure 2-2nd Harmonic resonant vertical vibrations of footbridge, updated model